Identifying the Role of His293 in Protein Arginine Methyltransferase 1 and Characterization of Agonists for Peroxisomal Proliferator Activating Receptors

by

Brittany Neasha Boykin

A thesis submitted to the Graduate Faculty of
Auburn University
in partial fulfillment of the
requirements for the Degree of
Master of Science

Auburn, Alabama
May 8, 2016

Keywords: chemistry, computational, molecular dynamics, mutagenesis, PRMT, PPAR

Approved by
Orlando Acevedo, Chair, Associate Professor of Chemistry
Konrad Patkowski, Assistant Professor of Chemistry
Steven Mansoorabadi, Assistant Professor of Chemistry
Bradley Merner, Assistant Professor of Chemistry

Abstract

This thesis presents two proteins of interest: (1) protein arginine methyltransferase 1 (PRMT1) and (2) peroxisome proliferator activated receptors (PPARs). The purpose of this thesis is to assess the intermolecular interactions between substrate and important active site residues of PRMT1 and to characterize the major conformational changes induced by compound **9** upon PPAR and PPAR-γ coactivator 1 alpha (PGC-1α) to target diabetes.

An overview of theoretical background of the computational methods applied in this research can be located in chapter 2. Chapter 3 dissects the PRMT1 active site, and gains insight into the significance of the H293 active site residue in product formation control. Chapter 4 decribes the efforts of a combined computational and experimental study of PPAR/PGC-1α/agonist complexes that were performed to explain the differences between agonists compounds **9**, rosiglitazone, and other selective PPARγ modulators.

Acknowledgments

I would like to start off by saying thank you to Dr. Acevedo for his guidance, support, and believing in my abilities. Also, I would like to thank him for introducing me to a new form and outlook of chemistry. I will carry this experience throughout my journey in life. To the research collaborators Drs. Amin and Hevel, thank you for the fun field, interesting to say the least, projects that I took part in. To all of my committee members, Drs. Patkowski, Mansoorabadi, Merner, thank you for your time, availability, and efforts during my time here at Auburn University. To my past and present lab mates: Symon, Nicole, Bin, Robel, and Brian, thank you for your guidance, conversations and overall being great colleagues.

I would like to thank Dr. Jenda, NSF LSAMP Bridge to Doctorate, and the President's Graduate Opportunity Program (PGOP) for providing full funding for my duration in the chemistry and biochemistry department. I would like to express my deepest gratitude to my family and boyfriend for being a tremendous support to me during my time of decision and throughout my studies. Their encouragement and understanding, made this work possible. To my friends in the department and in the community, thank you, you made my time here, well spent. I owe my success to my mentor Dr. Gilmore, without her, I would not have even considered graduate school.

Table of contents

List of Tables

List of Figures

List of Abbreviations

PRMT	Protein Arginine Methyltransferase
ADMA	Asymmetric di-methylated arginine
SDMA	Symmetric di-methylated arginine
MMA	Mono-methylated arginine
SAM	S-adenosyl methionine
SAH	S-adenosyl homocysteine
PPAR	Peroxisome Proliferator Activated Receptor
RXR	Retinoid X Receptor
DBD	DNA Binding Domain
LBD	Ligand Binding Domain
AF-2	Activation Function 2
TZD	Thiazalodinedione
PGC-1	PPAR-gamma coactivator 1
NCOR1	Nuclear Receptor Corepressor 1
SMRT	Silencing mediator for retinoid or thyroid hormone receptors
MD	Molecular Dynamics
aMD	Accelerated Molecular Dynamics
WT	Wild type

Chapter 1: Introduction

1.1 Peroxisome Proliferator Activated Receptor (PPAR)

1.1.1 Nuclear Receptors

Nuclear receptors (NRs) are a superfamily of ligand-inducible transcription factors that coordinately regulate gene transcription in response to specific ligands. This superfamily is widely involved in diverse physiological functions that control processes such as embryonic development, homeostasis, differentiation, reproduction, and organ physiology.[1] Amongst this superfamily includes: steroid and thyroid receptors, vitamin D, fatty acids, prostaglandins and retinoic acid.[2-3] NRs are highly implicated in biological research, which target specific chronic diseases such as cancer, diabetes, osteoporosis and hormone resistance syndrome.[2] This superfamily can be divided into two major subtypes: (type I receptors) consist of steroid receptors such as progesterone, while the second subtype (type II receptors) consists of the essential retinoid X receptors (RXRs) and peroxisome proliferator activated receptors (PPARs) which are independent of ligand binding. RXR plays a central role in dimerization of nuclear receptors, specifically PPARs, to form a heterodimer. NRs comprised of 49 members have a similar mode of action and structural organization.[4] This includes target genes to be controlled by the DNA binding domain (DBD), which is a highly conserved region along the center of polypeptides that regulate replication, repair and storage. Compared to other nuclear receptors, PPARs have a large ligand-binding domain (LBD) pocket which bind specific natural and synthetic ligands.[5] Located in the C-terminal region, NRs LBD is responsible for hormone binding and is required for heterodimerization and interaction with transcriptional cofactors.[6] The remaining two regions, N- and C- terminals contain

a regulatory domain, which size and sequence links the DBD and LBD. The C- terminus is essential for the nuclear localization of PPARs and interactions with activator proteins.[7-10]

1.1.2 PPAR Mode of Action

PPARs are ligand-dependent receptors composed of three isoforms (α, β, γ), which regulate glucose and lipid homeostasis in response to endogenous and exogenous agonists leading to the modulation of gene expression.[11-12] RXRs also exist of three subtypes (α, β, γ); whose ligands are retinoids, a functional analogue of vitamin A.[13] In the absence of ligand, the receptor heterodimer is bound to the DNA binding domain in an inactive or basal transcription. The binding of specific agonists activates PPARs response to form a heterodimer complex with the retinoic X receptor (RXR) that triggers a conformational change to reorient and stabilize the AF-2 helix.[7-10] Upon the binding of agonists results in the release of histone deacteylase (HDAC) corepressors, such as nuclear receptor corepressor 1 (NCOR1) and the silencing mediator for retinoid and thyroid hormone receptor (SMRT), which repress target gene expression. Corepressors bind weakly to the PPARγ/RXR heterodimer on the peroxisome proliferator response element (PPRE) in absence of ligand. The binding of agonist on the surface of the LBD creates an interface that directly interacts with the LXXLL motif, to facilitate the recruitment of coactivators to interact with the heterodimer.[13] To this complex, the recruitment of coactivator proteins modifies chromatin structure and stimulates the activity of RNA polymerase II. In addition, coactivators promote histone acetylation. In the succeeding complex, the PPAR/RXR heterodimer binds to specific (PPRE) regions in the DNA to target gene expression that regulates certain defects as insulin sensitization (Fig. 1.1).[11, 14-15]

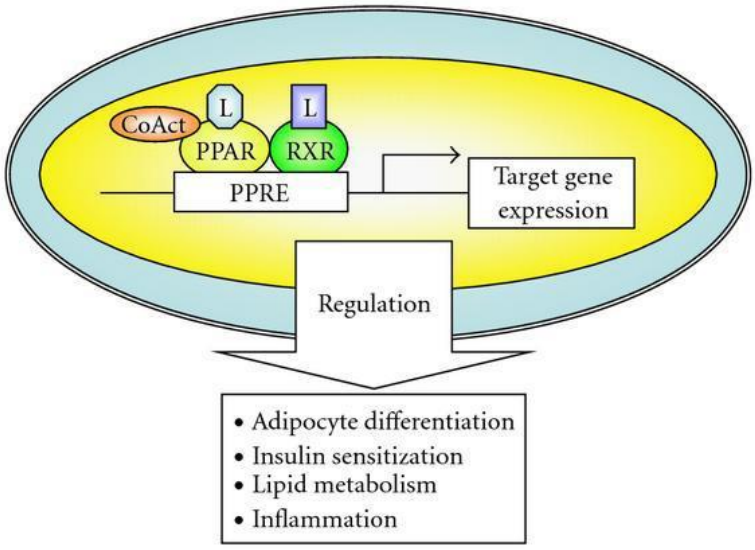

Figure 1 1.1

Shimizu, M., Moriwaki, H. PPAR Research 2008, 181047

Figure 1.1 - PPAR mode of action, PPAR/RXR heterodimer target gene expression

1.1.3 PPAR Subtypes: distribution and function

PPARs induce the proliferation of peroxisomes in cells to alterate in various metabolic reactions such as hepatic lipid metabolism and differentiation pathways.[16] The three human subtypes of PPAR (α, β, γ) promote distinct physiological roles and ligand specificity (Figure 1.2).[4, 17] The first PPAR, discovered by Isseman and Green, was cloned from mouse liver in the early 1990's, termed PPARα.[16, 18] All subtypes were cloned from Xenopus, a genus from the aquatic frog, while α, β/δ from humans, mouse and γ from a hamster.[16, 19-21] Since the discovery of isoform PPARα, followed two PPAR homologs identified as PPARβ/δ and PPARγ which share similar a structural homology and encode different cellular genes and tissues. The three subtypes differ as PPARβ/δ and PPARγ are activated by peroxisome proliferators in rodents unlike PPARα. PPARβ/δ nor PPARγ respond to peroxisome proliferators. The discovery of these three subtypes has promoted extensive research conducted on PPARs to regulate glucose homeostasis.

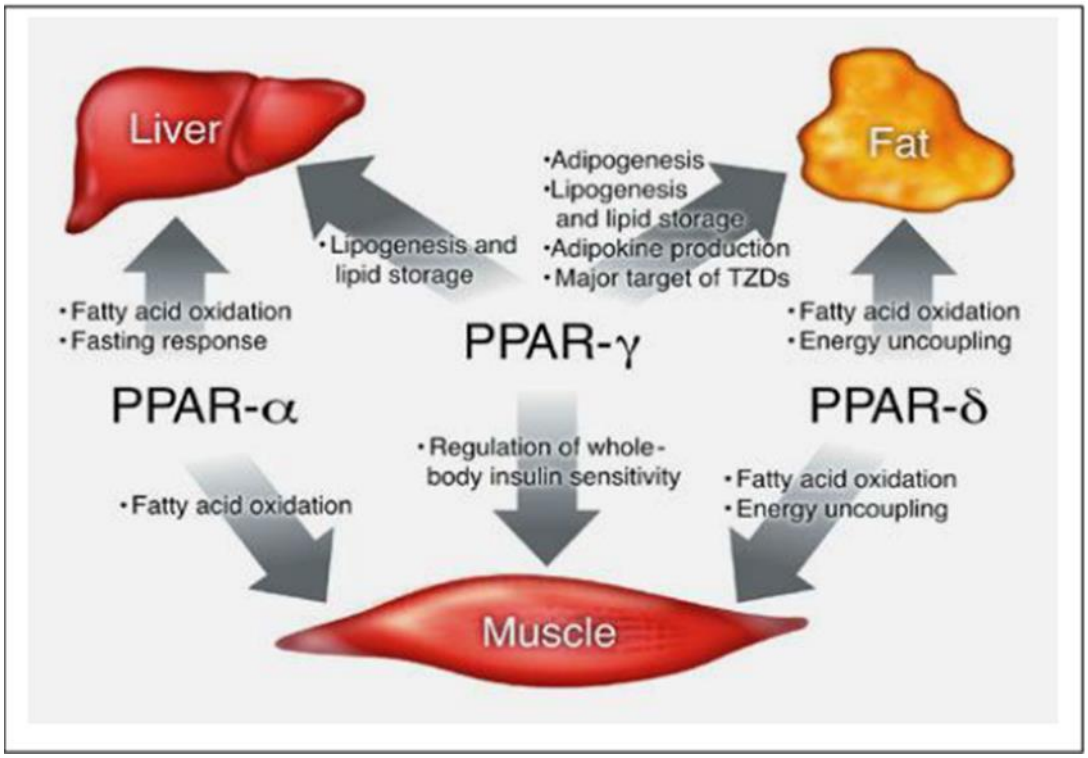

Figure 2 1.2

Nat Med. 2004; 10 (4):355-61

Figure 1.2 – PPAR subtypes physiological functions

PPARα expression is found abundantly in the liver, kidney, skeletal muscle, heart, macrophages and in tissue with high metabolic rates.[7-8, 22] PPARα is responsible for the cellular uptake and oxidation of FA lipoprotein metabolism.[3] PPARα induces gene expression of several enzymes such as acetyl – CoA synthase, which is highly involved in the β-oxidation pathway. Polyunsaturated fatty acids activate PPARα, like` docosahexaenoic acid (DHA), which prevents high-fat diet-induced obesity, used as a treatment of metabolic syndrome and increases in insulin sensitivity.[7-8, 22] This isoform is the target for lipid lowering fibrates, used as hypolipidemic drugs which are endogenous ligands for PPARα that cause a decrease in lipid levels in humans.

PPARβ/δ function is explored less extensively compared to the other two subtypes. PPARβ/δ expression is common in abundance as they favor fatty acid oxidation in absence of

PPARα or in tissues less expressed.[7, 23] PPARβ/δ is found in most cells, mainly the central nervous system and exhibit high concentrations in skeletal muscle. Agonists play a central role in cancer treatment and cell differentiation. Agonists of this subtype are known to act like PPARα and are involved in blood cholesterol, embryo development, and glucose homeostasis.[7, 24]

The four distinct variants of PPARγ (1-4) are expressed in fat, vascular tissue and lower intestine, while present in the brain and heart to reduce cardiovascular damage and neurodegeneration.[7, 25] Interestly, PPARγ is the most studied subtype. PPARγ is known as an antidiabetic agent that regulates genes involved in energy homeostasis, insulin sensitivity, lipid metabolism and improves adipocyte development in the body.[26-27] This subtype is activated by natural ligands such as linoleic acid (9- and 13-HODE) which facilitate an inflammatory response.[7, 10] PPARγ's clinical importance has risen due to its involvement in improving insulin sensitization. Activators of PPARγ, the thiazolidinedione (TZD) class (e.g. rosiglitazone (Avandia), and pioglitazone (Actos)) are used to reduce insulin resistance and lower blood glucose levels for the treatment of diabetes mellitus type 2 but cause scrutiny in the pharmacological world due to their adverse side effects.[7, 28-29]

Thus PPARs are key regulators for the translation of nutritional environments and prevail in pharmacological studies.

1.1.4 PPAR Binding/Structure

Similar to most nuclear receptors, PPAR proteins exhibit a molecular structure comprised of six functional domains: A/B, C, D, and E/F (Figure 1.3).[16]

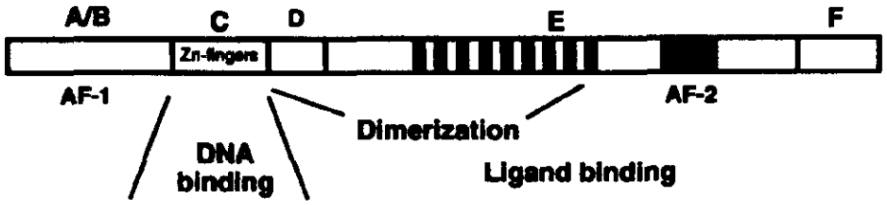

Figure 3 1.3

J Lipid Res. 1996 Vol. 37:907-925

Figure 1.3 – Functional Domains of the nuclear receptors

Unit A/B, located in the N-terminal is expressed as the least conserved domain, which controls the activation of the region, by the AF-1 (activating function 1) agonist. The C domain (DNA binding domain) specifically, consists of ~66 amino acids which bind receptors to DNA sequences or PPRE.[7] The PPAR D-box is said to be involved in protein-protein interactions, particularly, receptor dimerization.[16, 30-31] Both the C and D domains include two zinc fingers which bind to four invariant cysteine residues to further stabilize the DNA binding domain. PPARs D-box differs from other nuclear receptors due to the number of amino acids present.[16] A main region in PPARs, the C-terminal region encompasses a ligand-dependent activating domain, termed AF-2 (activating function 2), found in the E-domain, essential for the activation of proteins. The multifunctional domain, unit E/F (ligand-binding domain), embodies dimerization, nuclear localization, intermolecular silencing, as well as ligand-dependent transactivation[16, 30-31].

As of July 2006, the Protein Data Bank is comprised of twenty-eight co-crystal structures available to the public[3, 32-33] as well as countless X-ray structures in liganded and apo forms of PPAR (α, β, γ).[3, 5]

1.1.5 PPAR LBD

The ligand-binding domain in nuclear receptors is a standard in all three subtypes which molecules possess a bundle of thirteen helices and four small stranded β-sheets.[3] The PPAR structure is comprised of structure elements; helices H1 to H12 and β-strands S1 to S4 which allow the receptor to bind to similar but not identical ligands.[3, 16] The LBD's rather large cavity displays a Y-shape, which consists of three important parts: an entrance that extends to two pockets, arm I and arm II. Arm I can be described as the polar cavity, which extends toward the AF-2 (H12) helix, while arm II (located between helix H3 and β-sheet) and entrance are hydrophobic regions (Figure 1.4).[3, 34]

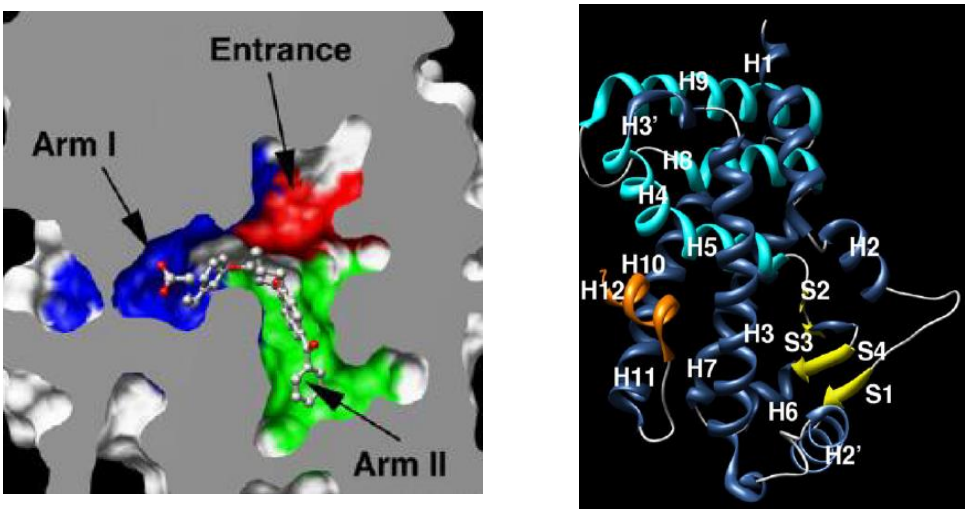

Figure 4 1.4

Biochimica et Biophysica Acta 1771 2007, 915-925

Figure 1.4 – Ligand Binding domain of PPAR and helices displayed

The ligand entrance easily adapts to natural and synthetic ligands, allowing large ligands to bind in the active site without affecting the overall structure of the LBD. Most agonists exhibit a polar head (carboxylate function) and a hydrophobic tail which stabilizes the AF-2 helix and several conserved polar residues: His323, His449, Ser289, and Tyr473 of PPARγ; Thr289, His323,

His449, and Tyr473 of PPARβ/δ; Ser280, Tyr314, His440, and Tyr464 of PPARα of the protein-ligand interaction.[3] These essential residues and ligands, such as eicosanoic acids and rosiglitazone in the LBD of PPAR (α, β, γ) are part of a hydrogen-bond network that conserves the protein-ligand interaction.[3, 35]

1.1.6 Partial, Full Agonists, Antagonist and Selective Modulators

Extensive research has been carried out for PPARs due to their therapeutic actions and benefits as drug targets. PPARs have a significant flexibility in the range of conformations that are induced from different ligands. This is of significance as these different ligands can promote distinct coactivator interactions, which trigger different biological responses. Synthetic agonist can range from displaying full, partial, and/or antagonist characteristics. Partial agonists promote submaximal activity. For example, rosiglitazone and troglitazone, two target drugs, induce PPARγ in different conformational changes, which in return result in different transcriptional activity. Troglitazone displays a portion of maximal activity to rosiglitazone of PPARγ, therefore, exhibits as a partial agonist. Partial and full agonist can be characterized by their hydrogen bond interactions with several conserved residues in the active site, particularly polar residues of arm I. Generally, full agonist display a hydrogen bond interaction with residues: Ser289, His323, His449, and Tyr473. Contact with residue Tyr473 is crucial for the stabilization of the AF-2 (H12) helix to further allow the recruitment of coactivators to activate genes responsible for adipogenesis.[34, 36] Partial agonists display a lesser degree of interaction with the AF-2 helix, exhibiting negligible effects upon lipid accumulation in adipocytes. Full agonists are more prone to have a direct interaction with Tyr473 compared to partial agonist. Clinically, partial agonists lack the deleterious side effects of lipid accumulation, development of edema, weight gain and risk of adverse cardiovascular events to full agonists.[34, 37]

Antagonists are classified as distinct ligands that bind to the receptor but fail to induce transcriptional activity. This failure to reorient the C-terminal, leads to competition of binding to the receptor, which results to a complex that does not recruit coactivators. Antagonists are not mentioned as extensively as partial and full agonist.

Recently, an additional ligand has been characterized due to its tolerability in preclinical species.[38] Gene-selective PPARγ modulators (SPPARγMs) have anti-diabetic efficacy comparable with full and partial agonist. SPPARγMs interact with PPARγ differently than full agonist; hence their novel affects as pharmacological agents. SPPARγMs have improved insulin sensitization and inflammation without side effects compared to full agonist. This agonist results in distinct patterns of gene expression that alters the conformational stability of the LBD in PPARγ.[39-40] Unlike most full agonist, SPPARγMs correspond to partial agonist, no direct hydrogen bond with the AF-2 (H12) helix.

Thus, advancing studies in the understanding of PPAR agonists holds potential to further provide the efficacy of PPAR therapeutic and pharmacological agents for the treatment of diabetes mellitus type 2.[38]

1.1.7 Coactivators and Corepressors

The transcriptional activity of NRs is regulated by their interactions with a variety of coactivators: p160/SRC-1 family members, GRIP1, ACTR, mediator complex (TRAP220, DRIP205, CBP, p300), and metabolic regulator (PGC-1α) or with corepressors such as SMRT and NCOR1.[4] Coactivators, upon ligand binding, undergo a conformational change that stabilizes the AF-2 (H12) helix and recruits an activator. These ligand-dependent activators contain an LXXLL that forms a two-turn α-helix to bind into a hydrophobic cleft on the surface of the receptor to promote histone acetylation (Figure 1.6).[41] This hydrophobic groove of the LXXLL motif, contacts

the hydrogen-bonded side chains of PPAR (α, β, γ) and the coactivator backbone, labeled as the charge clamp. The charge clamp stabilizes the coactivator to the PPAR LBD.

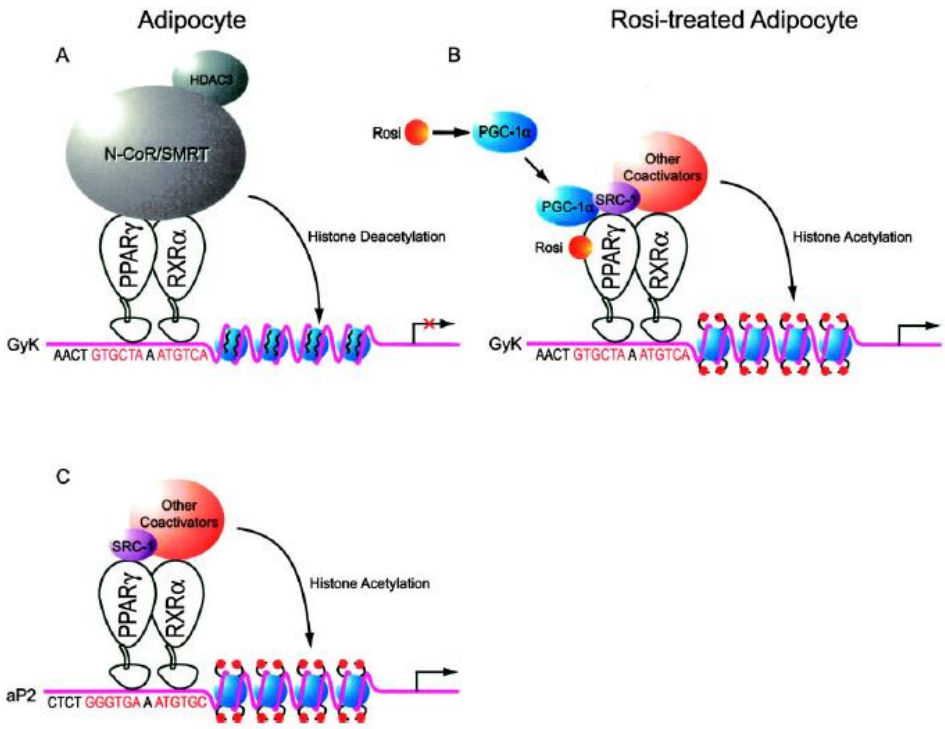

Figure 5 1.5

Genes and Development 2005, 19:453-461.

Figure 1.5 – PPAR mechanism with emphasis of coactivators and corepressors

Corepressors bind to unliganded receptors and promote histone deacetylation until agonist generates a dismissal followed by the recruitment of coactivators (Figure 1.5).[41] NCOR1 and SMRT bind to NRs by overlapping the surface bound region of coactivators by NR-box-like motifs[41-43]. PPARs can interact with both NCOR1 and SMRT but may posses a weak binding affinity (e.g. PPARγ displays a weaker interaction compared to other NRs).[41, 44]

1.1.8 PPARγ Coactivator 1 alpha (PGC1-α)

The PGC-1 family is known to enhance transcriptional activity through direct protein-protein interactions.[45] PGC1-α is a leading coactivator amongst many in drug discovery such as SRC-1, DRIP205, TRAP220, GRIP1, etc. PGC1-α was discovered by Bruce Spiegelman's laboratory to distinguish brown adipose tissue from white adipose tissue.[45] This coactivator is a key regulator of energy homeostasis and metabolic regulation.[46] PGC1-α is expressed in brown adipose tissue, heart, kidney, and skeletal muscle[41] as well as induces adaptive thermogenesis. PGC1-α, down regulated in diabetes, is critical to differentiate. specific functions of PPARγ such as triglyceride (TG) accumulation and insulin signaling.[34] This cofactor can induce expression of mitochondrial biogenesis and uncoupled respiration in brown adipocytes as well as drives oxidative phosphorylation. PGC-1α expression is activated by exercise training, where fatty acids and glucose utilization is increased to meet the demand of ATP (Finck and Kelly PGC-1α in Cardiac Physiology and Disease).

Compared to other coactivators such as the p160 family, PGC1-α coactivates the glycerol kinase (GyK) gene but not the adipose specific fatty acid-binding protein (aP2). Moreover, PGC1-α binds to PPARγ in a ligand-independent manner, to a region between the DBD and LBD[46], critical for corepressor interaction and induces contacts with other coactivators including SRC-1, TRAP/DRIP, CBP, and p300. Partial and full agonists display high recruitment of PGC1-α compared to p160 coactivators, therefore, exhibiting a high binding affinity to PPARγ. For example, even in the absence of ligand, PGC1-α displays a strong interaction to PPARγ due to the high basal activation of the protein. By PGC1-α binding to the GyK gene, this recruitment enhances corepressor removal and additional coactivator recruitment.[41] The intermolecular interaction and hydrophobic effect with Lys145 of PGC1-α and Asn312 of PPARγ stabilizes the

coactivator and PPARγ (Figure 1.6).[41] Residues Ser142 and Lys145 of PGC1-α contribute to the ability to coactivate PPARγ. This nuclear coactivator interacts with most NRs.

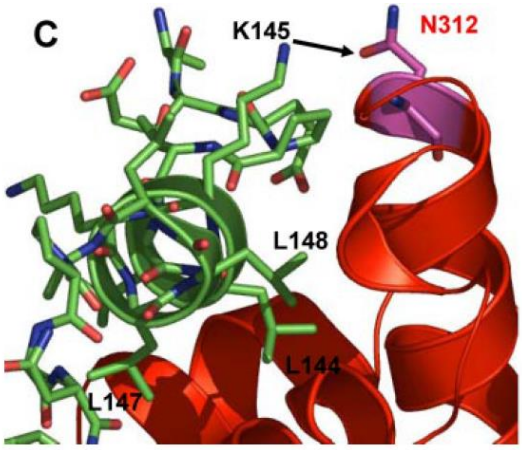

Figure 6 1.6

J Bio Chem. Vol. 283, No.27, pp. 19132-19139

Figure 1.6 – Molecular Interaction of PGC1-α/PPARγ

1.2 Protein Arginine Methyltransferases 1 (PRMT1)

1.2.1 Post-translational Modifications

The human proteome is vastly more complex than the human genome, comprised of 20,000+ human genome genes compared to the estimated 1 million human proteome proteins.[47] The complexity of the genome to proteome can be described by post-translational modification (PTM). This is a step in biosynthesis observed in all known living organisms, which protein function is created by ribosomes translating mRNA in to polypeptide chains.[48] PTM is a significant cellular control mechanism that alters the physical and chemical properties of a protein including, folding, conformation, distribution, stability, activity, and function.[49] Remarkably, there are 200+ types of post-translational modifications that include kinases, phosphatases, transferases,

and ligases, which add or remove lipids and functional groups.[50] PTMs are highly accepted cellular process that initiate and ensure particular protein functions.

1.2.2 Arginine Methylation

Protein arginine methylation is mainstream in all eukaryotic cells. Arginine methylation is a post-translational modification that regulates protein functions in cell processes and human diseases. This modification regulates stability, localization, and activity of proteins.[51] Protein methylation is biologically reversible in modification.[52] N-methylation of histones occurs in lysine and arginine side chains and is important for gene expression and pathogenesis.[52] Arginine is an abundant, positively charged amino acid that is known for its interaction with amino-aromatic groups and mediating hydrogen bonding.[53] It has been known for forty years that arginine displays methyl groups, but a greater focus on arginine methylation is becoming prominent in biological studies.[53-54] Arginine methylation is simply defined as nitrogen atoms of arginine within the protein can be post-translationally modified to contain one to two methyl groups[53, 55] from cofactors such as S-adenosyl-methionine (AdoMet or SAM) to produce S-adenosyl-homocysteine (AdoHcy or SAH) (Figure 1.7).[56]

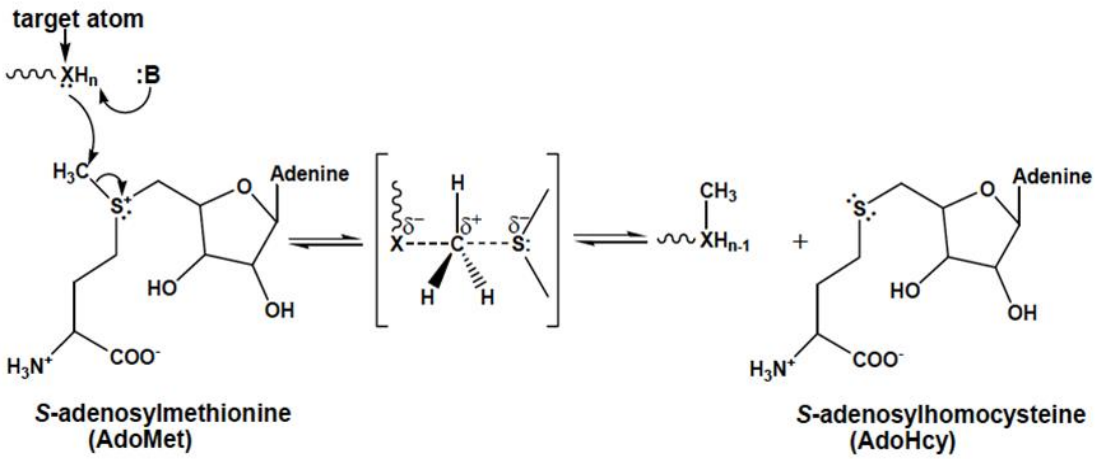

Figure 7 1.7

Trends in Biochemical Sciences 2003 28:6

Figure 1.7 - General Mechanism for AdoMet-dependent methyltransferases

The addition of the methyl group to an arginine residue affects the shape of the residue and increases the hydrophobicity and bulkiness[56] of the protein. Protein arginine methylation can form three products: monomethylarginine (MMA), asymmetric dimethylarginine (ADMA), and symmetric dimethylarginine (SDMA) (Figure 1.8).

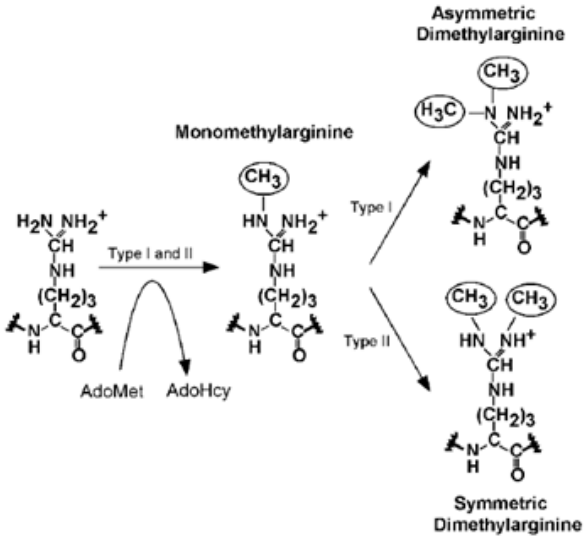

Figure 8 1.8

The EMBO Journal Vol. 19 No. 14, 2000, pp. 3509-3519

Figure 1.8 – Major types of PRMTs

1.2.3 Protein Arginine Methyltransferases (PRMTs)

Protein arginine methylation is catalyzed by protein arginine methyltransferases.[55] Protein arginine methyltransferases (PRMTs) is a family of enzymes widely involved in biological processes, including transcription, RNA splicing, signal transduction, DNA repair, neuronal cell differentiation, and chromatin remodeling.[57] PRMTs have become an expanded field, which are known to methylate and regulate coactivators, and histones[56], which are important for many benign cellular processes.[58] In recent years, deregulation of PRMT activity has been expressed in various diseases, specifically, cardiovascular disease[59-60] viral pathogenesis, cancer[61-62] and spinal muscular atrophy.[56]

Currently, there are eleven PRMT isoforms identified in eukaryotes from fungi, to plants, and mammals (Figure 1.9).[63]

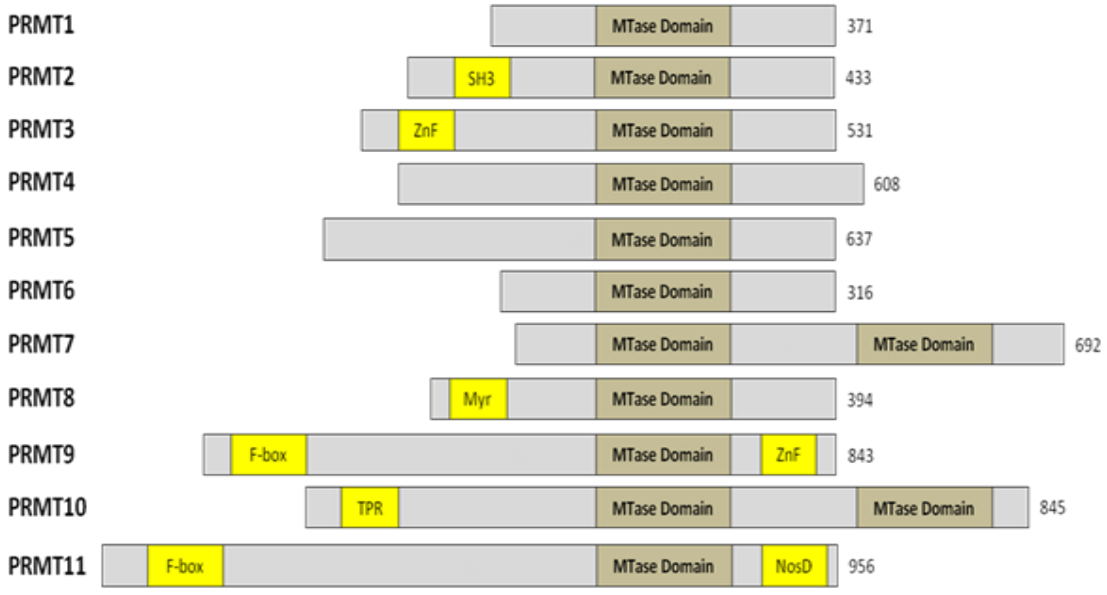

Figure 9 1.9

Cell. Mol. Life Sci. 2009 66:2109

Figure 1.9 – PRMT Human Isoforms

PRMTs are classified into specific forms, according to their methylation status. While type II and type I PRMTs generate (MMA), type I (PRMTs 1, 2, 3, 4, 6, and 8) further convert to catalyze (ADMA) and type II (PRMT 5) catalyzes to form (SDMA). Type III PRMTs (PRMT 7) found in yeast[58] specifically form (MMA). ADMA is known to reduce heart rate in persons with cardiac disease.[64] The specific physiological function of SDMA is not known as extensively as ADMA.

1.2.4 Protein Arginine Methyltransferase 1 (PRMT1)

PRMT1 is a widely expressed member in the PRMT family, which performs an estimated 85% of arginine methylation in mammals[65-66] and prefers to methylate arginine residues in GAR sequences (glycine and arginine rich).[58] PRMT1 is localized in the cytoplasm and nucleus. PRMT1 activity results exclusively MMA and ADMA products.

1.2.5 PRMT1 Structure

PRMTs are a 2-ring like dimer connected by a disulfide bond (Figure 1.10). Dimerization is strictly conserved in all known PRMTs[64] and is essential for SAM/substrate binding and enzymatic activity.[63] PRMT1 exists as a homodimer consisting of two 353-residues ~42 kDa in weight.[55] The PRMT structure is divided into four conserved regions in the PRMT monomeric structure: SAM binding domain (green), β-barrel (yellow), and dimerization arm (light blue) (Figure 1.9).[67]

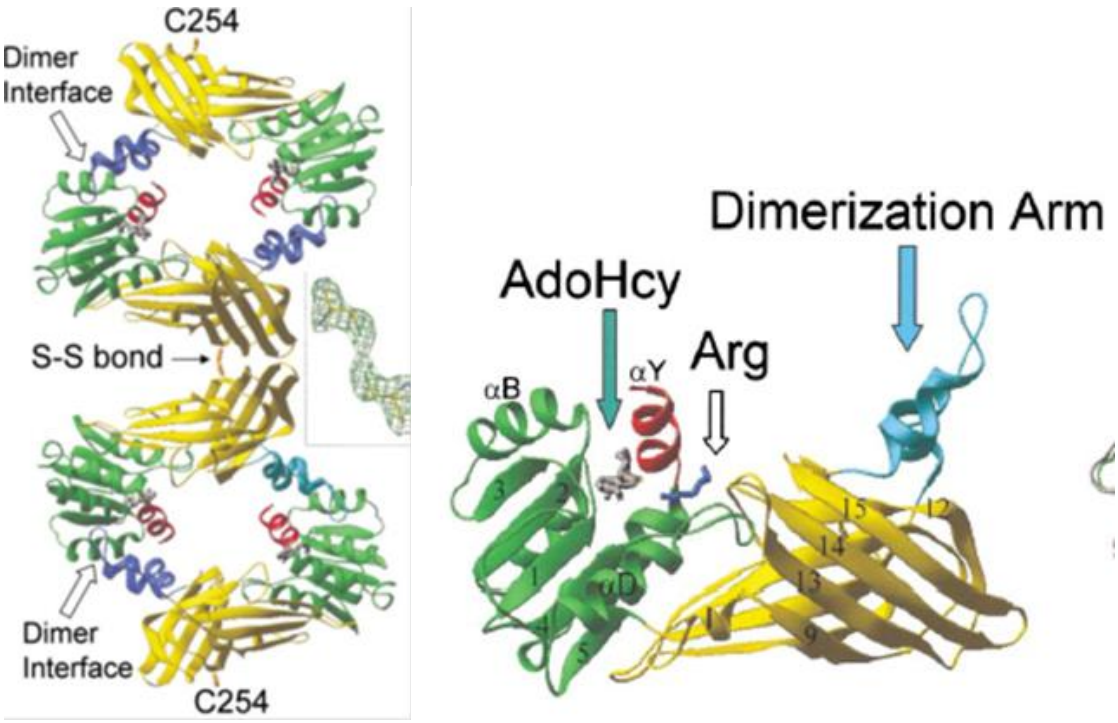

Figure 10 1.10

Cantoni, G. L. J Am Chem. Soc. 1952, 74, 2942

Figure 1.10 – **PRMT1 Structure**. Dimeric structure (left), monomeric structure (right).

The reported PRMT1 crystal structure contains the cofactor AdoHcy and a R3 peptide derived from fibrillarin (GGRGGFGGRGGFGGRGGFG).[68] The R3 peptide is known as a common peptide substrate in arginine methylation, as it was discovered to co-crystallize with rat His-PRMT1 in 2003.[63] The SAM binding domain is conserved in all SAM-dependent methyltransferases[69] while the β-barrel is seen as unique to the PRMT family.[63] Observed in the PRMT family, PRMT1 has a helical N-terminus (red) and C-terminus.

1.2.6 Active Site of PRMT1

The active sites of type I PRMTs are remarkably conserved.[70-71] Common active site residues in PRMT1 are as follows (Figure 1.11): two conserved glutamates (Glu144 and Glu153)

known as the “double-E” loop stabilize SAM and arginine substrate binding; Tyr39, although not visible in the PRMT1 crystal structure, plays a key role in cofactor binding; Arg54 is known to help position the Nη2 region of the guanidinium group of arginine substrate for attack on the methyl group of SAM; Glu100 forms a hydrogen bond with ribose moiety of SAM; Met48 and Met155 are essential to regulate product formation and affects SAM binding; and lastly, His293 plays a role in catalysis, potentially via salt bridge formation.[55]

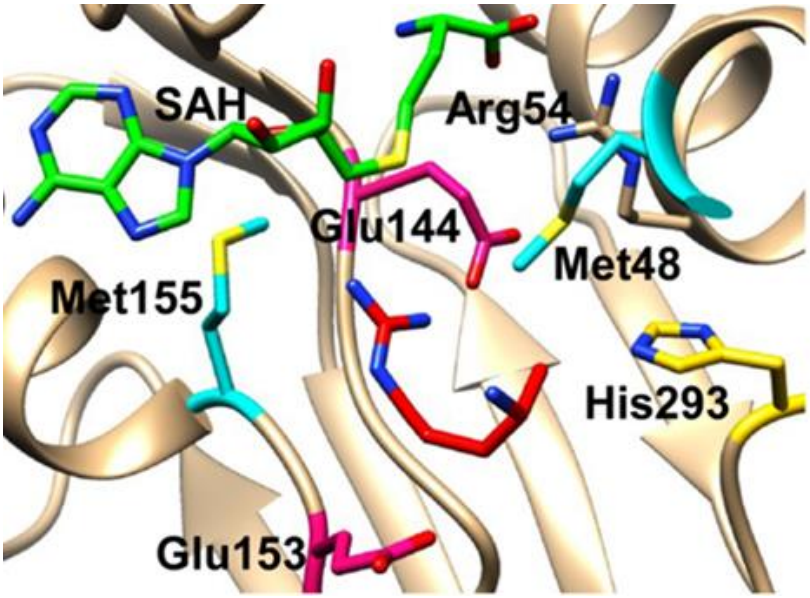

Figure 11 1.11

J. Bio. Chem. Vol. 289, NO. 13, 2014, pp. 9320-9327

Figure 1.11 – PRMT1 Active Site

1.2.7 H293 Importance

Rust et al. characterized the catalytic mechanism of PRMT1 by mutating several highly conserved active site residues (Y39, R54, E100, E144, E153, and H293) which play a role in SAM recognition, substrate binding, and catalysis by pH-rate studies, and solvent isotope effects to determine how MMA binds.[55] Due to H293’s distance of 6 Å away from the approximate position

of the Nη2 of the guanidino group of arginine substrate, it was deemed too far away to act as the general base and/or enhance nucleophilicity.[55] Mutagenesis studies of H293 to Ala and Gln residues resulted in a loss of activity.[55] The H293 residue is believed to form a salt-bridge with residue Asp51 (Figure 1.12), responsible for the formation of a two-helix boundary that separates SAM and peptide binding in the active site.[55] Disruption of the salt-bridge may result in an improper formation of the binding pocket. However, simulations suggest that H293 may have a larger effect on the active site beyond the salt-bridge formation.[57]

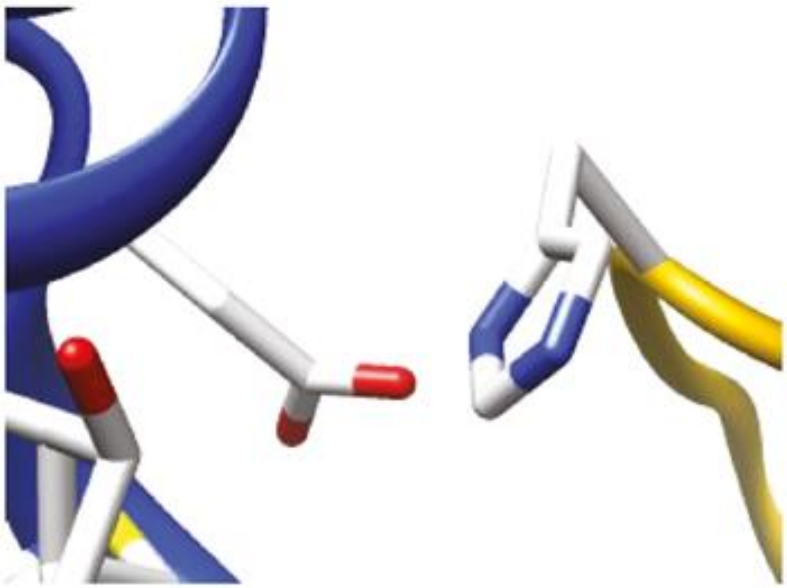

Figure 12 1.12

Biochemistry 2011; 50(16): 3332-3345

Figure 1.12 - H293 salt-bridge to conserved residue Asp51

Chapter 2: Methodology

2.1 Molecular Dynamics (MD) Simulations

Time-scale molecular dynamics (MD) is a computational method with complete atomistic detail, which calculates the time dependent behavior of molecular systems determined by trajectories generated by Newton's equation of motion of interacting particles. The usage of MD is to compute macroscopic behavior from microscopic interactions.[72] MD simulations can address multiple questions of properties of a molecular system, which is often easier than performing experiments on the actual system.[73] Alder and Wainwright were the first to perform molecular dynamics on a condensed phase system in the late 1950's.[74] They calculated equilibrium properties, specifically the equation of state of hard spheres. Atomic simulations were conducted in the 1960's for liquid argon by Rahman[75] and conformational simulations of protein molecules were first reported in the 1970's by McCammon.[76] MD today is routinely applied to complex systems[34, 77] and is increasing rapidly in refining structures using experimental procedures including X-ray crystallography and NMR[76].

In this thesis, molecular dynamics using AMBER was performed on Peroxisome Proliferator Activated Receptor (PPAR) and Protein Arginine Methyltransferase 1 (PRMT1) to determine various conformational changes of endogenous agonist compound 9, when bound to the PPARγ-PGC1-α complex and investigate how His293 controls product specificity using PRMT1. This section will highlight the theory of molecular dynamics using the AMBER force field and provide a fundamental overview of the techniques employed during each study.

2.1.1 Statistical Mechanics: Ensemble Averaging

Statistical averages can define the connection between the microscopic interactions and macroscopic behaviors of molecular systems. An ensemble can describe the position and momenta contained in a molecule. This can be defined as a collection of statistically identical time series from which different microscopic states can be determined.[78] Moreover, the ensemble average (equation 2.1) provides the mean of a quantity that is a function of the individual states of a system. This average is a replica of the system considered simultaneously.

$$< A >_{ensemble} = \iint dp^N \, dr^N \, A(p^N, r^N)\rho(p^N, r^N) \qquad (2.1)$$

Where:

$A(p^N, r^N)$ – is the observable of interest, momenta is expressed by p, and position by r.

(< >) – is the ensemble average notation.

$\rho(p^N, r^N)$ – is the probability density of the ensemble.

MD simulations aim to generate a range of conformations, which sample all possible states, to compute properties such as dynamics, thermodynamics and structure. Various macroscopic systems (variable constraints) are related to the behavior of their microscopic constituents, resulting in different types of ensembles. Simulations can be performed under conditions including the number of particles (N), volume (V), energy (E), pressure (P), temperature (T), and chemical potential (μ).[79] MD is traditionally performed in the constant NVE ensemble.[78] The two most common alternative ensembles are NPT and NVT. Examples of simulations under various conditions are as followed:

- Canonical ensemble (NVT) – the mechanical variables where the number of particles (N), volume (V), and temperature (T) of the system are held constant describes a system in

contact with a heat bath. Boltzmann and Helmholtz free energy are constants for this ensemble.

- Microcanonical ensemble (NVE) – the number of particles (N), volume (V), and energy (E) are held constant. Compared to other ensembles, microcanonical describes an isolated system. This ensemble is used less frequently due to the difficulty of isolated systems.
- Grand canonical ensemble (μVT) – chemical potential (μ), volume (V), and temperature (T) of the system are held constant. This ensemble can be described as an open system consisting of a heat and particle bath where the particles and heat can be exchanged between the bath and system.
- Isobaric-Isothermal Ensemble (NPT) – the number of particles (N), pressure (P), and temperature (T) of the system are held constant. The system exchanges heat with the bath, and volume while working with the bariostat.

2.1.2 Equation of Motion

Newton's Second Law or equation of motion is the foundation of MD simulations. It describes a system's behavior in terms of motion as a function of time expressed in equation 2.2.

$$F_i = m_i a_i = m_i \frac{dv_i}{dt} = m_i \frac{d^2 r_i(t)}{dt^2} \quad (2.2)$$

Where variables are as follows:

(F) is the force exerted, (i) is the particle, (m) is the mass, (a) is the acceleration, (r) is the position, and (v) is the potential energy or velocity of the system.

The time integration is the engine of MD, required to integrate the equation of motion of interacting particles and follow a trajectory that encompasses the positions, velocities, and accelerations of particles as a function of time. From the trajectory of an atom, the state of a system can be predicted throughout the simulation, thus providing averaged properties. Position and velocity vectors of a trajectory can describe the evolution of time in phase space.[73] A particle's position in space can be defined by $r_i(t)$, while the velocity $v_i(t)$ of a system determines the kinetic energy and temperature using various numerical integrators.

There are various numerical integrators used to express the equation of motion. The Verlet algorithm derived by the French physicist Loup Verlet is predominantly used in MD. Known for its simplicity and stability, the Verlet Algorithm is used to calculate trajectories of atoms in MD using the Taylor expansion for the position and momenta at time (t). The aim is to express each step by a known position $r_i(t + \Delta t)$ and time (t + Δt).[73] The positions can be predicted by time, t – Δt and t + Δt, where Δt is the integration state. The basic idea of this algorithm can be expressed below in equation 2.3:

$$r_i(t + \Delta t) \approx 2r_i(t) - r_i(t - \Delta t) + \frac{F_i(t)}{m_i} \Delta t^2 \quad (2.3)$$

Explicit velocities are not expressed using the Verlet algorithm; however they can be determined from the trajectory by dividing the difference in position at time (t – Δt) and (t + Δt) by 2Δt. This algorithm has the disadvantage of having moderate precision. A modified version of the Verlet algorithm was introduced in 1970 by Hockney, termed the leap frog algorithm.[80] The leap frog algorithm refers to the velocities leap over the positions, followed by the positions leap over the velocities. This algorithm is known to conserve more energy, is computationally less expensive, and is essential for large-scale calculations. Using this algorithm, velocity is expressed explicitly, but is not calculated at the same time as the position.

The SHAKE algorithm, based on the Verlet integration scheme, is employed extensively in MD calculations.[81] Ryckart[82] derived this algorithm to allow a larger time step to be carried out to constrain bond lengths (i.e. hydrogen). Using AMBER, the SHAKE algorithm reduces and averages the highest frequency vibrations, which confines the degrees of freedom. SHAKE retains the simplicity of Cartesian coordinates, while integrating the effects of the constrained geometry of the molecule.[83] Also, SHAKE can be employed for flexible molecules with internal constraints.[83]

2.1.3 Interatomic Potentials and Force Field

Molecular dynamics is used to define the interatomic potential, defined as the interaction of a pair of atoms or the potential energy of a system with given positions in condensed space of particles in a system. The potential function describes the dependence of the potential energy of a system on the coordinates of the atom (Figure 2.1). Each potential must display a repulsive and attractive component if binding is to occur. This series of expansion depends on the positions and the forces acting on each atom to describe the potential energy expressed below (equation 2.4):

$$F_i = -\nabla r_i V\ (r_i, r_2, \ldots\ r_N) \qquad (2.4)$$

Where:

$V\ (r_i, r_2, \ldots\ r_N)$ describes the potential function, r_N denotes the potential energy, (r) is the position and (N) is the number of particles.

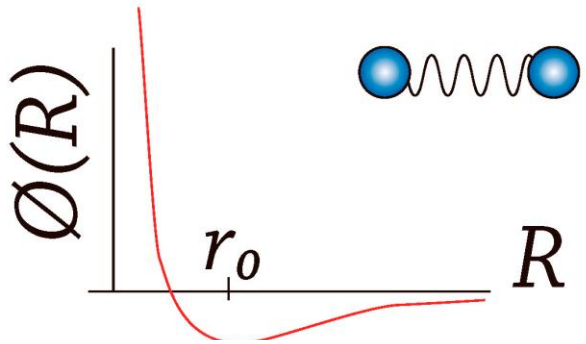

Figure 13 2.1

Spring-8 Information Vol. 14 No. 2 May 2009

Figure 2.1 – Potential energy function

Molecular modeling force fields used in molecular systems are used to interpret intra- and inter-molecular interactions by reproducing and predicting structural properties. A force field is based on an empirical potential, defined as a set of parameters and equations for usage in molecular mechanical simulations. There are several popular force fields: OPLS-AA, (Optimized Liquid System All Atoms), CHARMM (Chemistry at Harvard Molecular Mechanics), and AMBER (Assisted Model Building with Energy Refinement). The force field represents potential energy of the system with related parameters that describe the total energy of the system computed from bonded (i.e. bond stretching, angle bending, and torsions) and non-bonded interactions (electrostatics and van der Waals) (equation 2.5):

$$E_{total} = E_{bond} + E_{angle} + E_{dihedral} + E_{non-bond} \quad (2.5)$$

The AMBER force field defines structures and non-bonded energies for molecular systems (equation 2.6):

$$V(r^n) = \Sigma_{bonds} K_r (r - r_{eq})^2 + \Sigma_{angles} K_\Theta (\theta - \theta_{eq})^2 +$$

$$\Sigma_{dihedrals} \frac{V_n}{2} [1 + \cos(n\varphi - \gamma] + \Sigma_{i<j} \left[\frac{A_{ij}}{R_{ij}^{12}} + \frac{B_{ij}}{R_{ij}^{6}} + \frac{q_i q_j}{\varepsilon_r R_{ij}}\right] \quad (2.6)$$

Where:

r_{eq} and θ_{eq} are the structural equilibration parameters, K_r, K_θ, V_n are force constants, while *A*, *B*, and *q* represent the non-bonded potentials.[83]

The first three terms in the above equation represent the bonded terms including; bond stretching between two atoms, angle bending of covalently bound atoms, and the torsional energetics. A harmonic oscillator is displayed in the equation for the first two terms whereas the third term utilizes a Fourier series expansion. In the third term, *n* is the multiplicity (the number of possible orientations of spin angular momenta), φ is the dihedral angle (created by two intersecting planes), and γ is the phase angle (the number of suitable units of angular measurements between two points). The non-bonded interactions can be described by a combination of Lennard-Jones and Coulomb's law. The Lennard-Jones 12-6 ($r^{-12}$is repulsive; r^{-6} is attractive) potential models the Van der Waals interaction, which is the intermolecular attraction of atoms in a system. The electrostatic potential represents the Coulomb potential.[84] AMBER accounts for the non-bonded interactions by using the effective pair potential.[85]

2.1.4 Long-range Forces

Long-range forces are important when calculating specific properties (e.g. dielectric constant), these interactions are often greater in range than the half box length. Long-range forces can be divided in to short-range contributions (real space) and long-range contributions (Fourier transform). Focusing on the Ewald summation method specifically, which is a cell multiple method used to compute long-range interactions in periodic (or pseudo periodic). Developed in 1912,[78] the Ewald summations were used to calculate the energetics of ionic crystals. "In this method, each particle interacts with all of their images in an infinite array of periodic cells".[78] Each

box position consists of a cube of side *L* and contains *N* charges for simplicity. Each image box is related to a central box via the Coulomb potential by a vector ($\pm iL, \pm jL, \pm kL$), where *i, j, k* are positive integers. Utilizing a neutral periodic system of charge point ions; the Ewald summation is applied as each ion is neutralized describing (at long range) and the combined assembly of point ions and Gaussian charges become the real space, converted to (short range), treated by this method. For a box positioned at a cubic lattice point **n** (= $(n_x L, n_y L, n_z L)$, where $n_x n_y n_z$ are integers (equation 2.7) can be applied using electrostatic potentials:

$$V = \frac{1}{2} \sum'_{|n|} \sum_{i=1}^{N} \sum_{j=1}^{N} \frac{q_i q_j}{4\pi\varepsilon_0 |r_{ij}+n|} \qquad (2.7)$$

Where:

$q_i \; and \; q_j$ are nuclear charges, and |**n**| is all image boxes positioned at a cubic lattice point**.**

The long-range integration can be treated by a cut-off method in the potential energy function. Potential cut-off simply sets the potential to zero over some distance *r*. As it is not natural for the potential energy to instantly switch to zero, a switching function is applied to soften the potential truncation. The Ewald summation can be implemented on a grid using the Particle Mesh Ewald (PME) summation, where the charges on the nuclei are mapped on to grid points and the electrostatic potential is solved by the cut-off method. Outside the cut-off, the potential energy is not set to zero, whereas the inside is solved by the Poisson equation. The PME summation converges quickly, compared to the Ewald summation, which converges extremely slower. This method is essential for highly charged systems, such as nucleic acids, as they contain polyanionic backbones.

2.1.5 Periodic Boundary Conditions

Molecular dynamic simulations are used to predict and study the properties of a system in bulk. To eliminate any surface effects from the simulation, periodic boundary conditions (PBCs) can be applied for all system sizes. For example, when a small drop of water forms a spherical shape the surface forces overwhelm the structure of the system. PBCs approximate a large infinite system by using a unit cell. This boundary condition enables simulations to use a relatively small number of particles *N*, while allowing particles to experience forces in a bulk fluid.[86] During a simulation a molecule moves in the same orientation inside a central box and in its periodic image in every other box (Figure 2.2). If a molecule exits a box, a new image with the same velocity enters from the opposite end to keep the number of particles in each unit cell constant.[86] The central box does not contain any walls at the boundary of the box and the system has no surface, but rather serves as a coordinate system for measuring locations of particles.

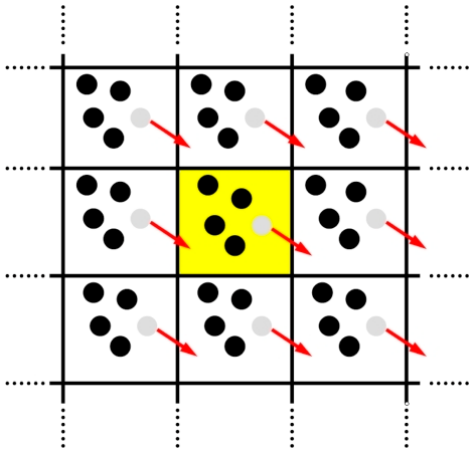

Figure 14 2.2

Int. J. Mol. Sci. 2009, 10(12), 5135-5216

Figure 2.2 – Two-dimensional Periodic Boundary Conditions

PBCs are not capable of evaluating interactions beyond the size of a periodic cell. Moreover, additional algorithms, such as Ewald sums, must be applied to consider long-range electrostatics and Lennard Jones interactions.

2.1.6 Accelerated Molecular Dynamics (aMD)

The MD simulation time scale is normally restricted to run in the nanosecond to microsecond range due primarily to computational requirements in time and disk space. As a consequence of this reduced time scale, simulations have the potential to get lodged in some local minima in the potential energy surface for extended periods, resulting in improper sampling of the system. Replica exchange[86] is one method used to overcome the multiple-minima problem associated with MD by exchanging non-interacting replicas of the system over a range of temperatures. Combining MD simulations with replica-exchange allows for optimal conformational sampling and free energy calculations of protein-ligand binding.[87]

An alternative procedure to enhance sampling is accelerated molecular dynamics (aMD). aMD was implemented in AMBER by McCammon and is described as an efficient simulation technique for biomolecules[88]. aMD is expressed as the threshold boost energy to display a raise in valleys and a lowering of barriers. Considering the statistical concept (primarily transition state theory), aMD allows users to follow the system from state-to-state, achieving time scales that conventional molecular dynamics cannot. This reduction of the energy barrier induces the acceleration of molecular system time scale. aMD only requires the evolution of a single copy, without former knowledge of the location of the potential energy wells.[89]

During a simulation, when the system's potential energy falls under the threshold energy, *E* (Figure 2.3), a boost potential ΔVr is added, such that the modified potential $V^*(r)$ and original potential $V(r)$ correspond via $V^*(\mathbf{r}) = V(\mathbf{r}) + \Delta V(\mathbf{r})$.

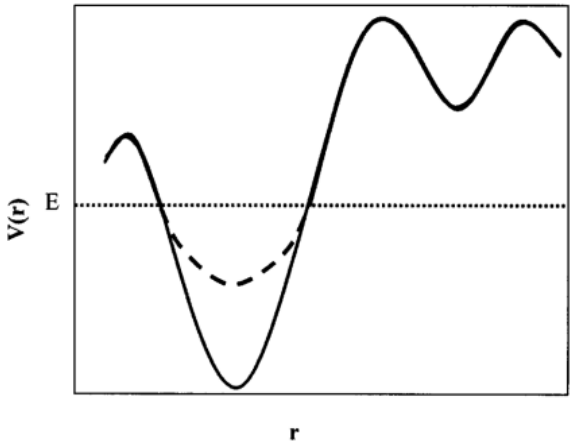

Figure 15 2.3

Hamelberg et al. J. Chem. Phys., 2004, 120(24), 11919

Figure 2.3 – Illustration of the normal and biased potential; displaying the threshold boost energy, *E*.

The threshold energy controls the section of the potential surface that is affected by the boost potential function. α describes the acceleration factor, which defines the orientation of the modified potential, which in turn cannot equal zero. The modified potential is displayed by smaller barriers, separated by neighboring energy basins (Figure 2.4).

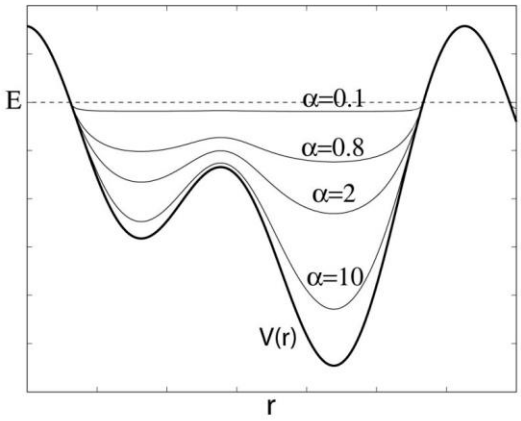

Figure 16 2.4

Hamelberg et al. J. Chem. Phys., 2004, 120(24), 11919

Figure 2.4 – **aMD method**. Normal potential (thick line); threshold energy E (dotted line); modified potential (thin lines).

AMBER supports the acceleration of every step, as well as the entire potential or the potential term arising from torsional contributions.[89] In addition to enhanced conformational sampling, the original free energy can be recovered by a reweighting procedure of the aMD simulation by the Boltzmann factor of the boost potential[87], however, accurate reweighting of aMD simulations are still being carried out.[90]

2.1.7 The AMBER simulations Package

AMBER can be defined as a collection of names for a suite of programs, which enables the usage of molecular dynamics for biomolecules. The AMBER force field provides a balance description of protein-ligand and protein-protein interactions in biological systems. The concept of AMBER dates back to 1978, where it was developed by Paul Weiner and Peter Kollman.[91] Weiner and Kollman's goal was to create a user-friendly general molecular mechanics program,

capable of performing energy component analysis, computer graphics, energy calculations as well as handling small molecules such as polymers.[91] The term *amber* refers to both an empirical force field and a code that can be used separately in computer packages and other force fields.[92] The AMBER package is very popular worldwide; with widest used AMBER force fields include ff94, ff99SB, ff03, ff14SB and GAFF for organic molecules, amino and nucleic acid parameters.[89]

The principal flow of Amber can be divided into three main components for an ideal system: preparation, production, and analysis (Figure 2.5).

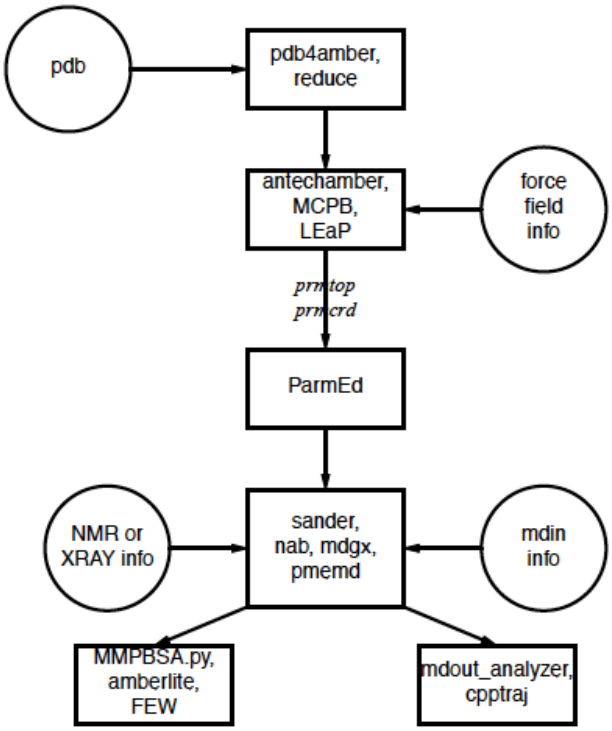

Figure 17 2.5

Case, D.A.; et. a. l. San Francisco, CA: University of California 2012

Figure 2.5 – The principal flow of the AMBER program

To prepare the system, several coding practices are applied including *LEaP* and *antechamber*. *LEaP* is a primary program written in C[92] to create or modify a system. Available as command-line programs *tleap* and *xleap*, it prepares the force field parameters required for each system.

Antechamber employs the general AMBER force field (GAFF) to prepare residues, as their parameters do not exist in the standard library. Secondly, the system undergoes simulation, using three MD simulation engines: *sander, pmemd, and pmemd.cuda*. *Sander* is the basic energy minimizer and molecular dynamics program, and an essential platform for both computation and development in AMBER.[92] *Pmemd* (Particle Mesh Ewald Molecular Dynamics) is a version of *sander* used for optimized speed and parallel scaling. *Pmemd.cuda* is based on *pmemd*, extended to specific CUDA (Compute Unified Device Architecture) kernels[92] for the GPU (graphics processing unit) acceleration. Both *pmemd* and *pmemd.cuda* are used to maximize performance of systems during production. Lastly, analysis of the system is conducted using *ptraj* or *mm-pbsa*. *Ptraj* is the main trajectory analysis used for superpositions, clustering of trajectories, calculation of bond/angle/dihedral values, hydrogen bond analysis and distance calculations. *Mm-pbsa* collects statistics and formats the output in a tabular form[92] of snapshots from a molecular dynamic simulation. This analysis is based on continuum solvation models.

2.2 Molecular Docking

Molecular docking is used to predict the preferred orientation of two molecules when superimposed to form the most stable complex. Molecular docking has been used widely since the 1980's and is an essential method in pharmaceutical research.[93] Most modern day drugs arise through discovery programs that identify bimolecular targets, which incorporate computer modeling of ligand-protein interactions[94]. This docking method characterizes the behavior of small molecules in a binding site of target proteins as well as validates the structure of the protein. The docking process is achieved by two basic steps: (1) prediction of ligand conformation and positions within the binding site and (2) the assessment of the binding affinity.[93] There are several

different molecular docking methods, but the three of interest here are: AutoDock[95], AutoDock Vina[96] and Surflex-Dock.[97]

2.2.1 Protein-Ligand Binding Affinities

In today's reality, computers and computational methods permeate all facets of drug discovery[98]. Modern drug discovery programs identify bimolecular targets, increasingly incorporating computer modeling of protein-ligand interactions. Advanced methods for determining protein-ligand binding currently include four classes of physical computer methods that can be grouped by fastest to slowest and least physical too most physical. The classes are as follows: [99]

1. Molecular Docking Methods: AutoDock,[95] Surflex,[97] and GLIDE[100]. These methods fabricate the most approximations, however, are considerably fast and desirable for screening large libraries.
2. Approximate free energy methods. Solvent and protein motions are considered with fewer approximations.
3. Relative binding free energy. This method considers the full solvent and protein motions, but require prior knowledge of the how the ligand binds to the protein complex.
4. Absolute binding free energy. This method is the most expensive computationally as the initial structure is the unbound protein and ligand to predict properties of interest.

The binding free energy included above has two main components, entropy S and enthalpy H, respectively. The binding free energy is related to the binding affinity (dissociation constant – $1/K_a$) represented in (equation 2.8) below:

$$\Delta G^\circ = -RTIn(C^\circ \frac{1}{K_a}) \tag{2.8}$$

Where each variable is expressed as:

R – gas constant

T – absolute temperature

C° - standard concentration (1M)

Docking techniques attempt to identify all the possible conformations of a known ligand when bound to a validated structure of the protein complex. This method positions the initial fragment based on shape complementarity. Docking treats the protein as a completely rigid structure, allowing for slight movement of active site residues in the receptor-binding site, while the ligand samples different conformations. Also, docking aims to correctly estimate the binding affinity of the protein-ligand interaction. Docking approaches are appealing for filtering out compounds and identifying native-like poses.[99] Docking can be achieved by two steps:[93] 1) examining multiple ligand orientations and identifying different potential binding sites and 2) ranking the ligand-protein conformations based on its free energy of binding via a scoring function, either force-field, empirical, or knowledge-based. The scoring function ranks the ligand orientations by evaluating the binding stiffness of each of the possible complexes.[101] In an ideal situation, the sampling method should reproduce the experimental binding mode, while the scoring function ranks its most highly.[93] This function can be simplified with a simple solvent model to correctly predict differences in effective electrostatic interactions in the receptor. Upon ligand binding, these approximations affect the ligand-protein prediction, as the loss of interactions between ligand polar groups and solvent are not captured.[102] A small molecule that binds to a receptor becomes less mobile, which will lead to a penalty in binding affinity, thus resulting in loss of configurational entropy.[103]

A scoring function can be explained by AutoDock's semi-empirical free energy force field.[104] This approach estimates the free binding energy by using six pair-wise evaluations (V) to

approximate the protein-ligand interaction and estimate the conformational entropy lost upon binding (ΔS_{conf}) (equation 2.9).

$$\Delta \square = [V_{bound} - V_{unbound}]^{L-L} + [V_{bound} - V_{unbound}]^{P-P} + [(V_{bound} - V_{unbound})]^{P-L} + \Delta S_{conf} \quad (2.9)$$

Where L and P refer to the "ligand" and "protein" of the complex.

This approach is used to evaluate the entropic contribution (all torsional degrees of freedom) of changes in solvation and conformational stability. The enthalpic contributions of each pair-wise energetic term includes analyses such as dispersion/repulsion (first term), H-bonding (second term), electrostatics (third term) and desolvation potential (fourth term) (equation 3.0).[104]

$$V = W_{vdw} \sum_{i,j} \left[\frac{A_{ij}}{r_{ij}^{12}} - \frac{B_{ij}}{r_{ij}^{6}} \right] + W_{hbond} \sum_{i,j} E \left(t \left[\frac{C_{ij}}{r_{ij}^{12}} - \frac{D_{ij}}{r_{ij}^{10}} \right] + W_{elec} \sum_{i,j} \frac{q_i q_j}{\varepsilon(r_{ij}) r_{ij}} W_{sol} \sum_{i,j} (S_i V_j + S_j V_i) e^{\left(\frac{-r_{ij}^2}{2\sigma^2}\right)} \right) \quad (3.0)$$

Where:

W – weighing constants

V – volume of atoms

S – solvation parameter

Σ – based on the distance

A and B – parameters taken from AMBER used for the dispersion/repulsion terms

C and D – assigned parameters to give a potential well depth of 5 kcal/mol at 1.9Å for bonds O-H and N-H and 1 kcal/mol at 2.5Å for bond S-H.

2.2.2 Synopsis of Molecular Docking Tools

AutoDock: This tool predicts the interactions of ligands with biomacromolecular targets. This free software is used to search for the best conformers of a biological system. AutoDock is known for its rapid grid-based energy evaluation as well as its efficient search for torsional freedom of a system. Conformational searching of AutoDock uses the Lamarckian Genetic Algorithm (LGA) and empirical free energy scoring function, which provides reproducible docking results for ligand-protein interactions.[95] AutoDock calculations are performed using four steps: (1) coordinated file preparation using AutoDockTools, for the parameterization of the protein-ligand interaction, (2) using AutoGrid, the atomic affinity potential is calculated for each atom type in the ligand docked, (3) docking of ligands using AutoDock and (4) analysis of results using AutoDockTools comprises various methods including visualizing conformations.

AutoDock Vina: AutoDock Vina is an open-source program utilizing the concepts in AutoDock. Oleg Trott implemented Vina for significant improvement of the average accuracy of the binding mode predictions compared to that of AutoDock.[105] AutoDock Vina utilizes a simpler scoring function, which allows a faster search method, thus providing more reproducible results. Vina automatically calculates the grid maps and clusters the results in a lucid manner.[105]

Surflex-Dock: Surflex-Dock is a ligand-receptor docking and virtual screening program implemented in the program Sybyl-X. This method allows one to visualize and explore the relationships between various properties of drug design and molecular discovery projects. Surflex-Dock offers users speed, accuracy, customization in scoring functions, considers protein flexibility, and detects multiple binding sites.[97]

2.3 Combined Quantum Mechanical/Molecular Mechanical Approach

Theoretical approach of combined quantum mechanics/molecular mechanics (QM/MM) method has become a popular technique for modeling reactions in bimolecular systems. This method is also a valuable tool for investigation of inorganic/organometallic and solid-state systems of examining systems in explicit solvent[98]. This method allows for the accurate modeling of the enzyme active site and proper basis of the protein environment.[106] The combined QM/MM approach was carried out to predict free energies of specific methyl transfer processes catalyzed[106] by the H293S-PRMT1 mutant, which is discussed in further detail in chapter 3.

Quantum mechanical (QM) methods describe the chemical reactions and other electronic processes such as electronic excitation. Typically, QM methods are usually restricted to a few hundred atoms, which in-turn creates problems when considering the size and conformational complexity of biomolecules. Simulating the majority of the protein is attained by using a force field based method, molecular mechanics (MM). In the QM/MM approach, the QM region treats substrates, and cofactors, in the catalytic site, whereas the MM region is composed of the surroundings, in particular, the protein and solvent of a system.[107] From here, reaction paths and free energy barriers will be determined. The QM/MM method uses the AMBER force-field equation (equation 3.1) characterized by a Hamiltonian, operating on the system's wave function.

Where:

ψ is dependent of the position of the QM and MM nuclei to further yield the system's energy E_{eff}. E_{MM} is calculated from the MM atom implemented in *sander*, while the H_{QM} is evaluated using the QM method.[108]

$$E_{eff} = < \psi \left| H_{QM} + H_{\frac{QM}{MM}} \right| \psi > + E_{MM} \qquad (3.1)$$

More recently, the QM/MM algorithm conserves energy for long MD simulations in AMBER. The fastest semi-empirical implementation available using this approach is provided by extensive optimization.[109] Explicit solvent long-range QM/MM electrostatic interactions are accounted for using a QM/MM compatible version of the PME approach,[110] while implicit solvents are considered by a QM/MM version of the regular AMBER GB model.[110] In the current version of *sander*, users can employ semi-empirical potentials for the QM region that include: MNDO (Modified Neglect of Diatomic Overlap), AM1 (Austin Model 1) or PME (Particle Mesh Ewald) Hamiltonian. Common semi-empirical methods are extensively used in QM/MM applications, as they provide fast and reliable QM calculations for energies and molecular properties.[92] In order to keep the QM and MM atoms from overlapping, interactions between the QM and MM regions include electrostatics and Lennard-Jones terms, arranged to imitate exchange-repulsion.

Thermodynamic integration (TI) is one of the familiar methods used to calculate free energy differences from MD simulations. TI is a conceptually simple method used to understand the interaction between work and free energy from the second law of thermodynamics. This efficient method is achieved by separating the interaction energy between the solute and solvent molecules into the constituent r^{-12}, r^{-6} and Coulomb terms. TI aims to compute the difference in free energy of a system, the reference state and the state of interest. Initially, time integration chooses a path between two points in which free energy is calculated; from here the path is termed the coupling parameter. Thus, the shape of the TI integrand as a function of the coupling parameters is determined by Coulombic terms, which is calculated by separate contributions of each term.[111] The path is reversible, as work measured is equal to the change in free energy.[112] After the path is determined, the TI approach is calculated as follows (equation 3.2):[111]

$$\Delta A = A_1 - A_0 \int_0^1 < \frac{dE(\lambda)}{d\lambda} >_\lambda \, d\lambda \qquad (3.2)$$

Where:

$<\ldots>_{\lambda}$ corresponds to an ensemble average with energy function $E(\lambda, X^{N})$ in the Boltzmann factor.

Chapter 3 – The role of His293 in PRMT13.1 Introduction

Numerous mutation studies have been conducted for PRMT1. Single and double mutations such as M48L, M155A, M48A, M48F, H293Q, H293A, and H293S-M48F, have led to the motivation of the current project. Gui et. al determined that the enzymatic specificity for double-methylation products, ADMA or SDMA, may be related to two highly conserved methionine PRMT1 active site residues.[113] The two methionine residues, M155 and M48, are essential for catalytic activity, product specificity of PRMT1, and are involved in the regulation of ADMA formation.[114] It was hypothesized that the mutation of M48L and M155A may transform a type I PRMT in to a type II PRMT capable of producing SDMA. However, M48A, M48L, and M155A generated exclusively MMA and ADMA.[113] Intriguingly, western-blotting experiments for a type II PRMT mutant, F397M-PRMT5 generated both ADMA and SDMA.[114] When comparing the crystal structures of PRMT1 and PRMT5 active sites, F397 was found in the same location as M48 in PRMT1 (Figure 3.1), suggesting that a larger residue, and not smaller as previously believed, may allow PRMT1 to produce SDMA.

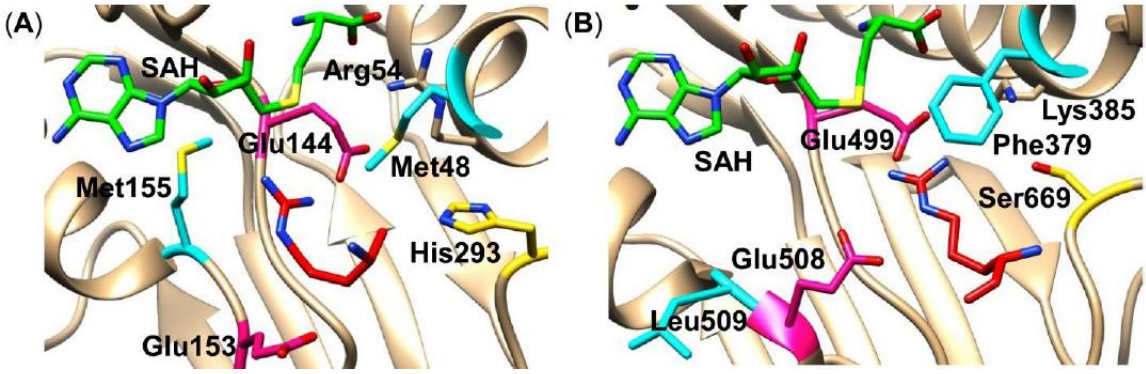

Figure 18 3.1

Figure 3.1 – a. PRMT1 Active Site (PDB ID: 1OR8) bound with S-adenosyl-L-homocysteine (SAH) and arginine substrate. **b.** PRMT5 Active Site (PDB ID 3UA3) bound with S-adenosyl-L-homocysteine (SAH) and arginine substrate.

In 2014, Gui et al. reported PRMT1 produced SDMA for the first time via the mutation M48F.[114] LC/MS confirmed that the WT-PRMT1 strictly produced MMA and ADMA, whereas M48F-PRMT1 generated MMA, ADMA and SDMA. The mutation M48F-PRMT1 enabled that a type I PRMT enzyme to exhibit type II characteristics. Gas-phase QM calculations were used to compute the free energies of activation, $\Delta G^{\neq}$, of MMA, ADMA, and SDMA formation. It was determined that the formation of SDMA is energetically more costly than ADMA, which results in a significant difference in the rate of which methylation occur for asymmetric and symmetric dimethylation.[114]

Molecular Dynamics (MD) calculations were carried out in our lab to determine the product specificity of double mutation H293S-M48F (Figure 3.2). This double variant inspired the current research to study the single mutation H293S, to evaluate if H293S resembles that of the double mutant and/or WT-PRMT1 or does it display other characteristics in determining the formation of MMA, ADMA, and potentially SDMA.

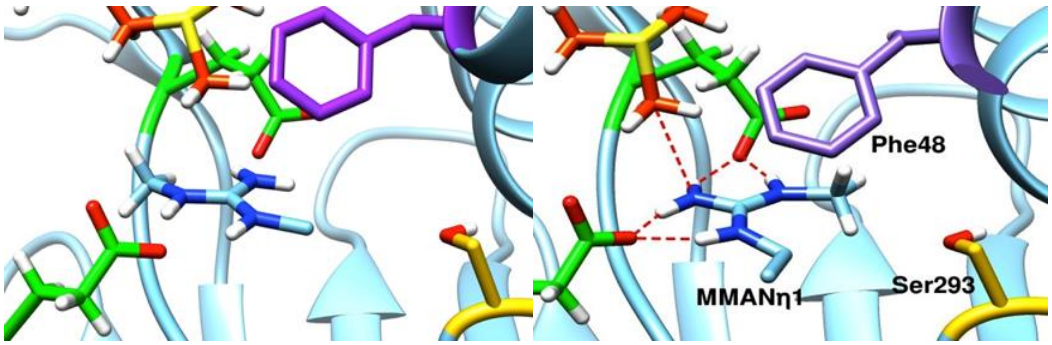

Figure 19 3.2

Figure 3.2 – H293S-M48F double mutation. How MMA binds, the images display an appreciable amount for forming SDMA and ADMA.

This study investigated the intermolecular interactions between substrate and important PRMT1 active site residues, by employing two methods including: accelerated molecular dynamic

(aMD) simulations and mixed quantum mechanical and molecular mechanical (QM/MM) calculations to understand how product specificity is regulated in the PRMT1 protein. The following are the simulated complexes:

1. H293S-Arg: H293S with SAM (S-adenosyl-methionine) and the arginine substrate.
2. H293S-MMA-Nη2: H293S with SAM and the monomethylated arginine substrate methylated on the Nη2 nitrogen.
3. H293S-MMA-Nη1: H293S with SAM and the monomethylated arginine substrate methylated on the Nη1 nitrogen.

QM/MM calculations were employed to compute free energies of activation $\Delta G^{\neq}$ for the formation of MMA, ADMA, and SDMA in PRMT1-H239S. These methods can consider nucleophilicity by exploring changes in charge distributions over the course of the reaction. For example, which nitrogen (Nη2, Nη1) is more nucleophilic and which nitrogen is methylated first?

3.1.1 Overall Motivation

3.1.1.1 PRMT1 Proposed Mechanism

In 2011, a PRMT1 mechanism was proposed by Rust et al. that exhibits a ternary complex: cofactor, protein, and arginine substrate bound to the enzyme.[115] In the proposed mechanism the arginine substrate is not required to be deprotonated to induce a methyl transfer.[115] The peptide binds in proximity with the cofactor S-methyl group and from here, leads to the binding of the substrate. A di-cation intermediate (Figure 3.3) is formed, which undergoes a loss in proton, to produce MMA product.

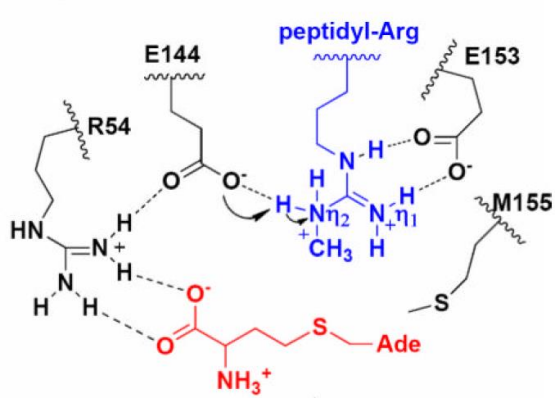

Figure 20 3.3

Biochemistry 2011; 50(16): 3332-3345

Figure 3.3 – Di-cation intermediate from proposed mechanism

The second methylation occurs via the same mechanism to produce the final product ADMA. In the proposed mechanism, residue H293 does not play a major role within the active site. The catalyzed mechanism involves three conserved residues (E144, E155, and R54) due to their support in positioning Nη2 of the substrate arginine for attack on the methyl group of SAM.[115] The mechanism proposed that the order of which the substrate binds to the enzyme and how the product is released from the enzyme is reversible. The overall mechanism was favored due to the transfer of the methyl group to the protonated arginine guanidinium substrate.[115] These specific residues evaluate the PRMT active site to formulate the control of product specificity.

3.1.1.2 Identifying H293 Significance

Research studies show H293 importance in catalysis, however, its predominant role is uncertain. Mutagenesis studies of H293Q and H293A resulted in a loss of activity,[115] having effects on both the kinetic parameters for SAM and the peptide substrate. The H293 residue is believed to form a salt-bridge with residue Asp51 (Figure 3.4), responsible for the formation of a two-helix boundary that separates SAM and peptide binding in the active site.[115]

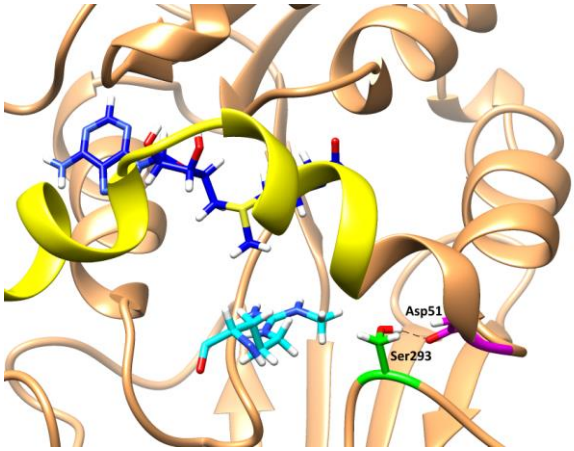

Figure 21 3.4

Figure 3.4 - H293 salt-bridge to conserve residue Asp51

Disruption of the salt-bridge may result in an improper formation of the binding pocket. However, simulations suggest that H293 may have a larger effect on the active site beyond the salt-bridge formation, such as rate enhancement and nucleophilicity.[114]

3.1.1.3 Alternative Mechanism

An alternative mechanism produced from the proposed mechanism by Rust et al., (Figure 3.5) takes in consideration that H293 may play a critical role in rate enhancement, substrate orientation and modulation of the nucleophilicity. In the crystal structure H293 is 6 Å from the substrate, but our previous simulations have shown that re-arrangement within the active site enables hydrogen bonding with the substrate. This H-bond is present in the WT enzyme suggesting its absence in H293S should therefore impact the nucleophilicity of the substrate. A second important residue, E153, in the alternative mechanism may offer a different role. This residue has been hypothesized by Rust et al. to induce electronic redistribution, which activates the Nη1 of the arginine substrate for the Sn2 reaction.[115] E153 charge and position are key components for catalysis. In our mechanism, E153 is proposed to be the general base instead of E144 as suggested by Rust.

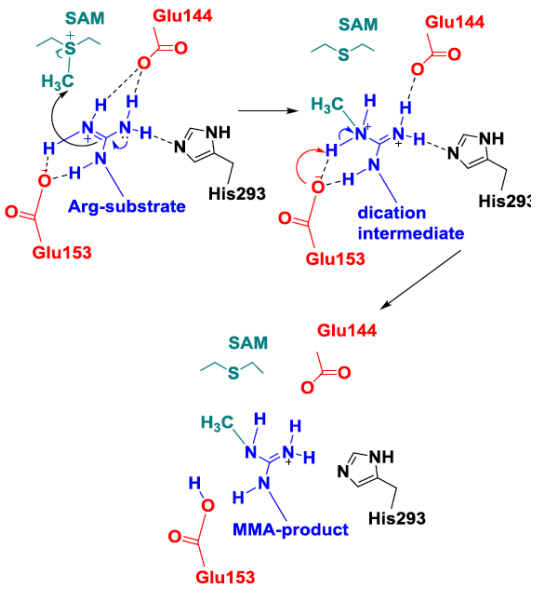

Figure 22 3.5

Biochemistry 2011; 50 (16), 3332-3345

Figure 3.5 – Alternative PRMT1 Mechanism

In Figure 3.5, the loss of the interaction between the substrate and H293 result from the current simulations as E144 abstracts a proton solely after the second methylation occurs at position 1 (Nη1). MMA bound to position 1 (Nη1) does not disrupt interactions between the arginine substrate and active site residues, due to the hydrogen of the methyl group of Nη1 forms a H-bond with E153, not E144. The di-cation intermediate involves three conserved residues (E144, E153, and H293) due to the support of position of arginine substrate to SAM.

3.1.1.4 Cation-π interactions

Cation-π interactions in protein structures are energy-based non-covalent binding interactions common in biological systems.[116] The arginine residue is more likely to be in a cation-π interaction than other residues such as lysine. Referring to former research by Gui et. al, the cation-π interaction between the arginine and phenylalanine in the (H293S-M48F-Arg) complex likely benefits from van der Waals interactions with the aromatic ring[114]. The positively charged guanidino moiety and phenylalanine's aromatic ring results in a much more favorable interaction than hydrogen bonding due to its altered positioning. Computationally, this interaction is deemed more favorable due to the T-shaped geometry of the arginine substrate.[116] In the double mutation Phe48 should perhaps affect the electron redistribution in the arginine substrate, consequently depressing the nucleophilicity. The presence of the stable Phe48 mutant in the polar active site lowers the H-bond percent occupancy when methylated on Nη1, hence the importance of the possible flexibility of the M48 residue. With the serine being present over the histidine, this allows for a decrease in H-bond occupancies across the H293S complexes. Thus, the cation-π interaction is considered more favorable than the H-bond formed between Met-Arg, perhaps explaining why

MMA binding on Nη1 is more unlikely in the H293S-MMANη1 complex compared to H293S-MMANη2.

3.1.2 PRMT1 Dimer

Dimerization of PRMT1 is essential for catalytic activity and can be regulated in a redox-sensitive manner.[117] Investigation of the PRMT1 monomeric active site versus the dimer will provide further insight into substrate recognition, sterics and nucleophilicity. PRMT1 was examined as a dimer with emphasis on two cysteine mutations (C101S, C208S) to identify the redox-sensitive manner of the system. The following systems were simulated using aMD.

1. C101S-C208S-dimer: Double variant of the PRMT1 dimer
2. WT-PRMT1-dimer: includes a protonated cysteine residue (Cys-SH)
3. WT-PRMT1-cys-deprotonated: includes a deprotonated cysteine residue (Cys-S^-)

3.2 Methods

3.2.1 Molecular Dynamics Simulations

The initial PRMT1 structure to simulate was obtained from the Protein Data Bank (PDB) as ID number (1OR8).[106] The original crystal structure is a dimer, but was reduced to a monomeric structure for the present calculations. This resulted in a 333-residue structure for each complex (H293S-Arg, H293S-MMA-Nη2, and H293S-MMA-Nη1). The Amber 12 program was employed in the simulations in conjunction with the parm99 force field[106] and TIP3P[118] waters. The AMBER GAFF force field was used for SAM, while ff99SB force field was used to develop the topology files. Following the protein preparation, hydrogen atoms were added to the cofactor and substrate. Antechamber and AM1-BCC[119] produced charges for each individual complex. The system was

neutralized by sodium counterions. A cubic water box circumvents the solute to a depth of 10 Å on each side of the complex. The AMBER[108] software was used for all MD simulations.

3.2.1.1 Minimization

Minimization is used to remove poor interactions that may lead to unstable molecular dynamics. For each complex, minimization was run in a dual stage, positioning restraints on all heavy atoms and only added hydrogens. First, minimization of water is strictly conducted for 200 steps. The first 50 steps were steepest descent, while the remainder was conjugate gradient. Lastly, all heavy atoms were minimized for 200 steps.

3.2.1.2 Equilibration

For each complex, a three-stage equilibration was conducted. Initial heating of the systems with volume held constant, started at a temperature of 0K and gradually increased to 300K over 50 picoseconds of simulation time. Equilibration steps using NPT with Periodic Boundary Conditions to adjust water density to experimental, was ran for 500 ps of constant temperature and pressure at 1 atmosphere. Particle Mesh Ewald (PME) method was used for all full systems periodic electrostatics. Constant pressure is expressed via Langevin Dynamics[120] while constant temperature used Berendsen[121] coupling algorithm. SHAKE was employed, maintaining all bonds including hydrogen atoms at their stationary state with a non-bonded cutoff of 10 Å.

3.2.1.3 Production

Production using accelerated molecular dynamics (aMD) was carried out at 300K using the NVT ensemble. In this study, MD simulations have been run on PRMT1 H293S mutation (H293S-Arg, H293S-MMA-Nη1, and H293S-MMA-Nη2) for 300 ns using the Verlet integration method with a 1-fs time step.

3.2.1.4 Analysis

After conducting MD simulations, each complex was analyzed using various methods. The atomic properties, backbone torsion angles, distance, their averages, standard deviation/fluctuation, hydrogen bond lengths and angles were specifically examined from the entire complex or from selected trajectories.[122] Root-mean-square-deviation (rmsd), root-mean-square-fluctuation (rmsf), clustering, hydrogen bond occupancy, distances, and angles between key residues, have been reported.

3.2.2 Combined QM/MM approach

After running the MD simulations, QM/MM and potential of mean force (PMF) simulations were applied to compute the activation free energies for the methyl transfer processes catalyzed via the PRMT1 H293S mutant.[108] During the simulation SAM and the target arginine substrate were treated in the QM region while the remaining system was treated by MM.[108] An MD equilibrated snapshot of the WT-enzyme-substrate complex was used as the initial structure for the QM/MM calculations.

Minimization and equilibration of the initial system was performed in an analogous fashion to the previous MD section. To generate accurate PMF and free energies of the three complex systems, aMD simulations were carried out to obtain useful sampling using umbrella sampling. This method generates the free energy profile along a specific reaction coordinate by breaking the reaction coordinate into a series of windows and applying a restraint that acts to force the reaction coordinate to remain in close proximity to the center of the window.[123] When conducting production, the windows must overlap (i.e. window one must sample a portion of window 2, etc.).

In this study, the C-N distance of the mono-methylated and di-methylated arginine substrate (Nη1 and Nη2) was computed from 3.8 to 1.3 Å for Nη1 and 4.4 to 1.4 Å for Nη2. The C is the carbon of SAMs methyl group while the N is the nitrogen of the guanidino group. The number of windows required and the size of the restraint depends solely on the specific complex, hence the difference in the window size of Nη2 to Nη1. Each window will be 0.1 Å apart for a total of thirty-one or twenty-six windows. The force constant of 400 kcal/mol rad^2 was employed. The force constant has to be large enough to ensure we sample the subset of phase space but not too forceful that the windows become narrow and prevents overlapping. Each window was ran for 30 ps, where the first 10 ps were disposed of, as they were simply relaxed. Thus for each window, relaxation using aMD and NPT was ran for 10 ps with a 1 fs time step, while data collection was ran for 20 ps with a 1 fs time step.

3.2.2.1 Analysis

Among multiple methods, analysis of the sampling was conducted using the Weighted Histogram Analysis Method (WHAM) of Alan Grossfeild[124] to generate PMFs. WHAM post-processes the results to remove the biasing of the restraints and recovers the PMF. The WHAM method simplifies considerably the task of recombining the various windows in complex systems.[125] A series of histograms representing sampling of the reaction coordinate values were generated.

3.3 Results and Discussion

3.3.1 Overall Molecular Dynamic Analysis

To determine the association between the structural changes that occur within the active site of PRMT1 bound cofactor and arginine substrate in the disparate methylated states, a thorough analysis from the MD simulations was conducted. The traditional MD analysis techniques root-mean-square deviation (RMSD) and root-mean-square fluctuations (RMSF) of the trajectories were calculated to display the structural stability and conformational changes by measuring the distance of a set of atoms from a specific reference over time of the simulations calculated. Figure 3.6 shows the RMSD of the three systems superimposed. All H293S systems were equilibrated after 300ns with average values of 3.5 Å, confirming good stability.

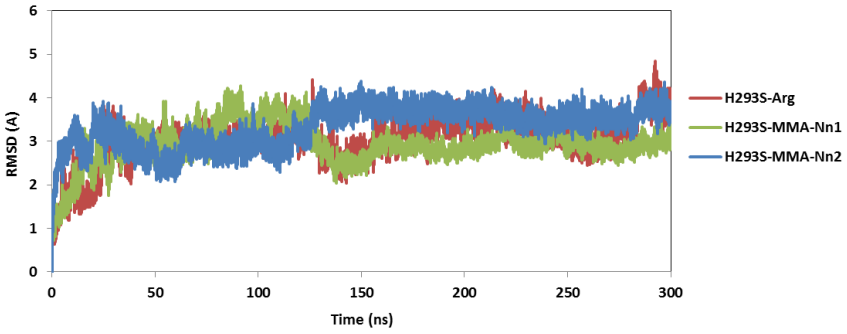

Figure 23 3.6

Figure 3.6 –RMSD of the protein backbone atoms (N, C, Cα) of the H293S complexes superimposed, relative to the first frame. H293S-Arg (red), H293S-MMA-Nη1 (green), and H293S-MMA-Nη2 (blue).

Figure 3.7 illustrates the positional fluctuations of the backbone atoms of the H293S mutation complexes. This encompasses two specific residues, Asp188 and Lys215, comprised of three helices joined by a loop: two α-helices, 188-194, 210-214 and one 3_{10} helix 196-199.When

viewing the residue number of each graph, the highest region 163-187 is the dimerization arm of the PRMT1 monomeric structure. H293S-MMA-Nη1 (green) exhibited the largest peak of approximately 10 Å, compared to the other examined complexes.

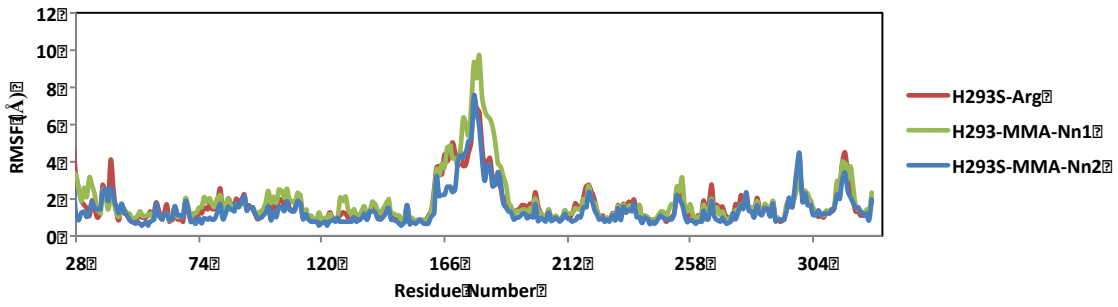

Figure 24 3.7

Figure 3.7 –RMSF of the N, C, Cα atoms relative to the average structure of the H293S complexes superimposed. H293S-Arg (red), H293S-MMA-Nη1 (green), and H293S-MMA-Nη2 (blue).

In addition, the substrates fluctuations possibly suggest that the movement of this region plays a major role on the substrate binding and/or product release, hence the two-step reaction of the substrate. Also, we should consider the hydrophobic interactions between the dimerization arm and SAM binding site, as this connection can lead to a major role within the PRMT1 structure. The calculated fluctuations of the protein are as follows (Fig. 3.5): the SAM binding site residues (28-145) exhibit modest flexibility, which consist of the N-terminus region (26-50) and the core binding site; the entrance of the binding site (43-63) located at the N-terminus fluctuates, as they open and close for substrate binding and product release. This specific region's fluctuations concur with the co-crystal structure of Zhang et al[63] as it lacks a lucid electron density.

3.3.2 Substrate, cofactor, and major residues Intermolecular Interactions

Hydrogen bonding: Hydrogen bonding is a key component in analyzing protein systems. Hydrogen bonding is typically expressed in energy (e.g., 5 to 30 kJ/mol) to define electrostatics, columbic interactions, and Van der Waals radii. The current analysis is focused on the percent occupancy. Out of the 60,000 frames conducted, if an intermolecular interaction occupies 3/5 of the fs-time scale, this implies that the hydrogen bond between two atoms is ~60% occupied.

SAM interactions: Essential interactions between SAM and active site residues involving H-bonding, e.g. Glu129, Arg54 and Thr81, have been examined from the MD simulation trajectories.

Table 3.1 H-bonds formed between SAM and active site residues

Table 1 3.1

		Complexes		
		H293S-Arg	H293S –MMANη1	H293S –MMANη2
H-acceptor	H-donor	% occupancy		
GLU100@OE1+OE2	SAM@H14	76.3	75.0	99.6
GLU100@OE1+OE2	SAM@H15	82.7	57.4	107.7
SAM@OXT+O	THR81@HG1	35.3	62.3	96.3
SAM@O+OXT	ARG54@HH22	27.5	33.8	79.5
SAM@O+OXT	ARG54@HH12	32.1	46.0	80.0
GLU129@OE1	SAM@H16	1.1	0.4	6.4
GLU129@OE2	SAM@H17	2.2	0	9.6

The carboxylate group of residue Glu100 forms a H-bond with the hydroxyl groups of the ribose moiety with SAM, which exhibits a very high percent occupancy from the H293S-MMA-Nη2 simulations compared to complexes, H293S-Arg and H293S-MMANη1 (Table 3.1). Glu100 simply anchors the cofactor in position, as the ribose ring is located towards the middle of SAM (Figure 3.8). Residues Thr81 and Arg54 form H-bonds with SAM's methionine moiety for all systems throughout simulation, whereas SAM's adenosyl region appears to be positioned by non-

electrostatic interactions as Glu129 forms a H-bond for a short amount of time, with an average value ~3% occupancy for each system.

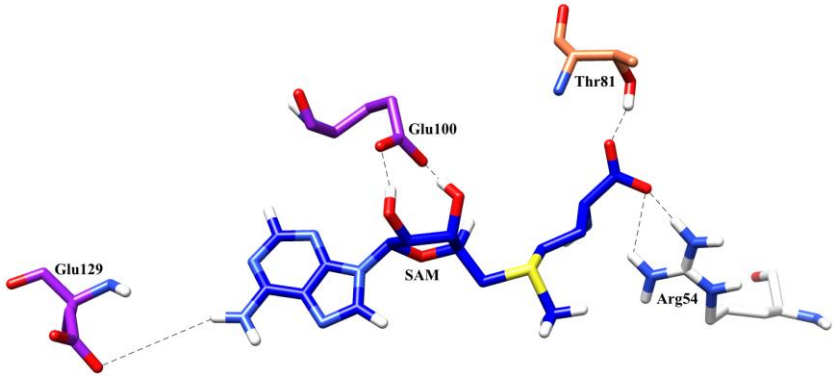

Figure 25 3.8

Figure 3.8 – Key residues that H-bond with SAM

Within this specific region, other important residue interactions are hydrophobic which include Met155, Met48, Tyr39 and Phe36. Moreover, the two methionines M155 and M48 are essential for catalytic activity and the product specificity of PRMT1 (113). M155 is a key residue that helps position the cofactor into place, as the simulations indicate that the side chain of this residue forms an electrostatic interaction with the purine ring.

Substrate interactions: Enzyme-substrate interactions yield high binding affinity complexes through a process termed transition state (TS) stabilization.[126] TS stabilization can be defined as the enzyme binds the transition state better than it binds to the substrate; moreover, the stability of the TS affects the reaction kinetics. The percentage occupancy of H-bonds formed by the substrate and oxygen atoms of Glu144 (96.3% and 46.0%) and Glu153 (85.0% and 59.0%) in H293S-MMANη2 were consistently high. This is in direct contrast to Ser293, which forms no hydrogen bonds with the substrate (Table 3.2). In our previous work, His293 was found to form long lasting hydrogen bonds between His293 and the substrate in the WT PRMT1.

Table 3.2 H-bonds formed between substrate and active site residues

Table 2 3.2

		Complexes		
		H293S-Arg	H293S –MMANη1	H293S –MMANη2
H-acceptor	H-donor	% occupancy		
GLU144@OE1+OE2	ARG@HH12	20.6	N/A	96.3
GLU144@OE1+OE2	ARG@HH22	22.6	5.9	46.0
GLU153@OE1+OE2	ARG@HE	19.7	5.4	85.0
GLU153@OE1+OE2	ARG@HH21	16.1	16.2	59.0
Ser293@NE2	ARG	4.7	0.4	0

The electrostatic interactions shown in (Figure 3.9) are important for the methylation reaction in terms of properly positioning the substrate nucleophilic attack of the methyl group of SAM.

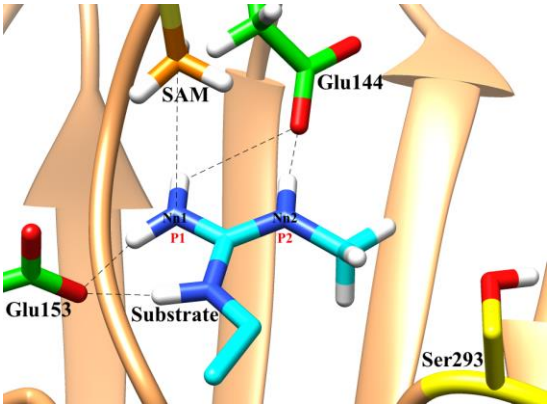

Figure 26 3.9

Figure 3.9 – Key active site residues that H-bond with the arginine substrate. P1 and P2 represent positions 1 (Nη1) and 2 (Nη2) of the substrate.

In the H293S-Arg system, this single mutation substantially reduces the substrate's ability to effectively interact with Glu144 and Glu153. Moreover, this indicates S293 may not play a major role in substrate positioning of the arginine guanidino moiety of PRMT1, therefore this system may be impaired.

The introduction of the methyl group on position 1 (Nη1) reduces the interaction with Glu144, as seen in H293S-MMANη1 (Figure 3.10). This mild interaction combined with the presence of a hydrophobic methyl group in a polar active site appears to give rise to why MMA containing peptides appear to be poor substrates for the enzyme.[127]

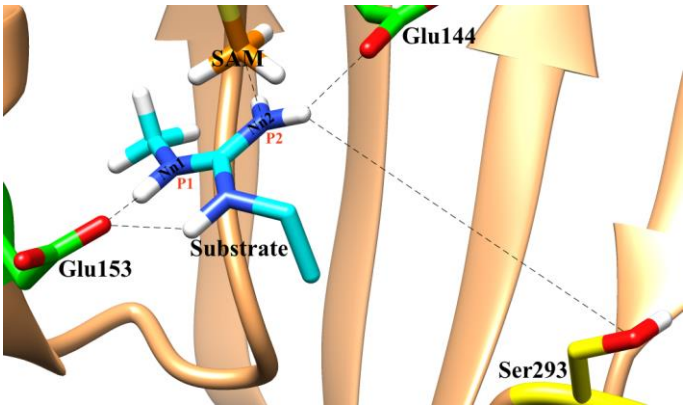

Figure 27 3.10

Figure 3.10 – H293S-MMANη1 interaction with Glu144.

H-bond network with substrate and active site residues: Arg54, Glu144, Tyr39, Glu153, Asp51, and His293: MD simulations confirms the intermolecular interactions between the arginine substrate, SAM, Arg51, and Glu144, are key components in stabilizing the complex for methylation. Arg54 forms crucial H-bonds with Glu144 and SAM, fixing these components in position for the reaction (Tables 3.1 and 3.3).

A similar interaction involving Tyr39 and Glu153 (Figure 3.11 & Table 3.3) display occupancies above 90%, specifically H293S-MMANη2, however H293S-Arg (80.1%) and H293S-MMANη1 (56.3%) exhibit lower values. This could possibly be due to E153 acting as the general base, which in turn reduces the interaction between Tyr39 and Glu153, due to the improper ability of the substrates interaction with E153. The Tyr39 and Glu153 interaction is of importance, as deprotonation and protonation must be attained for ideal activity (Biochemistry 2011, 50, 3332). Analysis finds that residues (Tyr39, Asp51, Arg54) interact with (Glu153, His293, Glu144) to

influence orientation and electronic arrangement to determine adequate nucleophilicity for catalysis.

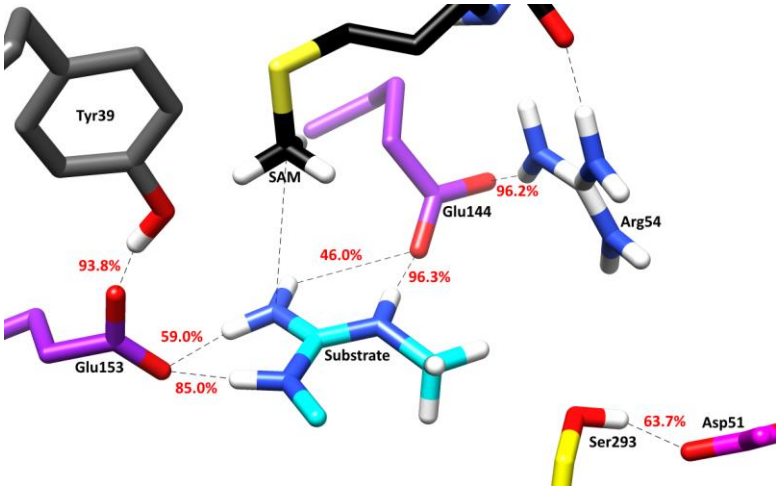

Figure 28 3.11

Figure 3.11 - Percent Occupancy of PRMT1 H293S-MMA-Nη2

Table 3.3 H-bond network in the active site

Table 3 3.3

		Complexes		
		H293S-Arg	**H293S –MMANη1**	**H293S –MMANη2**
H-acceptor	**H-donor**	**%occupancy**		
Glu144@OE1+OE2	**Arg54@HH11**	42.8	88.4	96.2
Glu153@OE1+OE2	**Tyr39@HH**	80.1	56.3	93.8
ASP51@OD1+OD2	**Ser293@HG**	19.5	24.7	63.7

Currently, highlighting the Glu153 residue, the H-acceptor (Glu153@OE1+OE2) to H-donor (ARM@HE) occupies 85.0%, in the H293S-MMA-Nη2 complex (Figure 3.11), while the remaining two complexes H293S-MMA-Nη1 (5.4%) and H293S-Arg (19.7%). This illustrates a strong interaction between the Glu153 residue and arginine substrate in the H293S-MMA-Nη2 complex relative to the remaining systems.

3.3.3 Origin of Product Specificity

Product specificity may be controlled by the initial binding of MMA by active site residues for methylation leading to production of ADMA and/or SDMA. The formation of MMA in the H293S mutation was evaluated by comparing probability distributions over time for each trajectory.

Distributions: Probability distribution is used to calculate confidence intervals for parameters and assigns a probability to each measurable subset of a hypothesized test. Probability distributions were computed to explore the formation of near-attack conformers (NAC) during the simulation that could lead to the formation of either ADMA or SDMA. The (d + 0.5*cos(θ)) displayed in radians can be described by distance and directionality. Sn2 reactions include distance and angles, if an angle is 180° or π using cosine x, it has a -1 value, therefore, reducing the distance to the subject. A linear system has more advantage than the un-favored right angle, as 90° or $\pi/2$ is further away from the subject.

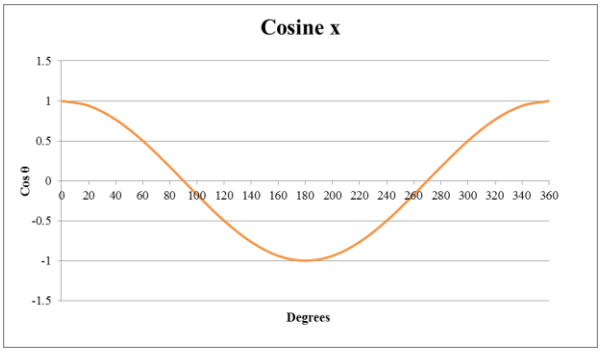

NAC can be defined as a chemical reaction situation, two reacting atoms form at a distance of van der Waals proximity and at an angle resembling the bond to form in the transition state (S-CH_3-N). The free energy for formation of NAC ($\Delta G_N°$) can be determined by use of free energy calculation methods. This free energy can be determined by equation $\Delta G^{\neq} = \Delta G_N° + \Delta G_{TS}$, after $\Delta G_N°$ is acquired, ΔG_{TS} is calculated by subtracting $\Delta G_N°$ from $\Delta G^{\neq}$, which is determined from

the experimental rate constant. NAC of SAM to the guanidino group involves two atoms forming a bond (CH_3 and Nη1 or Nη2) to be within van der Waals contact distance of 3.7 Å. NAC is a reasonable approach, when examining the bond formation of atoms, when it depends on the choice of boundary. For example, the H293S-Arg and H293S-MMANη1 both display broad peaks relative to H293S-MMANη2, which illustrate near attack conformers may not be in the proper position to bind as easily (H293S-Arg and H293S-MMA-Nη1) as if it displayed a narrow peak (H293S-MMA-Nη2) (Figure 3.12). MD simulations cannot determine this hypothesis to be true alone and the combined QM/MM technique has been applied to determine the integrity of the system.

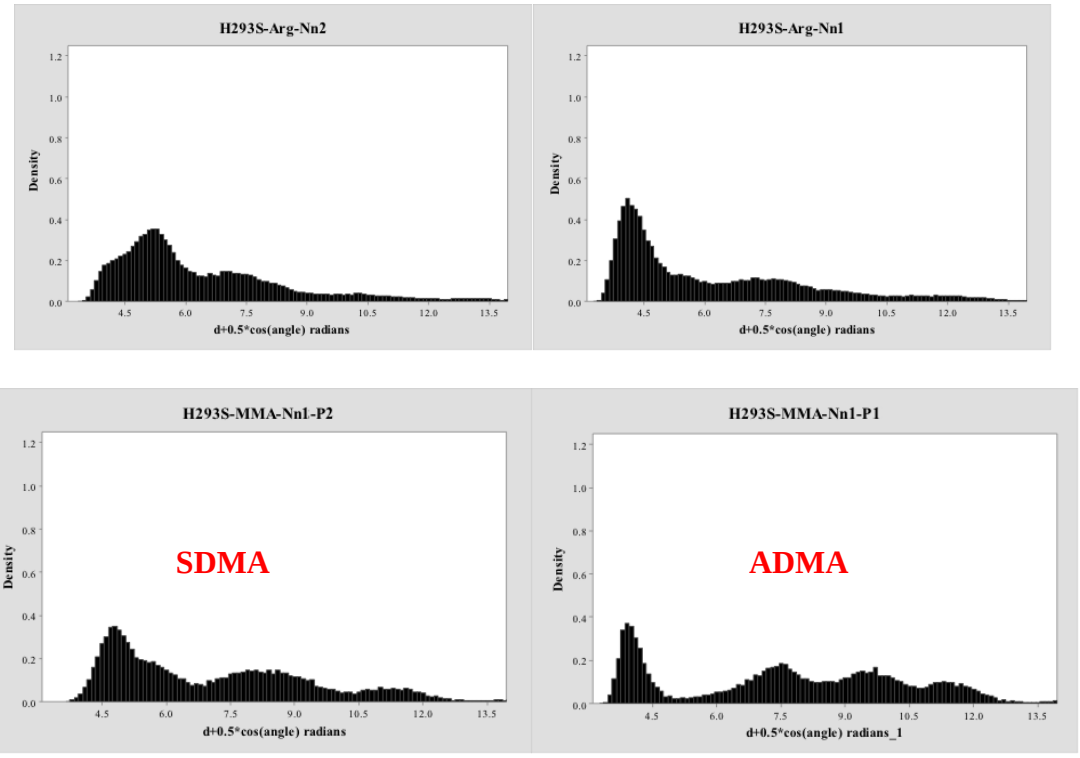

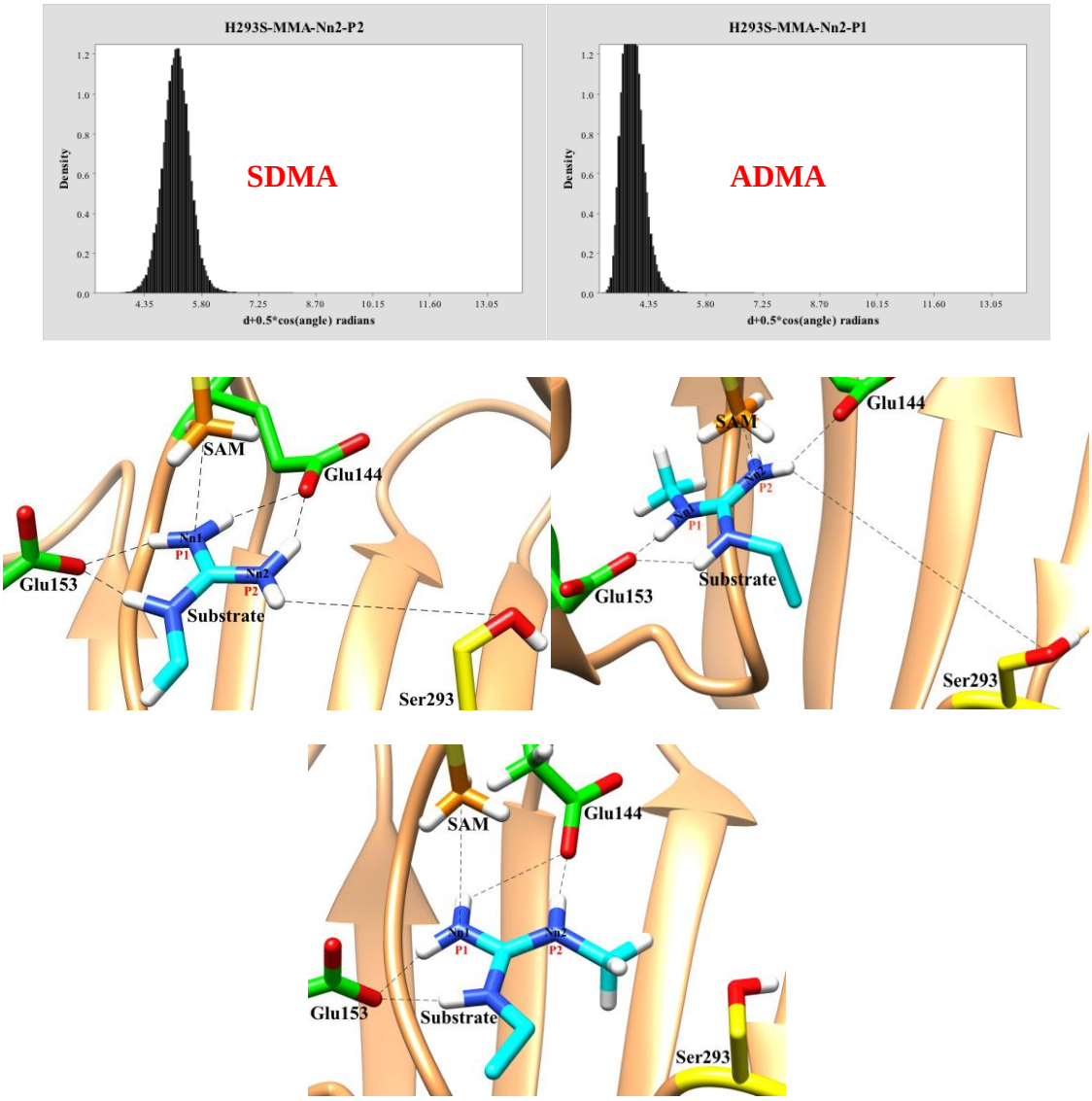

Figure 29 3.12

Figure 3.12 - Probability Distributions of the H293S-Arg, H293S-MMA-Nη1, and H293S-MMA-Nη2 guanidinium arginine substrate.

H293S complexes: The distributions (Figure 3.12) for H293S-Arg and H293S-MMANη1 display a wider spread and shifts to larger values (12-13.5Å). Additionally, the average distances are 4.6 and 5.6 for H293S-Arg Nη1/Nη2 and extremely high averaged distances 17.5 and 17.2 of H293S-MMANn1 complex for Nη1/Nη2 respectively (Figure 3.13).

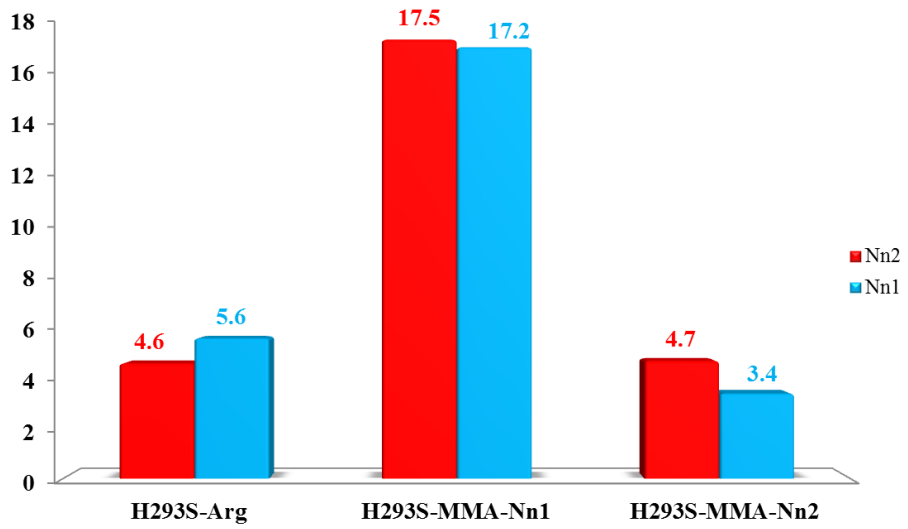

Figure 30 3.13

Figure 3.13 – The average near-attack distance between the arginine substrate nitrogen's (Nη1 and Nη2) and carbon of the methyl group of SAM.

The extremely long distances of H293S-MMANη1 is the results of the substrate extruding out of the active site after 130 ns of simulation time. With H293 being mutated to a smaller residue, the active site presents an ample amount of space for the substrate to move within. Steric bulk of specific residues can disturb the way in which the modified peptide interacts with PRMT1. However, the H293S-MMANη2 complex gives rise to lower values and narrow peaks. This system displays average distance values of 3.4 and 4.7 for Nη1 and Nη2. Methylation at position 2 (Nη2) does not allow the substrate to form an unfavorable bond, therefore, said not to disturb the substrate over time. Through electrostatics, E153 and S293 confine the substrate in position, as displayed in the H293S-MMANη2 complex (Figure 3.14).

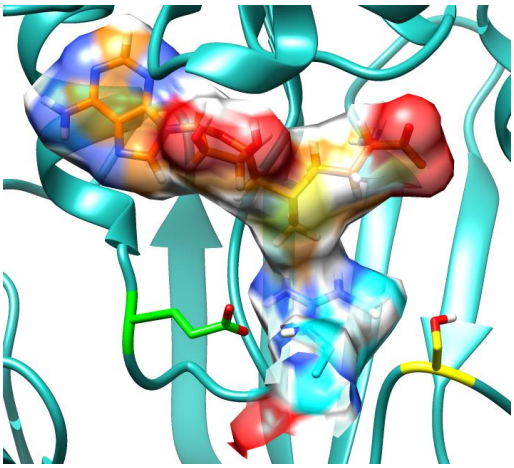

Figure 31 3.14

Figure 3.14 – E153 and S293 help localize the arginine substrate for methylation using H-bonds. The H293S-MMANη2 is a much more stable complex, therefore it becomes feasible that this mutation should permit MMA methylated on Nη2, due to the methyl groups electrostatic interaction with the serine residue, producing more SDMA than ADMA.

3.3.4 Combined QM/MM Analysis

H293 forms an H-bond with substrate arginine, which is suggested to pre-organize local conformations in the active site.[128] Our combined QM/MM calculations have characterized the theoretical understanding of the PRMT1 product specificity. The QM region consists of key active site residues (E153, E144, and mutation H293S), SAM, and the arginine substrate, while the rest of the system was treated by MM. To properly represent the electronic structure of the cofactor, the QM region for SAM was truncated at the Cα of the methionine moiety and at the oxolane ring of the adenosyl moiety. Moreover, the main function of the positively charged sulfur atom of SAM is to attract electron density from the carbon of the methyl group as the substrate Arg abstracts the methyl group. QM/MM calculations tabulated from the WT-enzyme structure yield a typical in-

line S_N2 nucleophilic substitution reaction, required for methylation.[128] The mutation of H293 to serine relieves steric effects, thus allowing enough room to accommodate the methyl group on the arginine substrate, more specifically position 2 (Nη2). In this complex the attack distance C-N displays a longer distance but near attack conformations are formed properly compared to shorter distance of Nη1. These results correspond to the MD simulations, that the product specificity of PRMT1 may be controlled by steric hindrance in the active site. Results from the frequency histogram graphs (Figure 3.15) compare to the MD simulations, which H293S mutant leads to decreased activity for the unmodified arginine (H293S-Arg) position 2 (Nη2) compared to position 1 (Nη1).

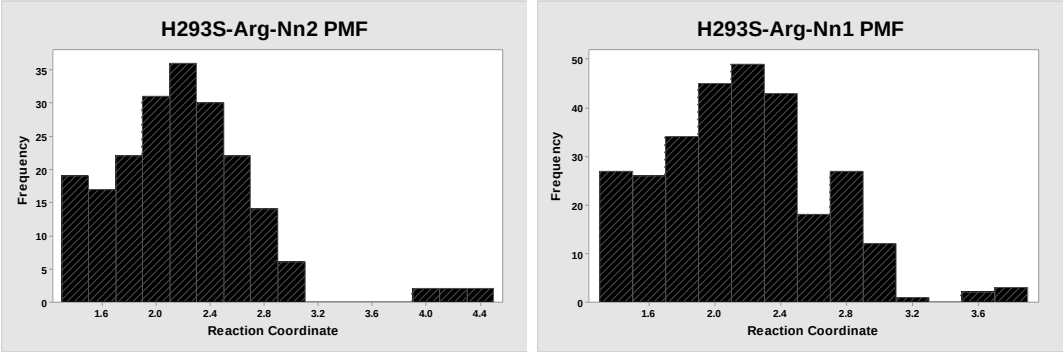

Figure 32 3.15

Figure 3.15 – Frequency Histogram graphs of the H293S-Arg complex Nη1 and Nη2.

The PMF for this system is highlighted in (Figure 3.16), as it displays how the systems energy changes as a function of the distance (4.4 for Nη2) and (3.8 for Nη1) between atoms C-N. As both graphs show similar peaks, the H293S-Arg-Nη2 displays a narrower peak with a decreased energy value (18.5 kcal/mol) compared to (26 kcal/mol) of position 1 (Nη1). The free energy barriers for the first methylation to Nη1 and Nη2 respectively, display that methyl addition to Nη1 is 7.5 kcal/mol higher compared to Nη2, indicating that the first methylation should occur on Nη2.

This suggests that methyl addition to Nη2 is likely more efficient than to Nη1. Thus, the arginine substrate can possibly display similar characteristics for the second methylation.

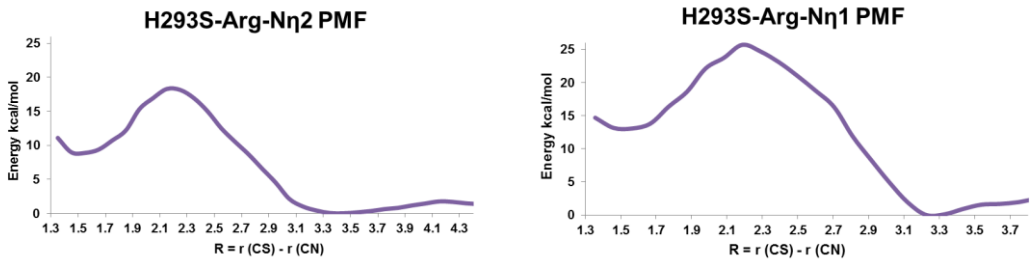

Figure 33 3.16

Figure 3.16 – The Potential Mean Force (PMF) of the H293S-Arg Nη1 and Nη2 complex.

For H293S-Arg, the guanidino nitrogen Nη1 and Nη2 is well aligned with the methyl group of SAM in the reactant complex for the first methylation (Figure 3.17) giving an ideal 180° attack angle. Moreover, this good alignment could make the methyl transfer easier. The guanidino nitrogen of the substrate appears to be stabilized within the active site through interactions with the surrounding residues, including h-bond interactions with E144 and E153. Residue E153 interacts with SAM and guides the methyl group towards Nη1. The active site residues (E144, E153, and S293) lead to the proper alignment of Nη1 and the CH3 of SAM. As the TS stabilization is reflected in reactant complex Nη1 and Nη2, this may not be the final TS, as the system did not fully converge, but this is roughly around the in-line conformation which correlates to the Sn2 reaction.[129]

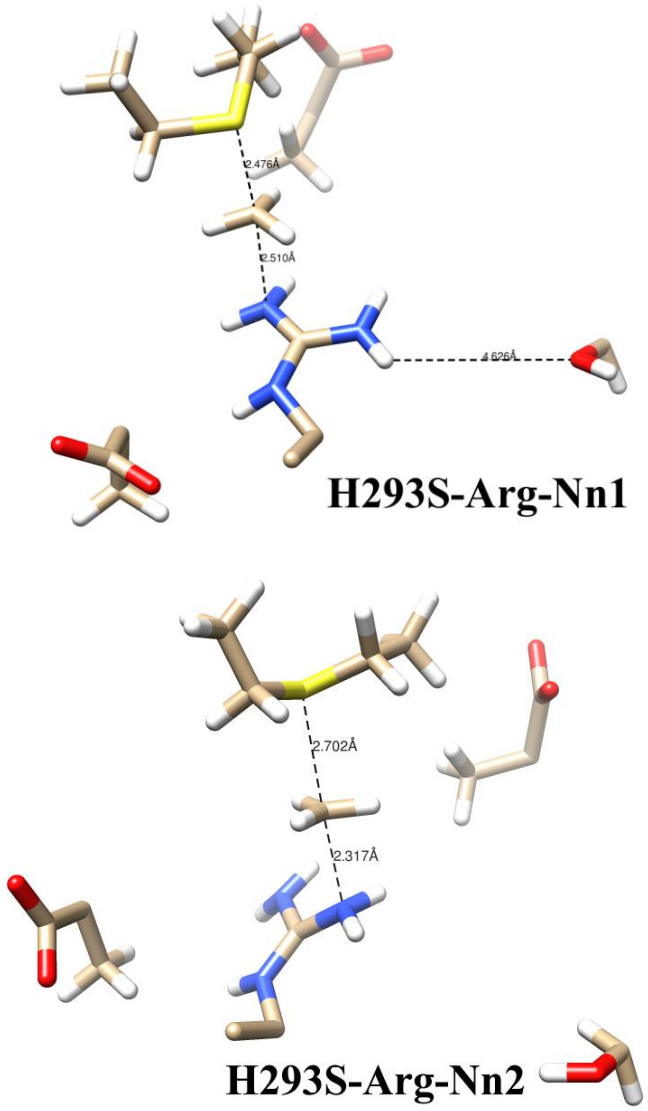

Figure 34 3.17

Figure 3.17 – QM region of H293S-Arg. H293S-Arg-Nη1 and H293S-Arg-Nη2 is well aligned with the methyl group of the arginine substrate.

3.3.5 Dimer Analysis

PRMT1 protein expression is assumed to increase under oxidative stress by further increasing free ADMA production; however, this point has been debated.[117] One or more cysteine residues play a role in stabilization of cofactor binding, but are said to disrupt the effect of substrate binding. Two specific Cys residues (C208 and C101) in the homodimer are currently being

examined, as they may be responsible for diminished PRMT1 methyltransferase activity under oxidative conditions. Cys101 can be found near the SAM binding pocket and interacts with the adenine ring of SAM while Cys208 is located on the dimer interface (Figure 3.18b).

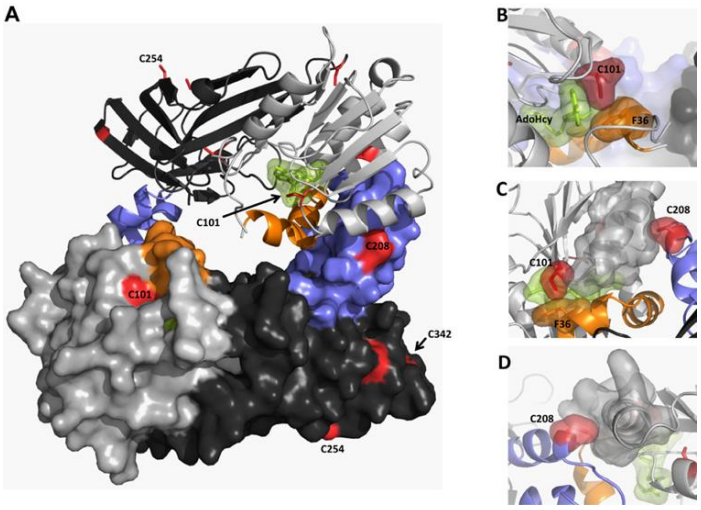

Figure 35 3.18

Protein Sci. 2014, 23, 193

Figure 3.18 - PRMT dimeric structure. (a) The cysteine residues in the homodimer are shown on (left). **(b)** Cys101 shown in the AdoMet binding domain (right) while Cys208 is shown in the dimer interface (right).

When the cysteine residues were mutated to serine, the double variant (C101S/C208S) displayed the same characteristics under oxidized and reduced conditions. Also, the activity is lower in the double variant compared to the WT-enzyme[117]. This suggests residues Cys101 and Cys208 may have an additional effect in PRMT1 activity. Oxidation of the two-cysteine residues destabilizes dimerization resulting in diminished methyltransferase activity while reduction of PRMT1 reverses the effects due to a uniformed, more oligomeric state, moreover, increasing catalytic activity. This hypothesis guides us to investigate mutants C101S-C208S of PRMT1 using MD

simulations to expand on the existing experimental research by using computational methods to examine the active site of the PRMT1 dimer further.

The goal of this study is to examine if oxidative conditions affect catalytic activity in PRMT1, experimentally.[117] Reversible concentration-dependent inhibition of PRMT1 activity by peroxide[117] indicated that two cysteine's are oxidized in the event. Interestly, the peroxide treated PRMT1 methyltransferase activity was substantially inhibited by peroxide in a dose-dependent manner.[117] Oxidized PRMT1 is characterized by impaired enzymatic activity, which in return can be rescued by reduction. The results provide insight in to the hypothesis that PRMT1 enzymatic activity can be governed in a redox-sensitive manner.[117]

To expound on the experimental research, analysis from MD simulations was conducted for each system (C101S-C208S-dimer, WT-PRMT1-dimer, and WT-PRMT1-dimer-cys-deprot); several rotations displayed in each complex, this perhaps indicates reversible activity. The reoccurring rotations during simulations may be due to a rotational shift over the course of the different trajectories behavior, which correlates to the protein's transition between an active and inactive state. Each system was re-analyzed twice to receive proper analysis. Figure 3.19 shows the RMSD of each system superimposed, which were equilibrated after 300 ns with average values of 3.0 Å, confirming good stability.

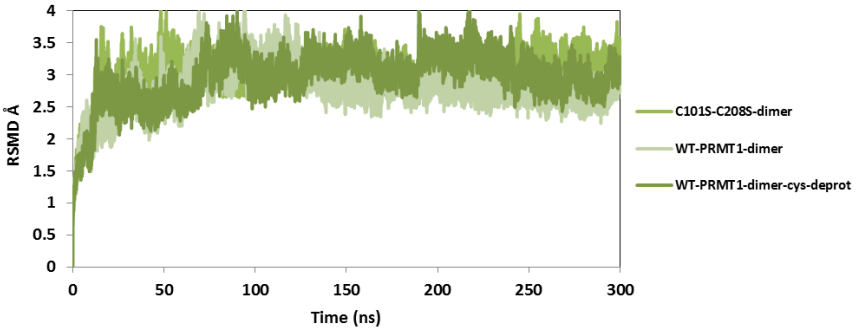

Figure 36 3.19

Figure 3.19 – RMSD of PRMT1dimeric structure superimposed.

The C101S-C208S-dimer and WT-PRMT1-dimer complexes exhibit high peaks approximately 8-10 Å as illustrated in (Figure 3.20); notice the slight decreased activity in the double variant compared to the WT-PRMT1-dimer. Fluctuations in the dimeric structure resemble to the monomeric structure, however the N-terminal displays the highest region in the system compared to the dimerization arm in the monomer structure.

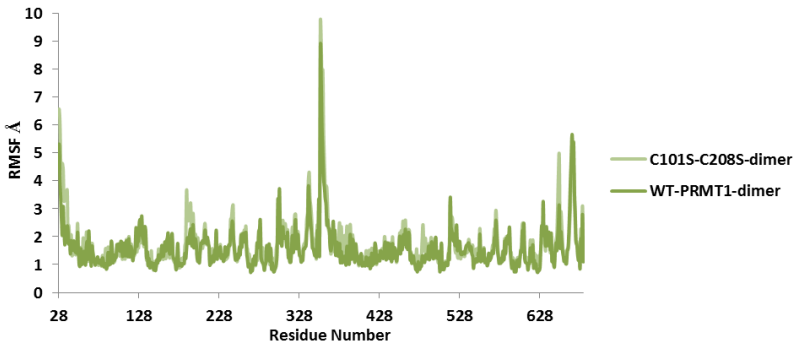

Figure 37 3.20

Figure 3.20 – RMSF of the PRMT1 dimeric structure superimposed.

C101S (Figure 3.21) is less susceptible to oxidation; therefore SAM near this serine residue is not as stable as the cofactor near C208S, which displays more –SOH acid formation. Mutation of C101S results in construct mimicking of the WT-PRMT1-dimer complex methyltransferase activity. The involvement of the two-cysteine residues, stabilize SAM binding. Each dimeric system will further be analyzed to fully grasp the theoretical aspect as compared to the experimental research.

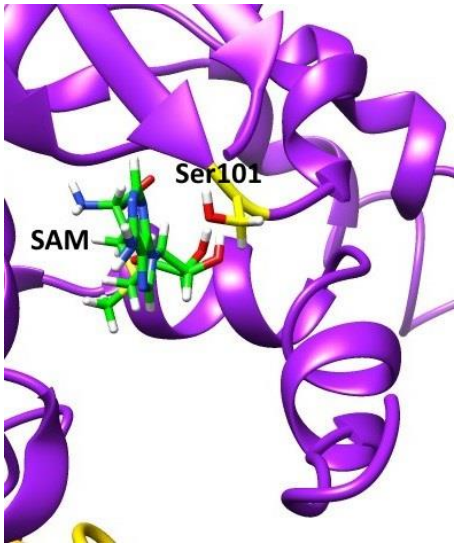

Figure 38 3.21

Figure 3.21 – C101S in the dimer active site.

3.4 Conclusion

From the Molecular Dynamics Simulations

1. After examining the H293S complexes, the serine mutation highlights the importance of the interaction between H293 and the arginine substrate in determining substrate orientation. Also, (Glu144, Glu153 and His293) modulate the substrate's charges activating it for the nucleophilic reaction, as exhibited by the H293S complexes. The H293S-Arg and H293S-MMANη1 complexes were very unstable and not localized well in the active site due to the generous amount of space available for movement.
2. Based on the MD simulations, the presence of the serine residue in H293S- PRMT1 mutation enables the system to form both SDMA and ADMA, as it appears to not disturb the substrate over time, due to the S293-substrate electrostatic/H-bonding interaction at the Nη2 position of the guanidino moiety.

3. The simulations support the hypothesis that the PRMT1 mutant H293S and/or the H293S/M48F systems might form SDMA. The H293S mutation displayed similar characteristics to both the WT-enzyme and the double mutation; however, MMA binding with the methyl group on the Nη2 position seems more likely than methylated on Nη1.

Chapter 4 – Identifying Protein Conformational Changes of Agonist-Induced PPAR-γ

4.1 Introduction

Diabetes mellitus (DM) is a chronic metabolic illness that is increasing in prevalence worldwide. Recently, DM has become a major health burden in the United States. This common disorder in modern society can be characterized by hyperglycemia (high blood glucose levels) resulting in impaired insulin secretion, action, or both. DM is associated with excessive cardiovascular dysfunction and failure of various organs such as eyes, kidneys, and blood vessels.[130] Abnormalities in carbohydrates, fat, and protein metabolism result from an autoimmune destruction of β-cells of the pancreas, a deficient action of insulin. Type 2 DM, the most common form of diabetes, is when the body does not employ insulin properly, termed insulin resistance. Type 2 DM is highly promoted by obesity. This prevalent type can be treated by lifestyle changes including exercise, insulin, oral medication, and diet.

The peroxisome proliferator-activated receptors (PPAR's α, β/δ, and γ) are ligand-regulated transcription factors that play a critical physiological role in lipid sensing and homoeostasis.[4] Synthetic PPAR-γ (thiazolidinedione) ligands have been used in the treatment of diabetes; however they have been limited due to adverse cardiovascular side effects.[34] These agonists bind to PPAR-γ causing the dismissal of co-repressors NCOR1/SMRT and the recruitment of co-activator PGC-1α. This promotes histone acetylation and further generates DNA-dependent events such as transcription, replication, and repair.

In a reported combined computational/experimental study, 23 PPARγ/δ agonists were designed, synthesized and evaluated.[34] After detailed analysis, docking simulations predicted compound **9** (Figure 4.1) as the most promising compound with high binding affinity for both PPAR-γ and PPAR-δ. Consequently, **9** was experimentally determined to inhibit gamma and

activate delta, and as a result did not exhibit the adverse side effects normally affiliated with full PPAR-γ agonists. Different endogenous ligands induce distinct structural changes to the protein that further dictate which genes to activate. For instance, compound **9** elevates expression of genes associated with fatty acid oxidation and insulin sensitivity.[34]

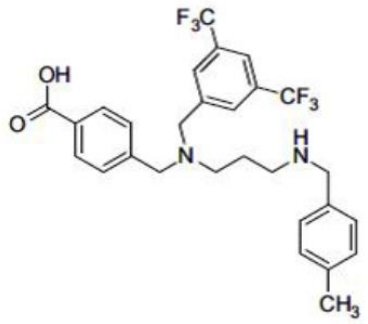

Compound 9

Figure 39 4.1

Bioorg. Med. Chem. Lett. 2013, 23(3), 873-9

Figure 4.1 – Compound **9** Structure

Our current effort was to characterize the major conformational changes induced by compound **9** upon PPAR-γ and PGC-1α. MD simulations of PPAR/PGC-1α/agonist complexes have been performed to explain the differences between **9**, rosiglitazone, and other selective PPAR modulators. PPAR-γ ligand-binding domain is more stable upon compound **9** binding, relative to agonist rosiglitazone.[34] Consequently, PPARγ/PGC1α/**9** complex may adopt a unique conformation relative to the PPARγ full agonist rosiglitazone.

4.1.1 Importance of the AF-2 Helix

The LBD of PPARγ typically triggers a conformational change of the receptor, stabilizing the activation function-2 (AF-2) domain, which aids in the recruitment of co-regulatory factors to regulate gene transcription.[131] This conformational change can either be subtle or dramatic, which leads to stabilization of the charge clamp between helices H3 and H12 to aid in the interaction with the LXXLL motif of the coactivator. When a corepressor is bound to PPARγ, the hydrogen bond between Tyr473 and other stabilizing residues is lost, preventing the AF-2 helix from occupying an active state.[132] Moreover, this eliminates the "charge clamp" (Glu471 and Lys301) between PPARγ and prospective coactivator. The charge clamp positions the LXXLL motif, allowing leucine residues to pack tightly in to the hydrophobic pocket of the receptor. In addition, the LXXLL motif is vital for mediating cooperative assembly of coactivator complexes.[5] Upon ligand binding, the AF-2 (H12) helix closes on the ligand-binding site, reducing the conformational flexibility, assuming an ideal structure for coactivator binding. Activation of PPARγ by partial and full agonist depends on the presence of the AF-2 helix in the receptor, as this activates the docking surface for coactivator recruitment.[133] Removal of the AF-2 helix allows for the receptor to recruit corepressors and not coactivators, leaving the LBD to be inactive. The LBD or F domain and AF-2 helix modulates access to the docking surface allosterically rather than direct binding to the cofactor itself.[134] The most important interaction is the hydrogen bond linking agonists and Tyr473 of the AF-2 helix of NRs, signifying its essential role in the LBD. Noteworthy, the type of ligand determines which coactivator associates with the heterodimer.[36]

4.2 Methods

4.2.1 Molecular Dynamics Simulations

The initial coordinates for the protein-ligand structures were obtained from the Protein Data Bank (PDB) as ID number (3ET3) and (3CS8) for coactivator PGC-1α.[135] The PPARγ model consisted of 287 residues for compound **9** and SPPARγM agonists, while rosiglitazone had 286 residues and the apo protein 275 residues. The PGC-1α peptide consisted of 55 residues. The protein target, PPARγ using compound **9**, rosiglitazone, SPPARγM agonists and apo were prepared for MD simulations using the AMBER 12 program and the parm 99 force field.[106] All ligands were constructed using the PyMOL[136] program. The PPARγ structures were prepared using the leap module where the appropriate hydrogen atoms were added and explicit waters with usage of aMD were carried out. The PPARγ complexes were solvated in an octahedral box of TIP3P[118] water molecules to a depth of 10 Å from the edge of each complex. Each solute was neutralized with sodium counterions. The AMBER Gaff force field was employed to generate the parameters for each ligand while the ff99SB force field was used to construct the topology files of the PPARγ protein.

4.2.1.1 Minimization

For each protein complex, minimization was conducted in a dual stage, positioning restraints on all heavy atoms and added hydrogens. Minimization began with 200 steps. The first 50 steps were steepest decent, while the remainder was conjugate gradient for the water molecules only, followed by 10,000 steps for the entire system. Lastly, all heavy atoms were minimized for 200 steps.

4.2.1.2 Equilibration

The solvated PPARγ complexes were equilibrated using the NVT ensemble and periodic boundary conditions in three stages. The system was gradually heated from 0K to 300K at NVT over 50 ps of simulation time. Equilibration steps using NPT to adjust water density to experimental was ran for 500 ps at constant pressure of 1 atmosphere using a coupling value of 2.0 ps. Lastly, 500 ps of NVT equilibration was carried out. Constant pressure is expressed via Langevin Dynamics[120] while constant temperature used Berendsen[121] coupling algorithm. The SHAKE algorithm was employed to restrict all covalent bonds involving hydrogen atoms.

4.2.1.3 Production

Accelerated molecular dynamics (aMD) was carried out at 300K using the NVT ensemble. In this study, simulations have been run of the molecular complexes for the PPARγ-ligand-PGC-1α systems (compound **9**, rosiglitazone, SPPARγM, and apo) for 310 ns using the Verlet integration method with a 1-fs time step.

4.2.1.4 Analysis

Following production, each complex was analyzed. Root-mean-square deviation (RMSD), root-mean-square fluctuation (RMSF) analysis were reported for the protein-ligand interactions.

4.3 Results and Discussion

4.3.1 Compound 9 binding to PPARγ

Compound **9** exhibited the highest binding affinity to both PPARγ/PPARδ, which was determined by luciferase assays.[34] Data from the assay showed that the PPARγ target is inhibited by compound **9** of the adipocyte protein 2 (AP2), and attached to PPRE, known for adipocyte growth and differentiation (Figure 4.2). Moreover, compound **9** minimally activates the AP2-PPRE. Also, this data showed that compound **9** activates PPARδ of the pyruvate dehydrogenase kinase isoenzyme 4 (PDK4), which regulates energy metabolism in the cell (Figure 4.2).

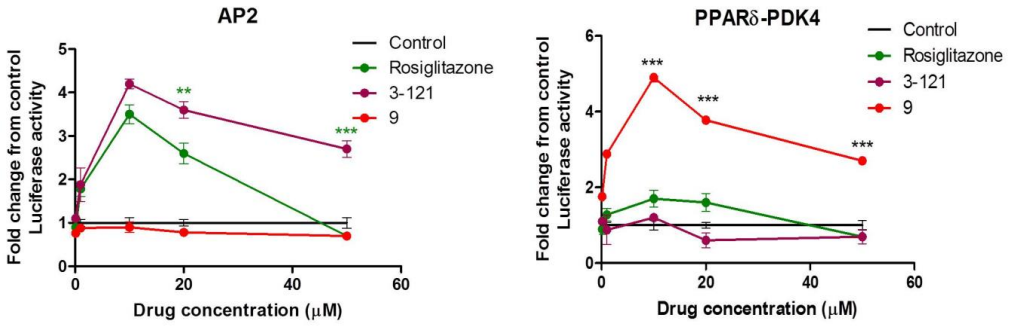

Figure 40 4.2

Bioorg. Med. Chem. Lett. 2013, 23(3), 873-9

Figure 4.2 – Lipid accumulation levels of PPARγ/PPARδ

Oil Red Staining of the cellular lipid was applied to determine the amount of lipid accumulation as a result of compound **9**. Compared to rosiglitazone, compound **9** induced negligible effects upon lipid accumulation in adipocytes (Figure 4.3). Marginally, compound **9** generates the expression of genes associated with lipid accumulation and synthesis. However, compound **9** stimulates the expression of genes affiliated with fatty acid oxidation and insulin sensitivity).[34]

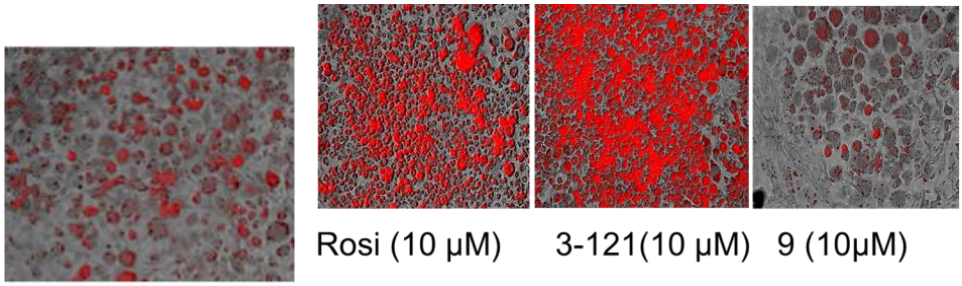

Figure 41 4.3

Bioorg. Med. Chem. Lett. 2013, 23(3), 873-9

Figure 4.3 – Compound **9** induces less lipid accumulation compared to rosiglitazone, the control and 3-121, demonstrated by the oil red-o stain

(red color).

4.3.2 Overall Molecular Dynamic Simulations

To define the major conformational changes induced by compound **9** and other selective PPARγ modulator (SPPARγM) agonists upon PPARγ and coactivator PGC-1α, a detailed analysis from the MD simulations was performed. Root-mean-square deviation (RMSD) and root-mean-square fluctuation (RMSF) were performed for all trajectories to monitor geometry stability of the complexes and global conformational changes of the simulations conducted. Figure 4.4 displays the RMSD of the PPARγ-ligand-PGC-1α complexes superimposed with average values of ~4.0 Å, extended over 310 ns, confirming good stability.

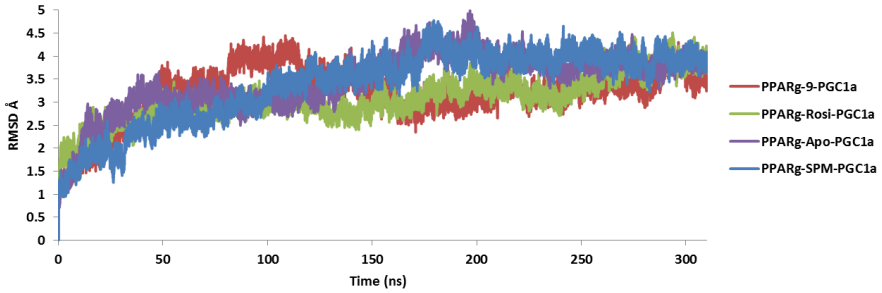

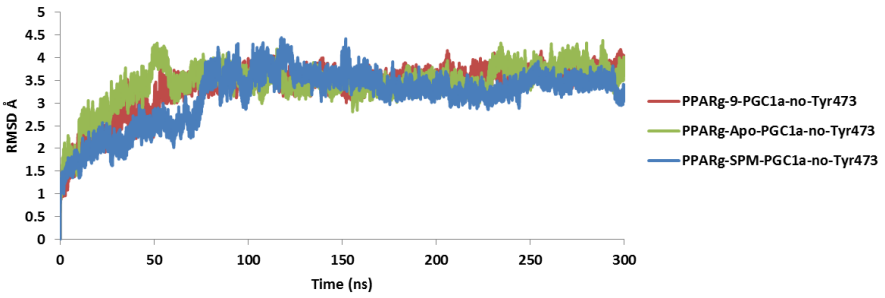

Figure 42 4.4

Figure 4.4 – RMSD of the PPARγ-ligand-PGC-1α complexes superimposed.

With the reported importance of Tyr473 in PPARγ binding pocket, significant effort has been placed upon determining the role of the residue in the enzyme.[36, 137] For example, what is the effect on conformational stability upon deleting Tyr473? Is Tyr473 essential for PGC-1α or coactivator recruitment? With full versus partial agonists, how does the removal of Tyr473 influence the complex towards coactivator recruitment? Moreover can RNA polymerase enter the LBD that lacks Tyr473? These posing questions motivated the current study to delete Tyr473 from the PPARγ LBD computationally to observe the effects towards the receptor and coactivator recruitment. Using program Chimera, each PPARγ complex bound with compounds **9** and rosiglitazone were altered by simply eliminating Tyr473 from the AF-2 (H12) helix.

The RMSD (Figure 4.4) of the backbone protein atoms for all PPARγ-ligand-PGC-1α complexes with residue Tyr473 eliminated, extended over 310 ns, fall in good standing, except for the PPARγ-Rosi-PGC-1α complex. Perhaps this can be explained as Tyr473 of the AF-2 helix, is a critical site of interaction between the PPARγ LBD and full agonist.[137]

Figure 4.5 shows the protein fluctuations of PPARγ helices of the ternary complexes with and without residue Tyr473. These differences in fluctuations accentuate the importance of this critical residue in the PPARγ LBD. The residue number displayed can identify the flexible helices, as H1-H12 from each individual complex exhibits more or less movement depending on agonist present,

hence several peaks. These peaks correspond to the movement from either the helix or loop of the receptor, indicating the geometry of each complex. Note the dramatic conformations when Tyr473 is not present, as fluctuations rise to approximately 40 Å.

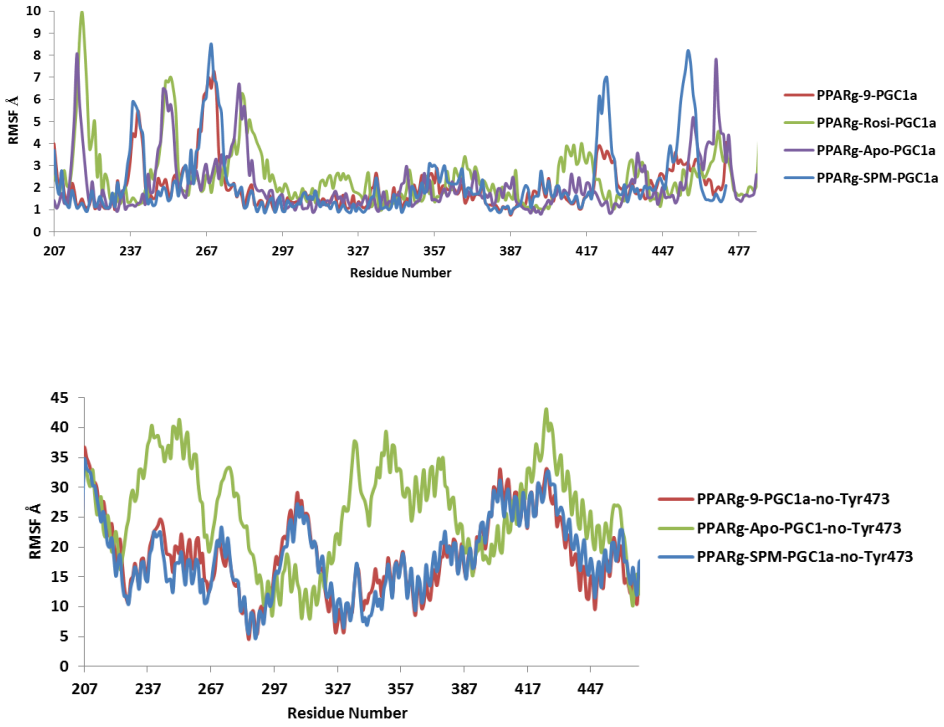

Figure 43 4.5

Figure 4.5 – RMSF of the PPARγ-ligand-PGC-1α complexes superimposed.

4.3.3 PPARγ LBD with Ligand/PGC-1α complex conformations: Tyr473 in binding pocket

To highlight each specific ligand (**9**, rosiglitazone, apo, and SPPARγM) in the PPARγ/PGC-1α complex LBD, major conformational changes were identified as of follows**:**

PPARγ-9-PGC-1α: Compound **9** exhibits several turns and flips compared to each system, however, compound **9** stabilizes the AF-2 helix due to the large binding affinity of the partial agonist. These rotations indicate the various conformations that compound **9** can display at different trajectories of simulations within the LBD. This agonist allows for the LBD to display

minor movement but in turn becomes more compact throughout simulations. Figure 4.6 displays that compound **9** is more likely not to make a direct interaction with Tyr473.

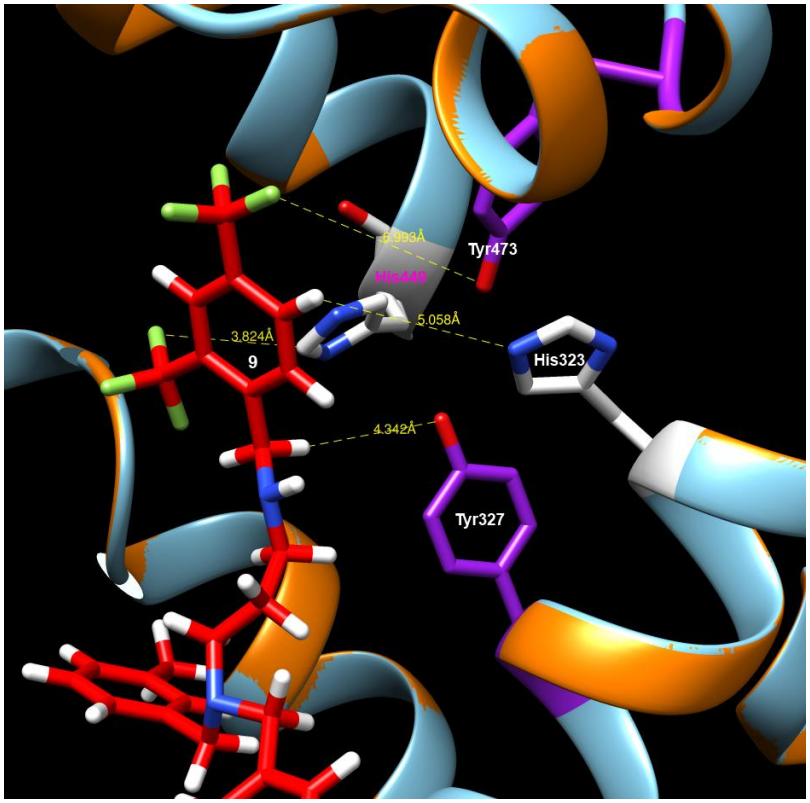

Figure 44 4.6

Figure 4.6 – Compound **9** in the PPARγ LBD

The tri-fluromethyl di-substituted phenyl ring adopts a N-H-π bond from His449, as this interaction holds the ring moiety in place, therefore avoiding Tyr473 (Figure 4.7). The amine group donates an H-bond to the sulfur atom of Cys285 in Arm 1. Several leucine and phenylalanine residues surround the methyl substituted phenyl ring, which also stabilizes compound **9** in the LBD.[34]

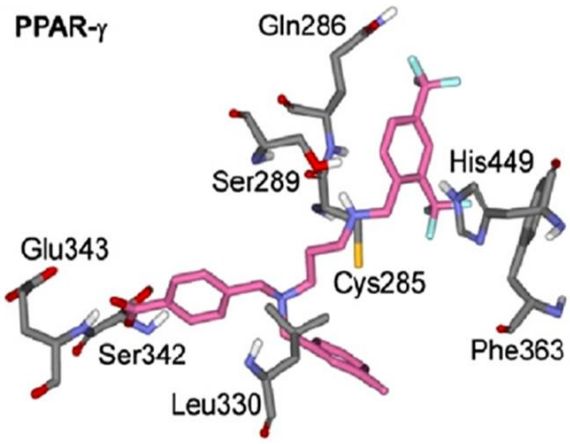

Figure 45 4.7

Bioorg. Med. Chem. Lett. 2013, 23(3), 873-9

Figure 4.7 – 9 in PPARγ LBD with common residues

Tyr473 on the AF-2 (H12) helix seems to allow the pocket to slightly open up, possibly suggesting specific enzymes, e.g. RNA polymerase, could enter the LBD. Compound **9** displays a "S-shaped" conformation, implying the "S" pocket occupancy in the absence of direct interaction with Tyr473 favors a correct balance of coactivator and corepressor binding favoring insulin sensitivity (Figure 4.8).

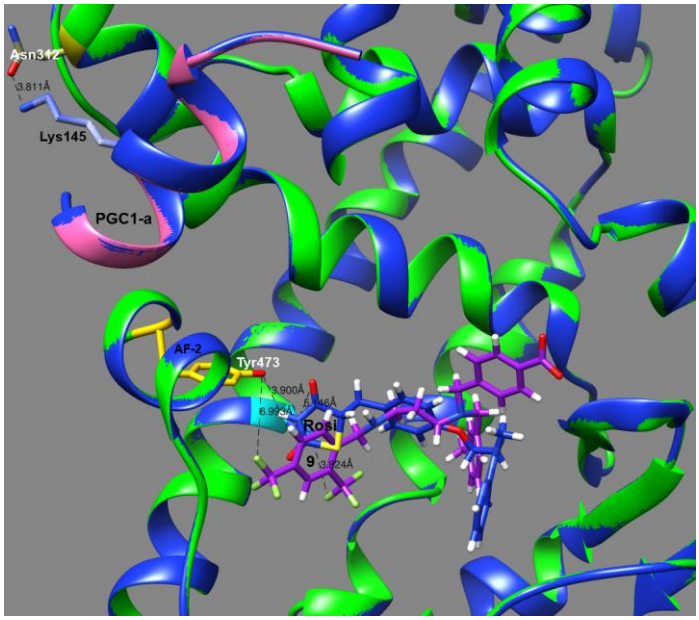

Figure 46 4.8

Figure 4.8 – Compound **9** and Rosi superimposed in the PPARγ LBD.

The H3 helix is more rigid with partial agonist compound **9**, compared to the flexibility available in the PPARγ-Apo-PGC-1α complex. The H11 helix, adjacent to the AF-2 (H12) helix, flexibility increases during simulations compared to full agonist rosiglitazone. In this complex, helices H1 (residues 213-223), H2 (residues 266-274), and H9 (residues 423-432) (Figure 4.5) exhibit modest flexibility. Coactivator PGC-1α, residues alanine, proline, and serine are the flexible amino acids within the peptide, as the LXXLL motif is stabilized being bound to PPARγ.

PPARγ-Rosi-PGC-1α: Compared to **9**, rosiglitazone directly interacts with Tyr473, stabilizing the C-terminus or AF-2 helix. TZDs bound to PPARγ generate two key hydrogen bonds between His323 and His449 that essentially lock the AF-2 (H12) helix into position.[138] Rosiglitazone binds in the pocket in a "U-shaped" conformation (Figure 4.7), wrapping around helix H3 with central benzene ring directly behind this helix.[131] The negatively charged nitrogen of the TZD head group forms an hydrogen bond with the Tyr473 side chain hydroxyl head group.[137] The Tyr473 residue appears to enclose the binding pocket, implying that no other enzyme could possibly enter the LBD of this complex. In this complex, the modest flexible helices differ from the PPARγ-9-PGC-1α by one (H1 (residues (208-212), H2 (residues (240-244), and H11 (residues 454-464), as the H11 helix is quite stable initially, but increases movement towards the end of the simulation. PGC-1α exhibits the same characteristics in this complex relative to the PPARγ-9-PGC-1α system. Rosiglitazone bound to the PPARγ LBD induces a strong interaction with this particular coactivator, as it displays a high binding affinity to the protein.[45] From simulations, rosiglitazone displays several different characteristics compared to **9**, as hypothesized.

PPARγ-SPM-PGC1-α: The SPPARγM agonist displays that Tyr473 is not a critical interaction, as it seems to not exhibit direct contact with the AF-2 helix residue, similar to **9**. The COOH moiety of such agonist is not in hydrogen bonding distance of Tyr473. Tyr473 mediates the interaction of full agonist but not SPPARγMs, thereby providing a precise determinant for their differing pharmacologies.[137] During simulations, similar rotations of the SPPARγM agonist occur relative to **9**, as each ligand has common moieties. This complex appears to be more stable with in the PPARγ LBD, perhaps caused by H-bonds with common active site residues. Ribbon 456-463 of the H11 helix acts to block the binding pocket, which resembles full agonist, rosiglitazone, however it gains flexibility similar to **9**. These helices (H1 (residues 207-213), H2 (residues 238-244), H6 (residues 265-276) and H9 (residues 423-430)) give rise to more movement compared to both complexes, PPARγ-9-PGC-1α and PPARγ-Rosi-PGC-1α during simulation. Alternatively, PPARγ-SPM-PGC-1α should resemble similar conformations relative to **9**.

PPARγ-Apo-PGC-1α: In this complex, the LBD is not stable, as no agonist is present. As PGC-1α stabilizes PPARγ, it allows the protein to not enclose on the LBD. Helices H11 and H12 somewhat display an open/close movement in the binding pocket. Helix H11 (residues 446-452) fluctuates to a larger extent in apo-form than partial agonists. In the absence of ligand, the AF-2 helix fluctuates more in the PPARγ-Apo-PGC-1α complex, but correlates to this region of **9** and SPM. In the apo-complex, helices (H1 (residues 207-210), H2 (residues 235-245), H6 (residues 264-273), and H9 (residues 423-429)) show moderate movement throughout the MD simulations. Coactivator peptides with high binding affinity such as PGC-1α to the receptor can bind to the LBD in the absence of any agonist.[139]

4.3.4 PPARγ LBD with Ligand/PGC-1α complex conformations: Tyr473 removed from binding pocket

Agonist compound **9** and rosiglitazone in the PPARγ-PGC-1α complexes are highlighted to identify the substantial differences in conformational changes when Tyr473 is removed is as follows:

The **PPARγ-9-PGC-1α** displays different conformations, as lack of Tyr473 allows for the binding pocket to be inactive. Unlike Tyr473 being present, compound **9** exhibits a "U shaped" conformation, perhaps failing to achieve optimal PPARγ activity (Figure 4.9). PGC-1α, differs as it displays increased flexibility, possibly with extended simulations it may completely unravel. Increased movement of PGC-1α may be due to the H-bond or intramolecular interaction of backbone Ser142 and Glu140 of the LXXLL motif does not exist, as Tyr473 is eliminated. If ligand present does not activate the AF-2 (H12) helix it may not be able to induce formation of a coactivator-binding surface, therefore, displacement of corepressors is not complete.

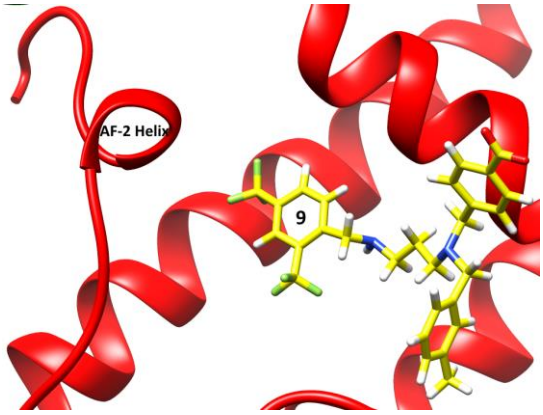

Figure 47 4.9

Figure 4.9 – Illustration of Compound **9** displaying a "U-shaped" orientation in the LBD, as Tyr473 is not present.

The **PPARγ-Rosi-PGC-1α** complex with lack of Tyr473 displays odd characteristics, as rosiglitazone and PGC-1α extrude out of the LBD, circling the receptor several times. These characteristics explain the significance of the Tyr473 and rosiglitazone interaction in the PPARγ LBD. Rosiglitazone continues to exhibit a "U-shaped" orientation, however, during simulations it appears to slightly form a "S-shaped" conformation. Rosiglitazone is not localized in the binding site, as the absence of Tyr473 allows clearance of the ligand. Compared to the PPARγ-9-PGC-1α complex, PGC-1α is not stable within this complex, as it circumvents the protein multiple times. Noteworthy, when rosiglitazone is lodged within the binding site, PGC-1α appears lost. This dramatic conformation perhaps can be explained as the charge clamp between PGC-1α and PPARγ is obstructing, this does not allow for proper dismal of corepressors. The interaction of PGC-1α to PPARγ is substantially increased by treatment with full agonist, rosiglitazone, indicating the significance of PGC-1α in rosi-regulated PPARγ activity.[140] This improper dismal of corepressors allows for PGC-1α to display energetic movement.

4.3.5 PPARγ-ligand-PGC-1α Possible Coactivators

PGC-1α binds to PPARγ in a ligand-independent manner, which facilitates interactions with other coactivators and plays a major role in RNA recognition. Partial and full agonist both display high recruitment of PGC-1α, but the lack of Tyr473 leads to an increase in the AF-2 helix opening, which can lead to a change in the ability of coactivator binding. In addition, a leading question still remains; will the ternary complex and/or heterodimer increase or decrease in selection of coactivators of compound **9** versus rosiglitazone? Rosiglitazone recruits coactivators (CBP, p300, SRC-1, TRAP220 and PGC-1α) to the receptor.[135] In a series of tests including coactivator (PGC-1α, TIF-2, SRC-1, and SRC-3), full agonist exhibited little selectivity between

the four peptides, marked by low (≤1) effect ratios; however partial agonist displayed high (≥1.5 to 6) effect ratios.[45] PGC-1α interacts directly with TRAP220/DRIP205 complexes to link with RNA polymerase II.[141] PGC-1α recruits HAT activity at 40%, including coactivators SRC-1, CBP, p300, and P/CAF, compared to the 48% of mediator complexes (TRAP220/DRIP205) (Figure 4.10).

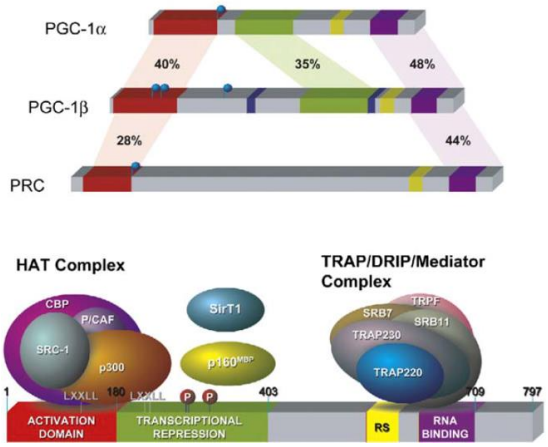

Cell Metabolism Vol. 1, 2005 pp.361-370

Figure 48 4.10

Figure 4.10 - PGC1-α recruits HAT activity and TRAP/DRIP/Mediator complexes.

Ligands bound to PPARγ and RXR were compared, interestly, CBP was not observed in the presence of either ligand alone or both ligands added simultaneously.[142] However, when PPARγ is associated with chromatin, acetylation occurs and eases the chromatin structure when compound **9** is bound to the protein, allowing for RNA polymerase to potentially enter the LBD. The more acetylation, the bigger the opening, confirming the prediction of the binding pocket opening and/or closing with specific agonist, therefore increasing transcription of PPARγ target genes displayed in (Figure 4.11) by coactivators (PGC-1α, CBP, and p300).

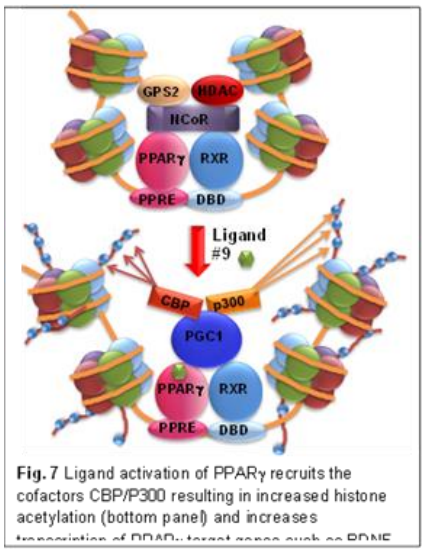

Fig. 7 Ligand activation of PPARγ recruits the cofactors CBP/P300 resulting in increased histone acetylation (bottom panel) and increases

Figure 49 4.11

Figure 4.11 – Ligand Activation of PPARγ recruits coactivators PGC-1α CBP/p300, increasing histone acetylation

DRIP205 bound to PPARγ requires higher concentrations of ligand than comparable binding of p160 coactivators to RXR; hence SRC-1 displays a higher binding affinity to the heterodimer. Moreover, p160 complexes will outcompete DRIP205, however, by dissociating SRC-1, this allows for higher recruitment of DRIP205. Anti-diabetic agents induce DRIP205 in a dose manner 10^{-6} M, but display inefficient recruitment of SRC-1, even at different concentrations. Thus, compound **9** can portray similar characteristics.[142] The AF-2 (H12) helix of the heterodimer is directly responsible for the recruitment of specific coactivators in response to their analogous ligands, possibly explaining why lack of Tyr473 leads to a change in coactivator binding. Halofenate, a PPARγ partial agonist, displayed inefficient recruitment of coactivators (CBP, p300, and TRAP220).[143] Compared to partial agonist, rosiglitazone induced a dose-dependent recruitment of coactivators (p300, CBP, and TRAP220). This should be consider when analyzing compound **9** and rosiglitazone, to understand which coactivator can further bind to the ternary complex with each individual agonist in the binding site.

4.4 Conclusion

From MD simulations

1. It was hypothesized that compound **9** should exhibit dramatically different effects to that of full agonist rosiglitazone, and this is deemed true, as they display different conformational changes with/out residue Tyr473 in the LBD. Without Tyr473 in the LBD, the receptor induces dramatic conformations, highlighting the significance of this residue bound to specific agonist. Tyr473 has a high influence on the recruitment of coactivators, as elimination allows PPARγ to form an improper molecular mechanism. Rosiglitazone displays adverse side effects (cardiovascular health) compared to compound **9**, as the partial agonist orientation in the PPARγ LBD improves adipocyte development, energy metabolism, insulin sensitization, and cardio protection.
2. In addition to the computational analysis, experimental work is still being conducted to further the current study using immunoprecipitation assays with PPARγ and PGC-1α in nuclear fractions to see if there is an increase in association of PPARγ with PGC-1α after ligand activation with compound **9** versus rosiglitazone. From here, additional coactivator recruitment by PGC-1α will also be detected, identifying which coactivator(s) binds to the ternary complex, with usage of compound **9** and rosiglitazone.

References

1. Vroling, B.; Thorne, D.; McDermott, P.; Joosten, H. J.; Attwood, T. K.; Pettifer, S.; Vriend, G., NucleaRDB: information system for nuclear receptors. *Nucleic Acids Res.* **2012,** *40* (D1), D377-D380.

2. Bertrand, S.; Brunet, F. G.; Escriva, H.; Parmentier, G.; Laudet, V.; Robinson-Rechavi, M., Evolutionary genomics of nuclear receptors: from twenty-five ancestral genes to derived endocrine systems. *Mol Biol Evol* **2004,** *21* (10), 1923-1937.

3. Robinson-Rechavi, M.; Garcia, H. E.; Laudet, V., The nuclear receptor superfamily. *J. Cell Sci.* **2003,** *116* (4), 585-586.

4. Zoete, V.; Grosdidier, A.; Michielin, O., Peroxisome proliferator-activated receptor structures: ligand specificity, molecular switch and interactions with regulators. *Biochim Biophys Acta* **2007,** *1771* (8), 915-925.

5. Nolte, R. T.; Wisely, G. B.; Westin, S.; Cobb, J. E.; Lambert, M. H.; Kurokawa, R.; Rosenfeld, M. G.; Willson, T. M.; Glass, C. K.; Milburn, M. V., Ligand binding and co-activator assembly of the peroxisome proliferator-activated receptor-gamma. *Nature* **1998,** *395* (6698), 137-143.

6. Bourguet, W.; Germain, P.; Gronemeyer, H., Nuclear receptor ligand-binding domains: three-dimensional structures, molecular interactions and pharmacological implications. *Trends Pharmacol Sci* **2000,** *21* (10), 381-388.

7. Quintanilla, R. A.; Utreras, E.; Cabezas-Opazo, F. A., Role of PPAR gamma in the Differentiation and Function of Neurons. *PPAR Res* **2014,** *2014*, 768594.

8. Rosen, E. D.; Spiegelman, B. M., PPARgamma : a nuclear regulator of metabolism, differentiation, and cell growth. *J. Biol. Chem.* **2001,** *276* (41), 37731-37734.

9. Kota, B. P.; Huang, T. H.; Roufogalis, B. D., An overview on biological mechanisms of PPARs. *Pharmacol Res* **2005,** *51* (2), 85-94.

10. Ahmadian, M.; Suh, J. M.; Hah, N.; Liddle, C.; Atkins, A. R.; Downes, M.; Evans, R. M., PPARgamma signaling and metabolism: the good, the bad and the future. *Nat. Med.* **2013,** *19* (5), 557-566.

11. Peters, J. M.; Shah, Y. M.; Gonzalez, F. J., The role of peroxisome proliferator-activated receptors in carcinogenesis and chemoprevention. *Nat. Rev. Cancer* **2012,** *12* (3), 181-195.

12. Schupp, M.; Lazar, M. A., Endogenous ligands for nuclear receptors: digging deeper. *J Biol Chem* **2010,** *285* (52), 40409-40415.

13. Jiang, M.; Strand, D. W.; Franco, O. E.; Clark, P. E.; Hayward, S. W., PPARgamma: a molecular link between systemic metabolic disease and benign prostate hyperplasia. *Differentiation* **2011,** *82* (4-5), 220-236.

14. DeFronzo, R. A.; Tripathy, D., Skeletal muscle insulin resistance is the primary defect in type 2 diabetes. *Diabetes Care* **2009,** *32 Suppl 2*, S157-163.

15. Shimizu, M.; Moriwaki, H., Synergistic Effects of PPARgamma Ligands and Retinoids in Cancer Treatment. *PPAR Res* **2008,** *2008*, 181047.

16. Miyata, K. S.; McCaw, S. E.; Marcus, S. L.; Rachubinski, R. A.; Capone, J. P., The peroxisome proliferator-activated receptor interacts with the retinoid X receptor in vivo. *Gene* **1994,** *148* (2), 327-330.

17. Evans, R. M.; Barish, G. D.; Wang, Y. X., PPARs and the complex journey to obesity. *Nat Med* **2004,** *10* (4), 355-361.

18. Issemann, I.; Green, S., Activation of a member of the steroid hormone receptor superfamily by peroxisome proliferators. *Nature* **1990,** *347* (6294), 645-650.

19. Aperlo, C.; Pognonec, P.; Saladin, R.; Auwerx, J.; Boulukos, K. E., cDNA cloning and characterization of the transcriptional activities of the hamster peroxisome proliferator-activated receptor haPPAR gamma. *Gene* **1995,** *162* (2), 297-302.

20. Dreyer, C.; Krey, G.; Keller, H.; Givel, F.; Helftenbein, G.; Wahli, W., Control of the peroxisomal beta-oxidation pathway by a novel family of nuclear hormone receptors. *Cell* **1992,** *68* (5), 879-887.

21. Gottlicher, M.; Widmark, E.; Li, Q.; Gustafsson, J. A., Fatty acids activate a chimera of the clofibric acid-activated receptor and the glucocorticoid receptor. *P Natl Acad Sci USA* **1992,** *89* (10), 4653-4657.

22. Forman, B. M.; Chen, J.; Evans, R. M., The peroxisome proliferator-activated receptors: ligands and activators. *Ann. N. Y. Acad. Sci.* **1996,** *804*, 266-275.

23. Ferre, P., The biology of peroxisome proliferator-activated receptors: relationship with lipid metabolism and insulin sensitivity. *Diabetes* **2004,** *53 Suppl 1*, S43-50.

24. Coll, T.; Rodriguez-Calvo, R.; Barroso, E.; Serrano, L.; Eyre, E.; Palomer, X.; Vazquez-Carrera, M., Peroxisome proliferator-activated receptor (PPAR) beta/delta: a new potential therapeutic target for the treatment of metabolic syndrome. *Curr. Mol. Pharmacol.* **2009,** *2* (1), 46-55.

25. Sundvold, H.; Lien, S., Identification of a novel peroxisome proliferator-activated receptor (PPAR) gamma promoter in man and transactivation by the nuclear receptor RORalpha1. *Biochem. Biophys. Res. Commun.* **2001,** *287* (2), 383-390.

26. Kersten, S., Peroxisome proliferator activated receptors and obesity. *Eur. J. Pharmacol.* **2002,** *440* (2-3), 223-234.

27. Grygiel-Gorniak, B., Peroxisome proliferator-activated receptors and their ligands: nutritional and clinical implications--a review. *Nutr J* **2014,** *13*, 17.

28. Krisanapun, C.; Lee, S. H.; Peungvicha, P.; Temsiririrkkul, R.; Baek, S. J., Antidiabetic Activities of Abutilon indicum (L.) Sweet Are Mediated by Enhancement of Adipocyte Differentiation and Activation of the GLUT1 Promoter. *Evid. Based Complement. Alternat. Med.* **2011,** *2011*, 167684.

29. Ryan, K. K.; Li, B.; Grayson, B. E.; Matter, E. K.; Woods, S. C.; Seeley, R. J., A role for central nervous system PPAR-gamma in the regulation of energy balance. *Nat Med* **2011,** *17* (5), 623-U145.

30. Green, S.; Chambon, P., Nuclear receptors enhance our understanding of transcription regulation. *Trends Genet.* **1988,** *4* (11), 309-314.

31. Evans, R. M., The steroid and thyroid hormone receptor superfamily. *Science* **1988,** *240* (4854), 889-895.

32. Berman, H. M.; Battistuz, T.; Bhat, T. N.; Bluhm, W. F.; Bourne, P. E.; Burkhardt, K.; Feng, Z.; Gilliland, G. L.; Iype, L.; Jain, S.; Fagan, P.; Marvin, J.; Padilla, D.; Ravichandran, V.; Schneider, B.; Thanki, N.; Weissig, H.; Westbrook, J. D.; Zardecki, C., The Protein Data Bank. *Acta Crystallographica. Section D: Biological Crystallography* **2002,** *58* (Pt 6 No 1), 899-907.

33. Berman, H. M.; Westbrook, J.; Feng, Z.; Gilliland, G.; Bhat, T. N.; Weissig, H.; Shindyalov, I. N.; Bourne, P. E., The Protein Data Bank. *Nucleic Acids Res.* **2000,** *28* (1), 235-242.

34. Gathiaka, S.; Nanayakkara, G.; Boncher, T.; Acevedo, O.; Wyble, J.; Patel, S.; Patel, A.; Shane, M. E.; Bonkowski, B.; Wieczorek, J.; Rong, Y.; Huggins, K.; Smith, F.; Amin, R. H.,

Design, development and evaluation of novel dual PPARdelta/PPARgamma agonists. *Bioorg. Med. Chem. Lett.* **2013,** *23* (3), 873-879.

35. Cronet, P.; Petersen, J. F.; Folmer, R.; Blomberg, N.; Sjoblom, K.; Karlsson, U.; Lindstedt, E. L.; Bamberg, K., Structure of the PPARalpha and -gamma ligand binding domain in complex with AZ 242; ligand selectivity and agonist activation in the PPAR family. *Structure* **2001,** *9* (8), 699-706.

36. Lewis, S. N.; Bassaganya-Riera, J.; Bevan, D. R., Virtual Screening as a Technique for PPAR Modulator Discovery. *PPAR Res* **2010,** *2010*, 861238.

37. Nesto, R. W.; Bell, D.; Bonow, R. O.; Fonseca, V.; Grundy, S. M.; Horton, E. S.; Le Winter, M.; Porte, D.; Semenkovich, C. F.; Smith, S.; Young, L. H.; Kahn, R.; American Heart, A.; American Diabetes, A., Thiazolidinedione use, fluid retention, and congestive heart failure: a consensus statement from the American Heart Association and American Diabetes Association. October 7, 2003. *Circulation* **2003,** *108* (23), 2941-2948.

38. Einstein, M.; Akiyama, T. E.; Castriota, G. A.; Wang, C. F.; McKeever, B.; Mosley, R. T.; Becker, J. W.; Moller, D. E.; Meinke, P. T.; Wood, H. B.; Berger, J. P., The differential interactions of peroxisome proliferator-activated receptor gamma ligands with tyr473 is a physical basis for their unique biological activities. *Mol Pharmacol* **2008,** *73* (1), 62-74.

39. Berger, J. P.; Petro, A. E.; Macnaul, K. L.; Kelly, L. J.; Zhang, B. B.; Richards, K.; Elbrecht, A.; Johnson, B. A.; Zhou, G.; Doebber, T. W.; Biswas, C.; Parikh, M.; Sharma, N.; Tanen, M. R.; Thompson, G. M.; Ventre, J.; Adams, A. D.; Mosley, R.; Surwit, R. S.; Moller, D. E., Distinct properties and advantages of a novel peroxisome proliferator-activated protein [gamma] selective modulator. *Mol Endocrinol* **2003,** *17* (4), 662-676.

40. Allen, T.; Zhang, F.; Moodie, S. A.; Clemens, L. E.; Smith, A.; Gregoire, F.; Bell, A.; Muscat, G. E.; Gustafson, T. A., Halofenate is a selective peroxisome proliferator-activated receptor gamma modulator with antidiabetic activity. *Diabetes* **2006,** *55* (9), 2523-2533.

41. Guan, H. P.; Ishizuka, T.; Chui, P. C.; Lehrke, M.; Lazar, M. A., Corepressors selectively control the transcriptional activity of PPARgamma in adipocytes. *Genes Dev.* **2005,** *19* (4), 453-461.

42. Hu, X.; Li, Y.; Lazar, M. A., Determinants of CoRNR-dependent repression complex assembly on nuclear hormone receptors. *Mol. Cell. Biol.* **2001,** *21* (5), 1747-1758.

43. Perissi, V.; Staszewski, L. M.; McInerney, E. M.; Kurokawa, R.; Krones, A.; Rose, D. W.; Lambert, M. H.; Milburn, M. V.; Glass, C. K.; Rosenfeld, M. G., Molecular determinants of nuclear receptor-corepressor interaction. *Genes Dev.* **1999,** *13* (24), 3198-3208.

44. Reginato, M. J.; Krakow, S. L.; Bailey, S. T.; Lazar, M. A., Prostaglandins promote and block adipogenesis through opposing effects on peroxisome proliferator-activated receptor gamma. *J Biol Chem* **1998,** *273* (4), 1855-1858.

45. Burgermeister, E.; Schnoebelen, A.; Flament, A.; Benz, J.; Stihle, M.; Gsell, B.; Rufer, A.; Ruf, A.; Kuhn, B.; Marki, H. P.; Mizrahi, J.; Sebokova, E.; Niesor, E.; Meyer, M., A novel partial agonist of peroxisome proliferator-activated receptor-gamma (PPARgamma) recruits PPARgamma-coactivator-1alpha, prevents triglyceride accumulation, and potentiates insulin signaling in vitro. *Mol. Endocrinol.* **2006,** *20* (4), 809-830.

46. Morley, S.; Cecchini, M.; Zhang, W.; Virgulti, A.; Noy, N.; Atkinson, J.; Manor, D., Mechanisms of ligand transfer by the hepatic tocopherol transfer protein. *J Biol Chem* **2008,** *283* (26), 17797-17804.

47. International Human Genome Sequencing, C., Finishing the euchromatic sequence of the human genome. *Nature* **2004,** *431* (7011), 931-945.

48. Ayoubi, T. A.; Van De Ven, W. J., Regulation of gene expression by alternative promoters. *Faseb J* **1996,** *10* (4), 453-460.

49. Wu, T.; Wang, J.; Liu, C.; Zhang, Y.; Shi, B.; Zhu, X.; Zhang, Z.; Skogerbo, G.; Chen, L.; Lu, H.; Zhao, Y.; Chen, R., NPInter: the noncoding RNAs and protein related biomacromolecules interaction database. *Nucleic Acids Res* **2006,** *34* (Database issue), D150-152.

50. Humbard, M. A.; Stevens, S. M., Jr.; Maupin-Furlow, J. A., Posttranslational modification of the 20S proteasomal proteins of the archaeon Haloferax volcanii. *J. Bacteriol.* **2006,** *188* (21), 7521-7530.

51. Bachand, F., Protein arginine methyltransferases: From unicellular eukaryotes to humans. *Eukaryot Cell* **2007,** *6* (6), 889-898.

52. Wolf, S. S., The protein arginine methyltransferase family: an update about function, new perspectives and the physiological role in humans. *Cell Mol Life Sci* **2009,** *66* (13), 2109-2121.

53. Bedford, M. T.; Richard, S., Arginine methylation an emerging regulator of protein function. *Mol. Cell* **2005,** *18* (3), 263-272.

54. Paik, W. K.; Kim, S., Enzymatic Methylation of Protein Fractions from Calf Thymus Nuclei. *Biochem Bioph Res Co* **1967,** *29* (1), 14-&.

55. Rust, H. L.; Zurita-Lopez, C. I.; Clarke, S.; Thompson, P. R., Mechanistic studies on transcriptional coactivator protein arginine methyltransferase 1. *Biochemistry* **2011,** *50* (16), 3332-3345.

56. Raman, B.; Guarnaccia, C.; Nadassy, K.; Zakhariev, S.; Pintar, A.; Zanuttin, F.; Frigyes, D.; Acatrinei, C.; Vindigni, A.; Pongor, G.; Pongor, S., N(omega)-arginine dimethylation

modulates the interaction between a Gly/Arg-rich peptide from human nucleolin and nucleic acids. *Nucleic Acids Res* **2001,** *29* (16), 3377-3384.

57. Gui, S.; Gathiaka, S.; Li, J.; Qu, J.; Acevedo, O.; Hevel, J. M., A remodeled protein arginine methyltransferase 1 (PRMT1) generates symmetric dimethylarginine. *J Biol Chem* **2014,** *289* (13), 9320-9327.

58. Di Lorenzo, A.; Bedford, M. T., Histone arginine methylation. *Febs Lett* **2011,** *585* (13), 2024-2031.

59. Vallance, P.; Leiper, J., Cardiovascular biology of the asymmetric dimethylarginine:dimethylarginine dimethylaminohydrolase pathway. *Arterioscler. Thromb. Vasc. Biol.* **2004,** *24* (6), 1023-1030.

60. Galassi, A.; Reynolds, K.; He, J., Metabolic syndrome and risk of cardiovascular disease: A meta-analysis. *Am J Med* **2006,** *119* (10), 812-819.

61. Jansson, M.; Durant, S. T.; Cho, E. C.; Sheahan, S.; Edelmann, M.; Kessler, B.; La Thangue, N. B., Arginine methylation regulates the p53 response. *Nat Cell Biol* **2008,** *10* (12), 1431-U1122.

62. Cloos, P. A.; Christensen, J.; Agger, K.; Helin, K., Erasing the methyl mark: histone demethylases at the center of cellular differentiation and disease. *Genes & development* **2008,** *22* (9), 1115-1140.

63. Zhang, X.; Cheng, X., Structure of the predominant protein arginine methyltransferase PRMT1 and analysis of its binding to substrate peptides. *Structure* **2003,** *11* (5), 509-520.

64. Morales, Y.; Nitzel, D. V.; Price, O. M.; Gui, S.; Li, J.; Qu, J.; Hevel, J. M., Redox Control of Protein Arginine Methyltransferase 1 (PRMT1) Activity. *J Biol Chem* **2015,** *290* (24), 14915-14926.

65. Herrmann, F.; Bossert, M.; Schwander, A.; Akgun, E.; Fackelmayer, F. O., Arginine methylation of scaffold attachment factor A by heterogeneous nuclear ribonucleoprotein particle-associated PRMT1. *J Biol Chem* **2004,** *279* (47), 48774-48779.

66. Lin, W. J.; Gary, J. D.; Yang, M. C.; Clarke, S.; Herschman, H. R., The mammalian immediate-early TIS21 protein and the leukemia-associated BTG1 protein interact with a protein-arginine N-methyltransferase. *J Biol Chem* **1996,** *271* (25), 15034-15044.

67. Cantoni, G. L., Activation of methionine for transmethylation. *J Biol Chem* **1951,** *189* (2), 745-754.

68. Volonte, D.; Galbiati, F., Polymerase I and transcript release factor (PTRF)/cavin-1 is a novel regulator of stress-induced premature senescence. *J Biol Chem* **2011,** *286* (33), 28657-28661.

69. Cheng, X.; Roberts, R. J., AdoMet-dependent methylation, DNA methyltransferases and base flipping. *Nucleic Acids Res* **2001,** *29* (18), 3784-3795.

70. Zhang, X.; Zhou, L.; Cheng, X., Crystal structure of the conserved core of protein arginine methyltransferase PRMT3. *Embo J* **2000,** *19* (14), 3509-3519.

71. Gui, S.; Wooderchak, W. L.; Daly, M. P.; Porter, P. J.; Johnson, S. J.; Hevel, J. M., Investigation of the molecular origins of protein-arginine methyltransferase I (PRMT1) product specificity reveals a role for two conserved methionine residues. *J Biol Chem* **2011,** *286* (33), 29118-29126.

72. Van Gunsteren, W. F.; Berendsen, H. J., Molecular dynamics: perspective for complex systems. *Biochem. Soc. Trans.* **1982,** *10* (5), 301-305.

73. Petrenko, R.; Meller, J., Molecular Dynamics. In *eLS*, John Wiley & Sons, Ltd: 2001.

74. Alder, B. J.; Wainwright, T. E., Phase Transition for a Hard Sphere System. *J Chem Phys* **1957,** *27* (5), 1208-1209.

75. Rossky, P. J., Perspective on "Correlations in the motion of atoms in liquid argon" - Rahman A (1964) Phys Rev 136 : 405. *Theoretical Chemistry Accounts* **2000,** *103* (3-4), 263-264.

76. Karplus, M.; Kuriyan, J., Molecular dynamics and protein function. *P Natl Acad Sci USA* **2005,** *102* (19), 6679-6685.

77. Gathiaka, S. M.; Gui, S.; Li, J.; Qu, J.; Hevel, J.; Acevedo, O. In *Mechanism and product specificity of PRMT1: Implications from QM and MD simulations*, ABSTRACTS OF PAPERS OF THE AMERICAN CHEMICAL SOCIETY, AMER CHEMICAL SOC 1155 16TH ST, NW, WASHINGTON, DC 20036 USA: 2014.

78. Leach, A., *Molecular Modelling: Principles and Applications (2nd Edition)*. Prentice Hall: 2001.

79. Gathiaka, S., Exploring the Mechanism and Product Specificity of Protein Arginine Methyltransferase 1 and Drug Discovery for Diabetes and Malaria. *Ph.D Dissertation* **2015,** (Auburn University, Auburn, AL).

80. Eastwood, J. W.; Brownrigg, D. R. K., Remarks on the solution of poisson's equation for isolated systems. *J. Comput. Phys.* **1979,** *32* (1), 24-38.

81. Allen, M. P.; Tildesley, D. J., *Computer Simulation of Liquids (Oxford Science Publications)*. Oxford University Press: 1989.

82. Ryckaert, J.-P.; Ciccotti, G.; Berendsen, H. J. C., Numerical integration of the cartesian equations of motion of a system with constraints: molecular dynamics of n-alkanes. *J. Comput. Phys.* **1977,** *23* (3), 327-341.

83. Wang, J.; Wolf, R. M.; Caldwell, J. W.; Kollman, P. A.; Case, D. A., Development and testing of a general amber force field. *J. Comput. Chem.* **2004,** *25* (9), 1157-1174.

84. Cornell, W. D.; Cieplak, P.; Bayly, C. I.; Gould, I. R.; Merz, K. M.; Ferguson, D. M.; Spellmeyer, D. C.; Fox, T.; Caldwell, J. W.; Kollman, P. A., A Second Generation Force Field for the Simulation of Proteins, Nucleic Acids, and Organic Molecules. *J. Am. Chem. Soc.* **1995,** *117* (19), 5179-5197.

85. Metropolis, N.; Rosenbluth, A. W.; Rosenbluth, M. N.; Teller, A. H.; Teller, E., Equation of State Calculations by Fast Computing Machines. *The Journal of Chemical Physics* **1953,** *21* (6), 1087-1092.

86. Sugita, Y.; Okamoto, Y., Replica-exchange molecular dynamics method for protein folding. *Chem. Phys. Lett.* **1999,** *314* (1–2), 141-151.

87. Miao, Y.; Sinko, W.; Pierce, L.; Bucher, D.; Walker, R. C.; McCammon, J. A., Improved Reweighting of Accelerated Molecular Dynamics Simulations for Free Energy Calculation. *J. Chem. Theory Comput.* **2014,** *10* (7), 2677-2689.

88. Hamelberg, D.; Mongan, J.; McCammon, J. A., Accelerated molecular dynamics: A promising and efficient simulation method for biomolecules. *The Journal of Chemical Physics* **2004,** *120* (24), 11919-11929.

89. Neese, F., The ORCA program system. *Wiley Interdisciplinary Reviews: Computational Molecular Science* **2012,** *2* (1), 73-78.

90. Shen, T.; Hamelberg, D., A statistical analysis of the precision of reweighting-based simulations. *The Journal of Chemical Physics* **2008,** *129* (3), 034103.

91. Pearlman, D. A.; Case, D. A.; Caldwell, J. W.; Ross, W. S.; Cheatham Iii, T. E.; DeBolt, S.; Ferguson, D.; Seibel, G.; Kollman, P., AMBER, a package of computer programs for applying

molecular mechanics, normal mode analysis, molecular dynamics and free energy calculations to simulate the structural and energetic properties of molecules. *Comput. Phys. Commun.* **1995,** *91* (1–3), 1-41.

92. Case, D. A.; Cheatham, T. E.; Darden, T.; Gohlke, H.; Luo, R.; Merz, K. M.; Onufriev, A.; Simmerling, C.; Wang, B.; Woods, R. J., The Amber biomolecular simulation programs. *J. Comput. Chem.* **2005,** *26* (16), 1668-1688.

93. Meng, X.-Y.; Zhang, H.-X.; Mezei, M.; Cui, M., Molecular Docking: A powerful approach for structure-based drug discovery. *Curr. Comput. Aided Drug Des.* **2011,** *7* (2), 146-157.

94. Jorgensen, W. L., The Many Roles of Computation in Drug Discovery. *Science* **2004,** *303* (5665), 1813-1818.

95. Morris, G. M.; Huey, R.; Lindstrom, W.; Sanner, M. F.; Belew, R. K.; Goodsell, D. S.; Olson, A. J., AutoDock4 and AutoDockTools4: Automated docking with selective receptor flexibility. *J. Comput. Chem.* **2009,** *30* (16), 2785-2791.

96. Trott, O.; Olson, A. J., AutoDock Vina: improving the speed and accuracy of docking with a new scoring function, efficient optimization and multithreading. *J. Comput. Chem.* **2010,** *31* (2), 455-461.

97. Jain, A., Surflex-Dock 2.1: Robust performance from ligand energetic modeling, ring flexibility, and knowledge-based search. *J. Comput. Aided Mol. Des.* **2007,** *21* (5), 281-306.

98. Hu, P.; Zhang, Y., Catalytic Mechanism and Product Specificity of the Histone Lysine Methyltransferase SET7/9: An ab Initio QM/MM-FE Study with Multiple Initial Structures. *J. Am. Chem. Soc.* **2006,** *128* (4), 1272-1278.

99. Mobley, D. L.; Dill, K. A., Binding of Small-Molecule Ligands to Proteins: "What You See" Is Not Always "What You Get". *Structure (London, England : 1993)* **2009,** *17* (4), 489-498.

100. Friesner, R. A.; Banks, J. L.; Murphy, R. B.; Halgren, T. A.; Klicic, J. J.; Mainz, D. T.; Repasky, M. P.; Knoll, E. H.; Shelley, M.; Perry, J. K.; Shaw, D. E.; Francis, P.; Shenkin, P. S., Glide: A New Approach for Rapid, Accurate Docking and Scoring. 1. Method and Assessment of Docking Accuracy. *J. Med. Chem.* **2004,** *47* (7), 1739-1749.

101. Huang, S.-Y.; Grinter, S. Z.; Zou, X., Scoring functions and their evaluation methods for protein-ligand docking: recent advances and future directions. *PCCP* **2010,** *12* (40), 12899-12908.

102. Gilson, M. K.; Zhou, H.-X., Calculation of Protein-Ligand Binding Affinities. *Annu. Rev. Biophys. Biomol. Struct.* **2007,** *36* (1), 21-42.

103. Chang, C.-e. A.; Chen, W.; Gilson, M. K., Ligand configurational entropy and protein binding. *Proceedings of the National Academy of Sciences* **2007,** *104* (5), 1534-1539.

104. Huey, R.; Morris, G. M.; Olson, A. J.; Goodsell, D. S., A semiempirical free energy force field with charge-based desolvation. *J. Comput. Chem.* **2007,** *28* (6), 1145-1152.

105. Trott, O.; Olson, A. J., AutoDock Vina: Improving the speed and accuracy of docking with a new scoring function, efficient optimization, and multithreading. *J. Comput. Chem.* **2010,** *31* (2), 455-461.

106. Senn, H. M.; Thiel, W., QM/MM Methods for Biomolecular Systems. *Angew. Chem. Int. Ed.* **2009,** *48* (7), 1198-1229.

107. Ribeiro, A. J. M.; Santos-Martins, D.; Russo, N.; Ramos, M. J.; Fernandes, P. A., Enzymatic Flexibility and Reaction Rate: A QM/MM Study of HIV-1 Protease. *ACS Catalysis* **2015,** *5* (9), 5617-5626.

108. Case, D. A.; Cheatham, T. E.; Darden, T.; Gohlke, H.; Luo, R.; Merz, K. M.; Onufriev, A.; Simmerling, C.; Wang, B.; Woods, R. J., The {Amber} biomolecular simulation programs. *J. Comput. Chem.* **2005,** *26* (16), 1668-1688.

109. Yilmazer, N. D.; Korth, M., Enhanced semiempirical QM methods for biomolecular interactions. *Computational and Structural Biotechnology Journal* **2015,** *13*, 169-175.

110. Walker, R. C.; Crowley, M. F.; Case, D. A., The implementation of a fast and accurate QM/MM potential method in Amber. *J. Comput. Chem.* **2008,** *29* (7), 1019-1031.

111. Resat, H.; Mezei, M., Studies on free energy calculations. I. Thermodynamic integration using a polynomial path. *The Journal of Chemical Physics* **1993,** *99* (8), 6052-6061.

112. Callen, H., *Thermodynamics and an Introduction to Thermostatistics*. Wiley: 1985.

113. Gui, S.; Wooderchak, W. L.; Daly, M. P.; Porter, P. J.; Johnson, S. J.; Hevel, J. M., Investigation of the Molecular Origins of Protein-arginine Methyltransferase I (PRMT1) Product Specificity Reveals a Role for Two Conserved Methionine Residues. *J. Biol. Chem.* **2011,** *286* (33), 29118-29126.

114. Gui, S.; Gathiaka, S.; Li, J.; Qu, J.; Acevedo, O.; Hevel, J. M., A Remodeled Protein Arginine Methyltransferase 1 (PRMT1) Generates Symmetric Dimethylarginine. *J. Biol. Chem.* **2014,** *289* (13), 9320-9327.

115. Rust, H. L.; Zurita-Lopez, C. I.; Clarke, S.; Thompson, P. R., Mechanistic Studies on Transcriptional Coactivator Protein Arginine Methyltransferase 1. *Biochemistry* **2011,** *50* (16), 3332-3345.

116. Gallivan, J. P.; Dougherty, D. A., Cation-π interactions in structural biology. *Proceedings of the National Academy of Sciences* **1999,** *96* (17), 9459-9464.

117. Morales, Y.; Nitzel, D. V.; Price, O. M.; Gui, S.; Li, J.; Qu, J.; Hevel, J. M., Redox control of protein arginine methyltransferase 1 (PRMT1) activity. *J. Biol. Chem.* **2015**.

118. Jorgensen, W. L.; Chandrasekhar, J.; Madura, J. D.; Impey, R. W.; Klein, M. L., Comparison of simple potential functions for simulating liquid water. *The Journal of Chemical Physics* **1983,** *79* (2), 926-935.

119. Jakalian, A.; Jack, D. B.; Bayly, C. I., Fast, efficient generation of high-quality atomic charges. AM1-BCC model: II. Parameterization and validation. *J. Comput. Chem.* **2002,** *23* (16), 1623-1641.

120. Brünger, A.; Brooks Iii, C. L.; Karplus, M., Stochastic boundary conditions for molecular dynamics simulations of ST2 water. *Chem. Phys. Lett.* **1984,** *105* (5), 495-500.

121. Berendsen, H. J. C.; Postma, J. P. M.; van Gunsteren, W. F.; DiNola, A.; Haak, J. R., Molecular dynamics with coupling to an external bath. *The Journal of Chemical Physics* **1984,** *81* (8), 3684-3690.

122. Sessions, R. B.; Gibbs, N.; Dempsey, C. E., Hydrogen bonding in helical polypeptides from molecular dynamics simulations and amide hydrogen exchange analysis: alamethicin and melittin in methanol. *Biophys. J.* **1998,** *74* (1), 138-152.

123. Sippl, M. J., Calculation of conformational ensembles from potentials of mean force. An approach to the knowledge-based prediction of local structures in globular proteins. *J. Mol. Biol.* **1990,** *213* (4), 859-883.

124. Kumar, S.; Rosenberg, J. M.; Bouzida, D.; Swendsen, R. H.; Kollman, P. A., Multidimensional free-energy calculations using the weighted histogram analysis method. *J. Comput. Chem.* **1995,** *16* (11), 1339-1350.

125. Roux, B., The calculation of the potential of mean force using computer simulations. *Comput. Phys. Commun.* **1995,** *91* (1–3), 275-282.

126. Wolfenden, R.; Snider, M. J., The Depth of Chemical Time and the Power of Enzymes as Catalysts. *Acc. Chem. Res.* **2001,** *34* (12), 938-945.

127. Obianyo, O.; Osborne, T. C.; Thompson, P. R., Kinetic Mechanism of Protein Arginine Methyltransferase 1†. *Biochemistry* **2008,** *47* (39), 10420-10427.

128. Kraus, J., The Biochemistry of Adenosylmethionine. *The Yale Journal of Biology and Medicine* **1978,** *51* (6), 669-670.

129. Chu, Y.; Li, G.; Guo, H., QM/MM MD and free energy simulations of the methylation reactions catalyzed by protein arginine methyltransferase PRMT3. *Can. J. Chem.* **2013,** *91* (7), 605-612.

130. Association, A. D., Standards of Medical Care in Diabetes—2010. *Diabetes Care* **2010,** *33* (Supplement 1), S11-S61.

131. Li, Y.; Wang, Z.; Furukawa, N.; Escaron, P.; Weiszmann, J.; Lee, G.; Lindstrom, M.; Liu, J.; Liu, X.; Xu, H.; Plotnikova, O.; Prasad, V.; Walker, N.; Learned, R. M.; Chen, J.-L., T2384, a Novel Antidiabetic Agent with Unique Peroxisome Proliferator-activated Receptor γ Binding Properties. *J. Biol. Chem.* **2008,** *283* (14), 9168-9176.

132. Gampe, R. T., Jr.; Montana, V. G.; Lambert, M. H.; Miller, A. B.; Bledsoe, R. K.; Milburn, M. V.; Kliewer, S. A.; Willson, T. M.; Xu, H. E., Asymmetry in the PPARγ/RXRα Crystal Structure Reveals the Molecular Basis of Heterodimerization among Nuclear Receptors. *Mol. Cell 5* (3), 545-555.

133. Liu, J.; Li, H.; Burstein, S. H.; Zurier, R. B.; Chen, J. D., Activation and Binding of Peroxisome Proliferator-Activated Receptor γ by Synthetic Cannabinoid Ajulemic Acid. *Mol. Pharmacol.* **2003,** *63* (5), 983-992.

134. Ruse, M. D.; Privalsky, M. L.; Sladek, F. M., Competitive Cofactor Recruitment by Orphan Receptor Hepatocyte Nuclear Factor 4α1: Modulation by the F Domain. *Mol. Cell. Biol.* **2002,** *22* (6), 1626-1638.

135. Li, Y.; Kovach, A.; Suino-Powell, K.; Martynowski, D.; Xu, H. E., Structural and Biochemical Basis for the Binding Selectivity of Peroxisome Proliferator-activated Receptor γ to PGC-1α. *J. Biol. Chem.* **2008,** *283* (27), 19132-19139.

136. Schubert, H. L.; Blumenthal, R. M.; Cheng, X., Many paths to methyltransfer: a chronicle of convergence. *Trends Biochem. Sci* **2003,** *28* (6), 329-335.

137. Einstein, M.; Akiyama, T. E.; Castriota, G. A.; Wang, C. F.; McKeever, B.; Mosley, R. T.; Becker, J. W.; Moller, D. E.; Meinke, P. T.; Wood, H. B.; Berger, J. P., The Differential Interactions of Peroxisome Proliferator-Activated Receptor γ Ligands with Tyr473 Is a Physical Basis for Their Unique Biological Activities. *Mol. Pharmacol.* **2008,** *73* (1), 62-74.

138. Nolte, R. T.; Wisely, G. B.; Westin, S.; Cobb, J. E.; Lambert, M. H.; Kurokawa, R.; Rosenfeld, M. G.; Willson, T. M.; Glass, C. K.; Milburn, M. V., Ligand binding and co-activator assembly of the peroxisome proliferator-activated receptor-[gamma]. *Nature* **1998,** *395* (6698), 137-143.

139. Zoete, V.; Grosdidier, A.; Michielin, O., Peroxisome proliferator-activated receptor structures: Ligand specificity, molecular switch and interactions with regulators. *Biochim. Biophys. Acta* **2007,** *1771* (8), 915-925.

140. Rha, G. B.; Wu, G.; Shoelson, S. E.; Chi, Y.-I., Multiple Binding Modes between HNF4α and the LXXLL Motifs of PGC-1α Lead to Full Activation. *J. Biol. Chem.* **2009,** *284* (50), 35165-35176.

141. Finck, B. N.; Kelly, D. P., Peroxisome Proliferator–Activated Receptor γ Coactivator-1 (PGC-1) Regulatory Cascade in Cardiac Physiology and Disease. *Circulation* **2007,** *115* (19), 2540-2548.

142. Yang, W.; Rachez, C.; Freedman, L. P., Discrete Roles for Peroxisome Proliferator-Activated Receptor γ and Retinoid X Receptor in Recruiting Nuclear Receptor Coactivators. *Mol. Cell. Biol.* **2000,** *20* (21), 8008-8017.

143. Allen, T.; Zhang, F.; Moodie, S. A.; Clemens, L. E.; Smith, A.; Gregoire, F.; Bell, A.; Muscat, G. E. O.; Gustafson, T. A., Halofenate Is a Selective Peroxisome Proliferator–Activated Receptor γ Modulator With Antidiabetic Activity. *Diabetes* **2006,** *55* (9), 2523-2533.